1997

Neutron scattering studies of RENi2B2C (RE=Lu,Y,Ho,Er): Lattice dynamics

Max Bullock
Iowa State University

INFORMATION TO USERS

This manuscript has been reproduced from the microfilm master. UMI films the text directly from the original or copy submitted. Thus, some thesis and dissertation copies are in typewriter face, while others may be from any type of computer printer.

The quality of this reproduction is dependent upon the quality of the copy submitted. Broken or indistinct print, colored or poor quality illustrations and photographs, print bleedthrough, substandard margins, and improper alignment can adversely affect reproduction.

In the unlikely event that the author did not send UMI a complete manuscript and there are missing pages, these will be noted. Also, if unauthorized copyright material had to be removed, a note will indicate the deletion.

Oversize materials (e.g., maps, drawings, charts) are reproduced by sectioning the original, beginning at the upper left-hand corner and continuing from left to right in equal sections with small overlaps. Each original is also photographed in one exposure and is included in reduced form at the back of the book.

Photographs included in the original manuscript have been reproduced xerographically in this copy. Higher quality 6" x 9" black and white photographic prints are available for any photographs or illustrations appearing in this copy for an additional charge. Contact UMI directly to order.

UMI

A Bell & Howell Information Company
300 North Zeeb Road, Ann Arbor MI 48106-1346 USA
313/761-4700 800/521-0600

Neutron scattering studies of $RENi_2B_2C$ (RE=Lu,Y,Ho,Er): Lattice dynamics

by

Max Bullock

A dissertation submitted to the graduate faculty
in partial fulfillment of the requirements for the degree of
DOCTOR OF PHILOSOPHY

Major: Condensed Matter Physics
Major Professor: Constantine Stassis

Iowa State University
Ames, Iowa
1997

Graduate College
Iowa State University

This is to certify that the Doctoral dissertation of

Max Bullock

has met the dissertation requirement of Iowa State University.

Signature was redacted for privacy.

Major Professor

Signature was redacted for privacy.

For the Major Program

Signature was redacted for privacy.

For the Graduate College

TABLE OF CONTENTS

LIST OF FIGURES

LIST OF TABLES

ACKNOWLEDGMENTS

The author would like to thank his advisor Professor C. Stassis for his guidance and support. Special thanks are also extended to Professor P.C. Canfield and Dr. B.K. Cho for growing excellent single crystals which were used in the experiments for this dissertation.

The author would also like to thank Dr. J. Zarestky, Prof. B.N. Harmon, Prof. A. Goldman, Dr. P. Dervenagas, Prof. W. Weber, Dr. Gen Shirane, Dr. S.M. Shapiro, and Mr. Z. Honda for their assistance during the course of this work. I would also like to thank my fiancee for giving me support.

The assistance and hospitality of the Neutron Scattering Groups at Oak Ridge National Laboratory and Brookhaven National Laboratory is greatly appreciated.

Finally, appreciation is extended to the many people at Iowa State University and Ames Laboratory who create an excellent scientific environment.

This work was performed at Ames Laboratory under Contract No. W-7405-Eng-82 with the U.S. Department of Energy. The United States government has assigned the DOE Report number IS-T 1820 to this dissertation.

CHAPTER 1. INTRODUCTION

Background-General

Superconductivity and magnetic order are two fundamental properties of matter that have been studied for decades. However, few materials exhibit both properties. The first such systems were made by introducing magnetic impurities into superconducting materials.[1,2] These systems gave great insight into the pair-breaking mechanisms of the magnetic impurities of these superconductors. However, magnetic ions would interact and destroy the superconductivity before enough of the ions had been added to the system to order magnetically.

In the 1970's, two systems were discovered that allowed for the study of the interaction between superconductivity and magnetic ordering. These two systems were the $REMo_6(S,SE)_8$, and $RERh_4B_4$ (where RE stands for a rare-earth element)[2] which are superconducting ternary compounds[3,4,5]. From these two systems, it was concluded that superconductivity can coexist with long range antiferro-magnetic order, but that ferromagnetism usually leads to the destruction of superconductivity[2-15]. Experimentally, these systems are hard to study because T_N(i.e. magnetic transition

temperatures) is very low; (≤1K) which is below the temperature of pumped liquid ^{4}He. Also $T_c >> T_N$ for most of these systems. Therefore you cannot examine comparable energy scales. In addition single crystal samples were very rare and not examined until 5-10 years after the discovery of a new system.

$RENi_2B_2C$-Introduction

The recent discovery of the rare-earth boride carbide family $RENi_2B_2C$ [16,17,18,19] has provided another system to study the interplay of superconductivity and magnetism. In addition, these compounds have much higher transition temperatures ($T_N \approx 1.5$-20K, $T_c \approx 6.2$-16.6K) which make them easier to work with experimentally. This system exhibits a variety of ground states from just superconductivity (in *Y*[20,21] and *Lu* compounds), superconductivity coexisting with magnetic order (*Tm*[22], *Er*[23], *Ho*[24], and *Dy*[25,26] compounds), and magnetic order without superconductivity (*Gd*[27] and *Tb*[28] compounds). The transition temperatures for these compounds are given in Table 1.1[29], with the highest superconducting temperatures, 16.6 and 15.6K for the Lu and Y compounds. The superconductors in these compounds are conventional superconductors even though they have a layered structure,

Table 1.1: Transition temperatures of the $RENi_2B_2C$ family.

RE	T_c(K)	T_N(K)
Y[21]	15.5	-
Lu[17]	16.6	-
Tm[22]	10.8	1.5
Er[23]	10.5	6
Ho[23]	8.5	6
Dy[25]	6.2	10
Tb[28]	-	15
Gd[27]	-	20
Sm[29]	-	9
Nd[29]	-	4.5

common to high T_c superconductors, which can be seen in Figure 1.1.

Incommensurate Magnetic Structure

Many interesting papers have been published on the $RENi_2B_2C$ system since the discovery of these compounds in 1994. Of particular relevance to this dissertation is the magnetic structure of a few of the magnetic compounds, specifically the magnetic ordering of Ho, Er, Gd, and Tb. These compounds order in an incommensurate modulation of the moments along **a*** with wave vectors of 0.585, 0.553, 0.553, and 0.551 to 0.545 for Ho[30,31,32], Er[33,34], Gd[35], and Tb[36], respectively. In Er (T_c = 10.5K), below 6 K, magnetic diffraction peaks appear in rows parallel to the reciprocal a-axis as in Figure 1.2. These peaks can be indexed as first and higher-order satellites of the allowed nuclear reflections with an incommensurate wave vector (0.553,0,0). A similar magnetic structure with wave vector (0.585,0,0) was also observed between approximately 6 and 4.7 K in the Ho compound.

It is interesting that an incommensurate magnetic structure with wave vector along **a*** is a common feature of the magnetic structures of several of these compounds(Ho, Er, Tb, and Gd). The magnitude of the wave vectors do not vary appreciably among these compounds and are close to the zone

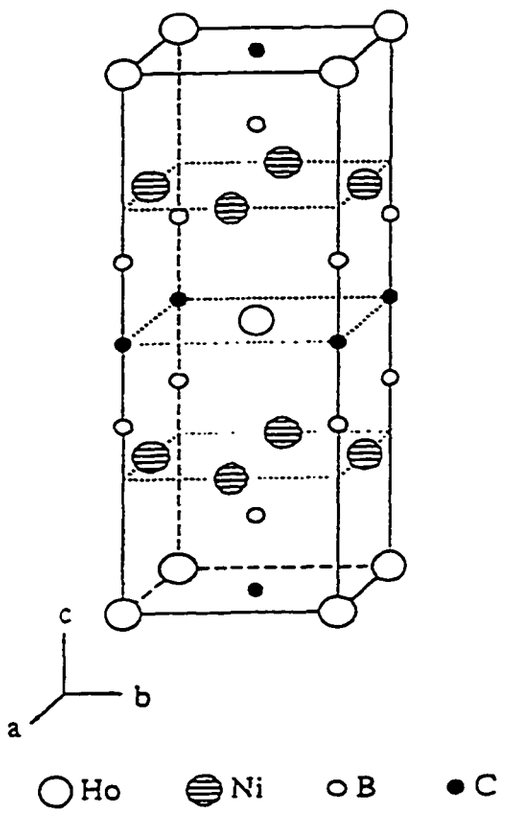

Figure 1.1: The crystal structure of $HoNi_2B_2C$. Ho can be replaced with any rare-earth element. (After Reference Grigereit[31])

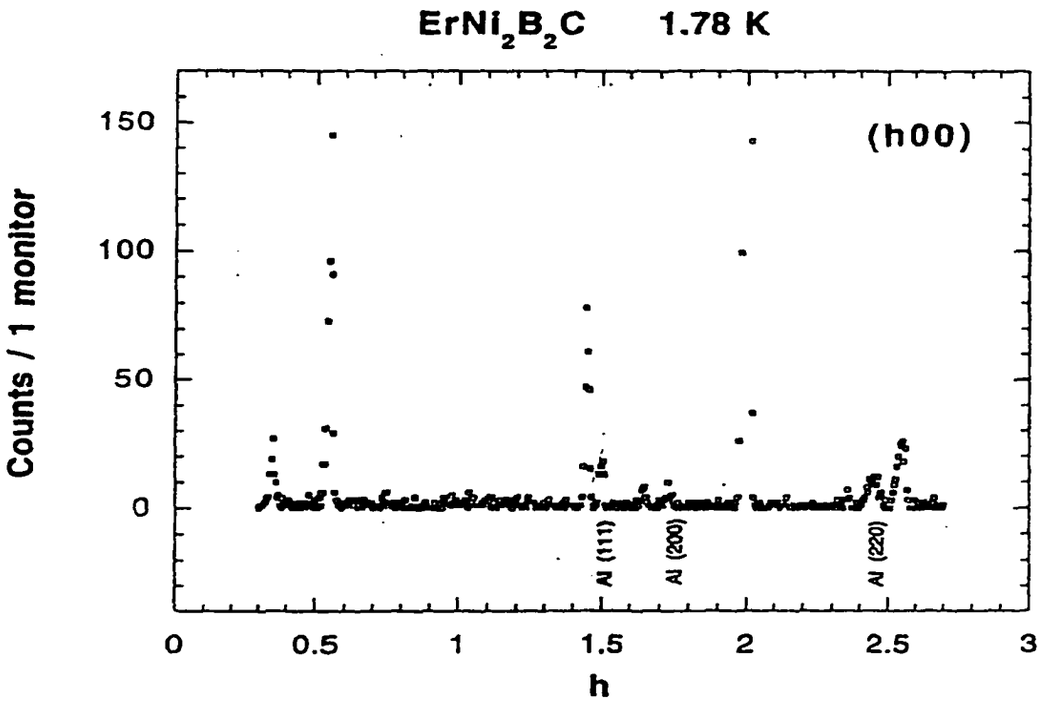

Figure 1.2: Neutron diffraction scan along the **a*** direction for $ErNi_2B_2C$. One monitor corresponds to a counting interval of approximately 1 sec. (After reference Zarestky[29])

boundary point G_1. This suggests that there are common Fermi surface nesting features along **a*** which cause the magnetic ordering of the rare-earth magnetic moments via the Ruderman-Kittel-Kasuya-Yosida (RKKY) mechanism.[37,38,39,40]

Phonon Softening-Kohn Anomaly

The lattice vibrations of the atoms are partly screened by the electrons. Essentially, a phonon of wave vector $\vec{q}$ and frequency ω sets up a potential field due to the motion of the ions in the metal. The electrons move to screen this field and modify the ion-ion interaction which in turn alters the phonon frequency. The screened field will be inversely proportional $\varepsilon(\vec{q})$, where $\varepsilon(\vec{q})$ is the dielectric function describing the screening of the electrons(see appendix A). By modifying the forces between the ions, the lattice frequency, ω, of this mode of vibration will depend on $\varepsilon(\vec{q})$. Hence, any singularity in ε will be reflected in the phonon frequency.[41]

Kohn[42] proposed that for metals this screening changes rather rapidly, depending on the Fermi surface's geometry. Thus, the electron-phonon interaction will be reflected in the phonon spectrum of some metals depending on the detailed electronic structure. In addition, $\varepsilon(\vec{q})$ will change when $\vec{q}$ is equal to a spanning vector connecting two pieces of Fermi

surface. This means that the electrons which usually screen the motions of the ions are unable to screen as effectively for $\vec{q} = \vec{q}_{ext}$,where $\vec{q}_{ext}$ is a q vector connecting two extremum pieces of Fermi surface. Kohn was the first person to point out that the drop in $\varepsilon(\vec{q})$ as $\vec{q}$ is increased through $\vec{q}_{ext}$, where $\vec{q}_{ext} = 2\vec{k}_f$ for a free electron gas with Fermi wave number $\vec{k}_f$, should lead to a small sudden change in the eigenfrequency $\omega(\vec{q})$ at the point $\vec{q} = \vec{q}_{ext}$.

This effect of the electron-phonon interaction on the phonon dispersion curves was first observed by Brockhouse[43] in lead. The dispersion curves of lead have several small anomalous kinks at wave vectors corresponding to nested pieces of the fermi surface. Since this time, numerous Kohn anomalies have been observed in other metals.

A calculation(without matrix elements) of the generalized electronic susceptibility $\chi(q)$, where

$$\varepsilon(\vec{q}) = 1 + 4\pi\chi(\vec{q}),$$

is shown in Figure 1.3. This electronic susceptibility for $LuNi_2B_2C$ is based on the normal-state electronic band structure of this compound which was made by Rhee et al.[44] The $\chi(q)$ showed a peak near wave vectors corresponding to those observed for the incommensurate magnetic structure observed in Ho, Er, Gd, and Tb. This peak in $\chi(q)$ is due to a nesting of the Fermi surface shown in Figure 1.4 by the solid arrow. Figure 1.4 is a cut of the Fermi surface (perpendicular to

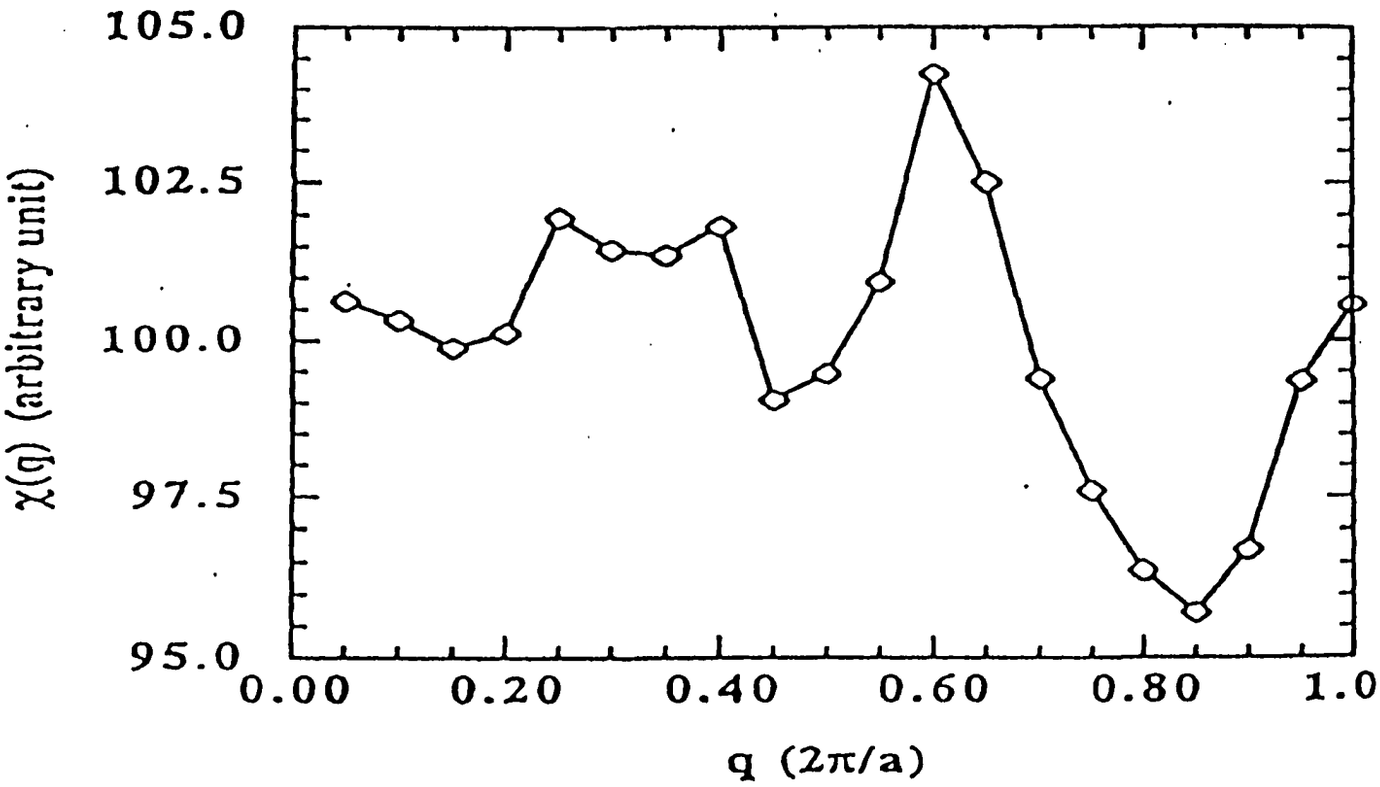

Figure 1.3: Generalized susceptibility along the a* axis. (After Reference Rhee[44])

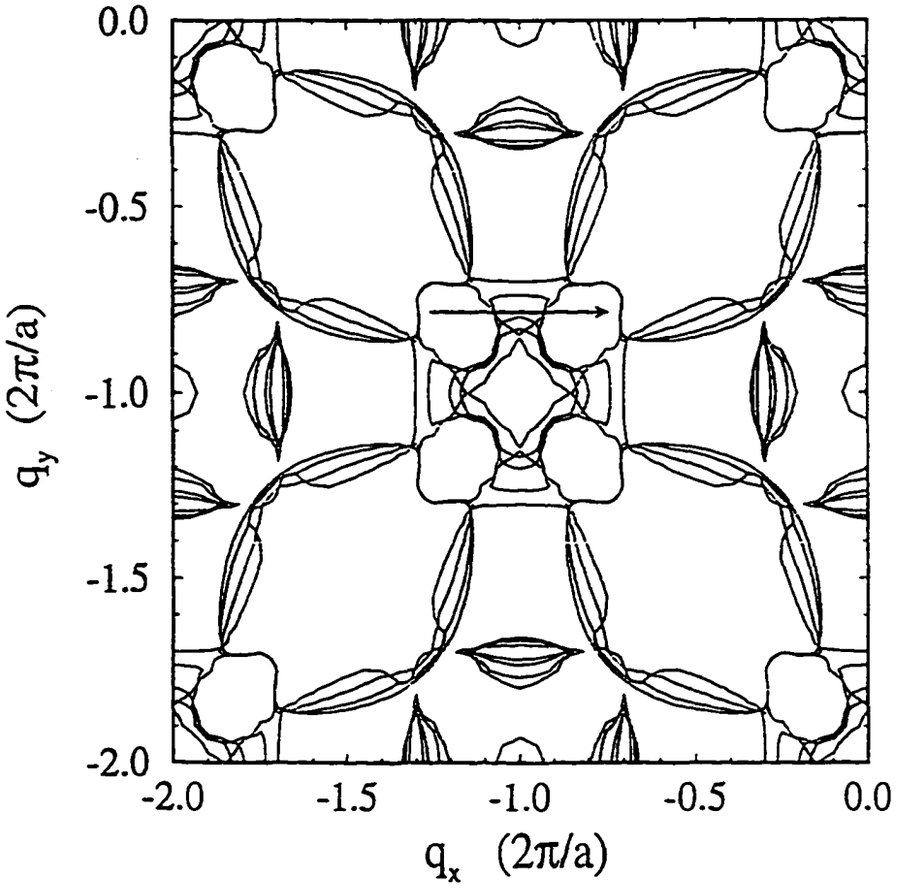

Figure 1.4: Fermi surface cross section on the planes perpendicular to the c axis.(After Reference Rhee[44])

the c axis) and the arrow shows the region of the Fermi surface that are nearly parallel and give rise to the peak in the generalized susceptibility $\chi(q)$ defined[45] as

$$\chi(\mathbf{q}) = \sum_{n,m,\mathbf{k}} \frac{f[E_m(\mathbf{k})]\{1 - f[E_n(\mathbf{k}+\mathbf{q})]\}}{E_n(\mathbf{k}+\mathbf{q}) - E_m(\mathbf{k})}$$

where f is the Fermi-Dirac distribution function and n, m are indexes of the electronic bands. Since there appears to be a strong nesting of the Fermi surface of $LuNi_2B_2C$[44], one would also expect strong Kohn anomalies in the phonon dispersion curves of this compound. This dissertation will detail the dispersion curves and Kohn anomalies in the Lu compound.

Other compounds in this family have been studied experimentally by other groups. Gompf et al.[46] found that the phonon softening in the $LuNi_2B_2C$ compound was so significant that it was observed in their phonon-density of states measurements. Likewise, Yanson et al.[47] found phonon softening in their point-contact spectra of these compounds. Kawano et al.[48] performed a detailed study of the low-lying excitations in the YNi_2B_2C compound and found softening as predicted above and claims that there may be a new type of excitations below the superconducting transition temperature.

Crystal Structure

The structure of these compounds[18] is body-centered tetragonal (space group I4/mmm) and consists of RE-C layers separated by Ni_2B_2 sheets as can be seen in Figure 1.1. The crystals used in these experiments were grown at the Ames Laboratory by the high-temperature flux technique.[49,50] With the high-temperature flux technique, crystals as large of 700 mg (7mm x 7mm x 0.5mm) can be grown. Typically the c-axis is around 3 times larger than the a-axis. Some typical lattice constants from neutron scattering experiments are given in Table 1.2.

Experimental-Neutron Scattering

This section will detail some practical aspects of neutron scattering directly related to this dissertation. Other texts cover the subject of neutron scattering[51,52,53,54,55,56] in much greater depth than this dissertation.

Unlike X-rays and electromagnetic radiation such as infrared radiation, neutrons have wavelengths and energies comparable with the interatomic spacing and phonon energies of solids. Taking this into account as well as the fact that neutrons have no electric charge, makes neutron

Table 1.2: Lattice constants from neutron scattering for $RENi_2B_2C$ (After Reference Siegrist[18]).

RE	Lat. Par. (a) Å	Lat. Par. (c) Å
Lu	3.467	10.63
Tm	3.494	10.6
Er	3.508	10.57
Ho	3.526	10.54
Dy	3.535	10.55
Y	3.544	10.47
Tb	3.561	10.43
Sm	3.629	10.23
La	3.803	9.795

scattering an ideal tool for the study of dynamical properties of crystalline solids. The neutron interacts with the nucleus primarily though the nuclear force. The range of the neutron-nucleon interaction is of the order of 1 Fermi while the wavelength of the incident neutrons is roughly 1 Å. This implies that neutron scattering is isotropic and can be characterized by a single parameter b, the scattering length. The value of b can be both positive, negative, or even complex depending on the nucleus involved. In addition, different isotopes and spin orientations of the neutron and nucleus also affect the scattering length.

Most crystals are made up of a variety of isotopes, and therefore b may vary from nucleus to nucleus. Only the mean scattering potential can give interference effects and thus have coherent scattering. Likewise, the variations in scattering potential from different nucleus is proportional to $(\overline{b^2}-\bar{b}^2)^{\frac{1}{2}}$ and give rise to incoherent scattering. The differential cross section for scattering of neutrons into the solid angle Ω can thus be represented as a sum of two terms:

$$\left(\frac{d\sigma}{d\Omega}\right)_{total}=\left(\frac{d\sigma}{d\Omega}\right)_{coherent}+\left(\frac{d\sigma}{d\Omega}\right)_{incoherent}$$

The differential cross section of one-phonon inelastic coherent scattering is given by

$$\left(\frac{\partial^2\sigma}{\partial\Omega\partial E_f}\right)_{coherent} = \frac{4\pi^3\hbar}{V_0}\frac{k_f}{k_i}\sum_{\vec{\tau},j,\vec{q}}\frac{(n+\frac{1}{2}\pm\frac{1}{2})}{\omega_j(\vec{q})}\left|F_j(\vec{Q})\right|^2_{coh}\delta(\hbar\omega\mp\hbar\omega_j(\vec{q}))\delta(\vec{Q}-(\vec{q}+\vec{\tau}))$$

where

V_0 is the volume of the primitive cell,

n = average occupation number = $n_{j\vec{q}} = \dfrac{1}{\exp[\frac{\hbar\omega_j(\vec{q})}{k_B T}]-1}$,

$\vec{q}$ = phonon wave vector,

$\hbar\omega_j(\vec{q})$ = energy of the phonon in the j^{th} mode with wave vector $\vec{q}$,

$\vec{\tau}$ = reciprocal lattice vector,

$\vec{Q} = \vec{k}_i - \vec{k}_f$ is the scattering vector,

$\hbar\omega = \dfrac{\hbar^2(k_i^2 - k_f^2)}{2M_n}$ is the energy change of the neutron,

$\left|F_j(\vec{Q})\right|^2_{coh} = \left|\sum_k \bar{b}_k[\vec{Q}\cdot\vec{e}(k\mid j\vec{q})]e^{i\vec{Q}\cdot\vec{r}(k)}\dfrac{e^{-W_k}}{\sqrt{M_k}}\right|^2$ is the inelastic structure factor,

$\bar{b}_k = \dfrac{1}{N_k}\sum_k b_k$ is the coherent nuclear scattering amplitude of atom k,

N_k = number of atoms of type k in the crystal,

$\vec{r}(k)$ = the position vector of atom k with respect to the origin of the unit cell,

and W_k = Debye-Waller factor for atom k.

The delta functions in the differential cross section requires conservation of energy and momentum up to a reciprocal lattice vector. The ± signs indicate the creation(upper) and annihilation(lower) of a phonon in mode j with wave vector $\vec{q}$. Since the average occupation number goes to 0 at low temperatures, most phonon low temperature experiments have to be done with the creation of phonons, or energy loss to the neutrons so that $\left(n+\frac{1}{2}\pm\frac{1}{2}\right)$ is equal to 1, and not 0 at low temperatures.

Experimentally, we want to maximize the coherent scattering so that we can observe the phonon peaks and hopefully minimize the background. By looking at the inelastic structure factor, we see that it contains the following expression $\vec{Q}\cdot\vec{e}(k,j\vec{q})$. By maximizing $\vec{Q}$ we will be increasing the inelastic structure factor. This same expression is what determines which phonon polarization, or mode, will be picked up in a certain configuration. If the phonon polarization is parallel to $\vec{Q}$ the phonon mode should be observed in a scan. The $RENi_2B_2C$ phonon modes do not have the typical longitudinal and transverse symmetry along the [100] as are observed in most simple systems. Instead, these modes develop both transverse(along **c***) and longitudinal components for the Ni and B atoms for two of the four representations. The RE and C atoms on the other had, do not

exhibit both transverse and longitudinal components. For example, for small wave vectors, the Δ_4 is transverse in nature, however, as the wave vector increases, the Ni and B atoms develop a longitudinal component. This means that it is theoretically possible to pick this mode up from a longitudinal configuration. Only a complete analysis of the inelastic structure factors will tell you which Q will give you the largest structure factor.

The incoherent scattering cross section does not depend on $\vec{Q}$ and will be treated as background for these experiments. Typically, phonons will have a peak height of a few hundred counts with a background of 50 or less. Figures 1.5 and 1.6 show two phonon profiles for $LuNi_2B_2C$ and YNi_2B_2C respectively.

Experimental-Triple Axis Spectrometers

A schematic diagram of HB3 triple axis spectrometer at Oak Ridge National Laboratory(ORNL) is shown in Fig. 1.7. A large single crystal (pyrolitic graphite for these experiments) is used as a monochromator to Bragg reflect neutrons of a particular wavelength from the reactor spectrum. By varying the angle of the monochromator $2\theta_m$, and θ_m, the wavelength of the monochromatic beam can be varied.

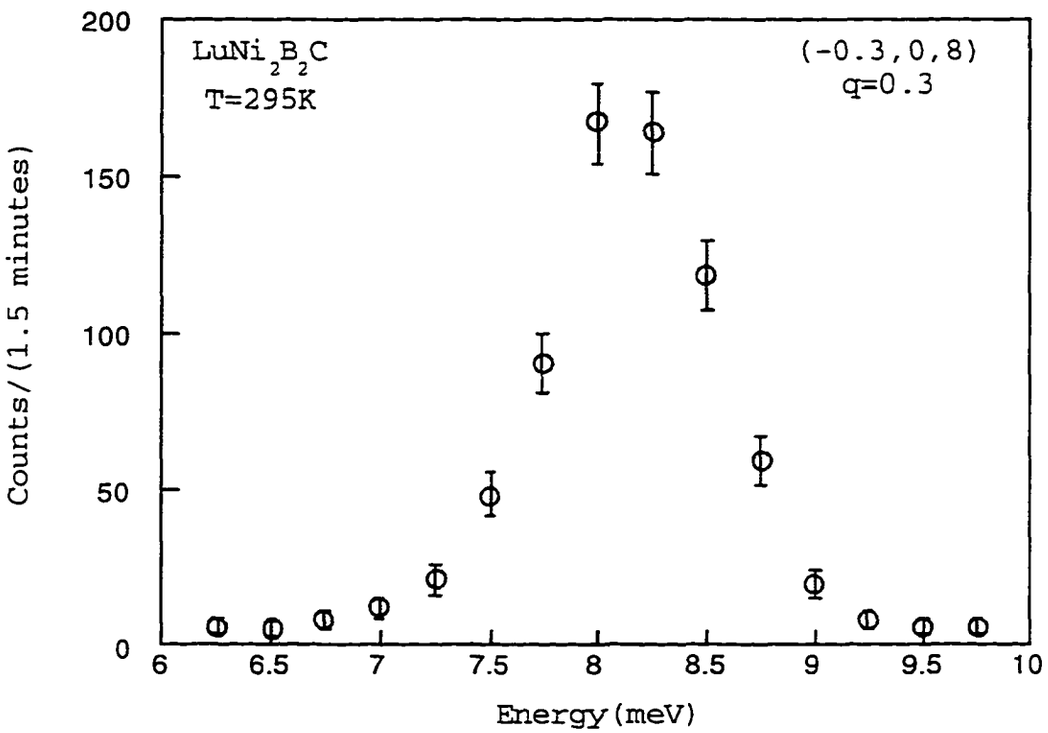

Figure 1.5: Phonon profile of $LUNi_2B_2C$ for Q=(0.3,0,8) at T=300K.

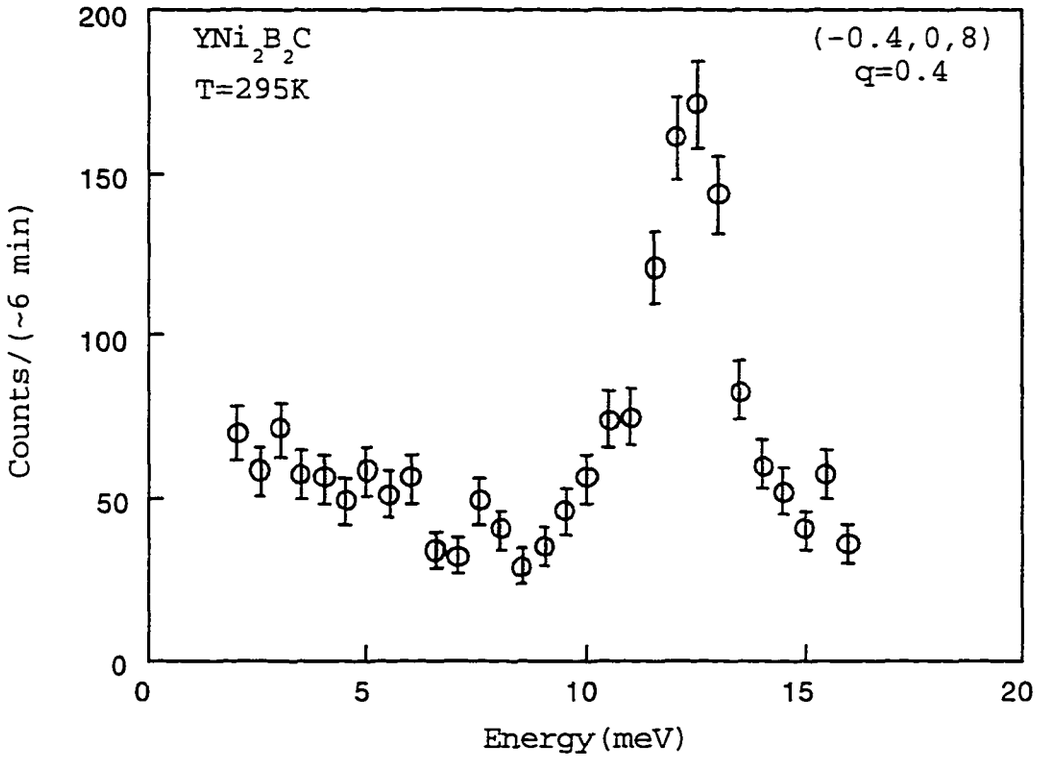

Figure 1.6: Phonon profile of YNi_2B_2C for Q=(0.3,0,8) at T=300K.

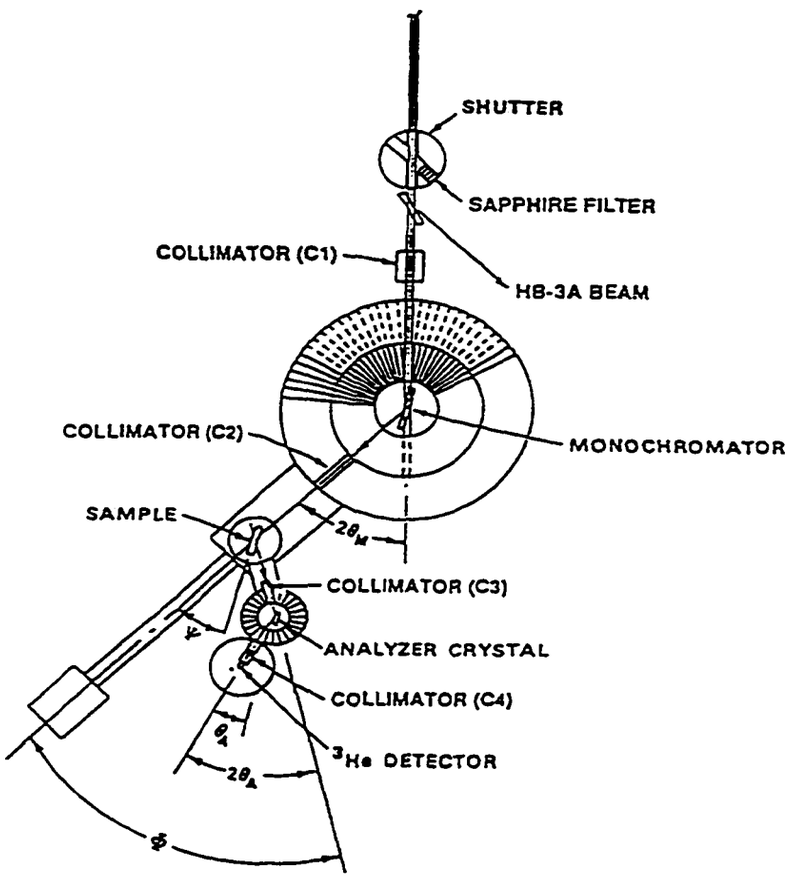

Figure 1.7: Diagram of the HB3 triple axis spectrometer at the HFIR reactor at Oak Ridge National Lab.

The momentum $\bar{k}_0$ of the incident neutrons of energy E_o is determined by the direction of the beam and the relation

$$E_0 = \frac{\hbar^2 k_0^2}{2M_n} = \frac{\hbar^2}{2M_n}\left[\frac{\pi \sin\theta_m}{d_m}\right],$$

where M_n is the mass of the neutron and d_n is the spacing of the reflecting planes of the monochromating crystal.

Next, the beam is incident on the sample crystal set at an angle ψ and is scattered at a scattering angle ϕ towards the analyzing crystal. The energy of the reflected beam of scattered neutrons is determined with the analyzer crystal. The final momentum of the neutrons is determined from the angle ϕ and the relation

$$E_f = \frac{\hbar^2 k_0^2}{2M_n} = \frac{\hbar^2}{2M_n}\left[\frac{\pi \sin\theta_a}{d_a}\right]$$

where θ_a is the glancing angle at the analyzer and d_a is the spacing of the reflecting planes of the analyzer.

Most of the experiments described in this dissertation were done at fixed analyzer energy of 14.5 meV, or 30.5 meV. These energies were chosen so that the pyrolitic graphite filters placed in front of the analyzer would attenuate higher-order contamination.

After the analyzer, the neutron beam travels into a detector. Since the neutron does not have any electric charge, a BF_3 or ^3He gas detector is typically used. The

neutron then interacts with the gas producing radiation by the relation

$$^{3}_{2}He + ^{1}_{0}n = ^{1}_{1}H + ^{3}_{1}H + 0.76\ Mev$$

Counters are typically cylindrical with a diameter of a few centimeters and a length of around 30 cm. These detectors have an efficiency of about 80%.

A typical spectrometer also has collimators along the path of neutrons to improve resolution of the instrument. Typically we use collimation of 40'-monochromator-40'-sample-40'-analyzer-80'-detector. Of course tighter collimation gives less background, but typically requires longer counting time to get the same intensity of the phonon peak. In addition, a sapphire filter was used before the monochromator in some experiments to eliminate higher energy neutrons.

Experimental-"Constant-Q" Method

The most common method used in determining the phonon dispersion relations using a triple axis spectrometer is the constant-Q method. In this method the scattering vector $\vec{Q} = \vec{k}_i - \vec{k}_f$ is held constant, while the energy transfer,

$$\hbar\omega = \frac{\hbar^2}{2M_n}\left(\vec{k}_i^{\,2} - \vec{k}_f^{\,2}\right)$$

is varied. This method is illustrated in Fig 1.8 and 1.9 for the (h0l) scattering plane[we assume this plane is parallel

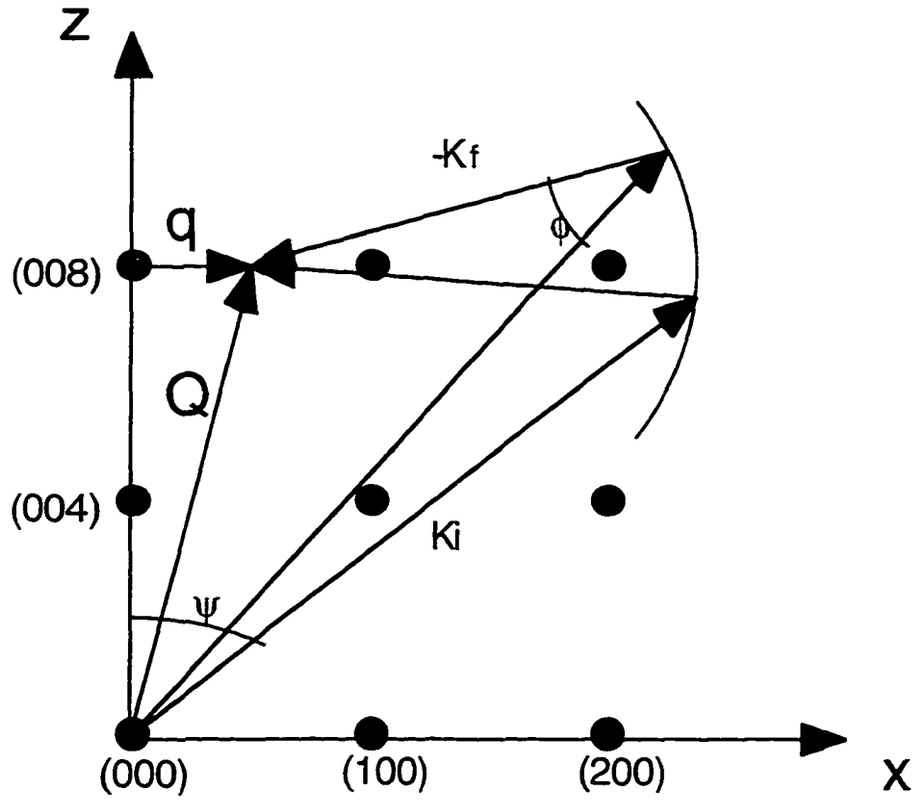

Figure 1.8: The constant Q method of phonon measurement. This figure illustrates the motion of momentum-space vectors in the (h0l) scattering plane for a constant Q scan using fixed final energy(i.e. fixed $|\vec{k}_f|$).

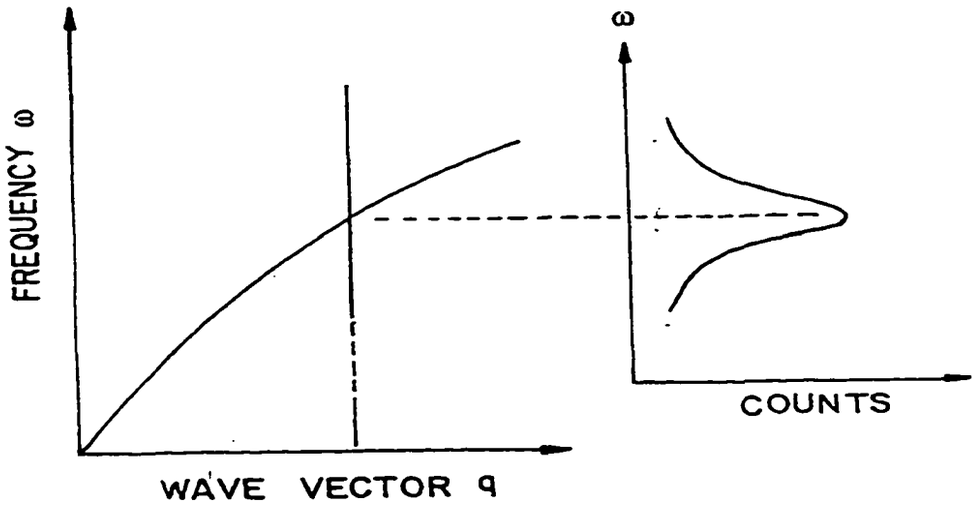

Figure 1.9: The constant Q method of phonon measurement. The left figure shows a scan through a dispersion curve as produced by this method, while the right figure shows the resultant scan we see experimentally.

to the scattering plane of the spectrometer]. This amounts to scanning along the solid line in Fig. 1.8. For these experiments, we usually fix the final energy, which in turn fixes the magnitude of $\vec{k}_f$. The magnitude and direction of $\vec{k}_i$ are then varied so that $\vec{Q}=\vec{k}_i-\vec{k}_f$ is held constant. This allows the energy transfer to be varied which results in a vertical scan through the dispersion curve as can be seen in the left side of Fig 1.9. This results in a peak of the 'neutron group' in the left side of Fig 1.9 which will define the frequency $\omega_j(\vec{q})$. By varying $\vec{q}$ we are then able to map out the dispersion curves for a sample. The different polarizations can be selected by using different $\vec{Q}$ which will favor certain modes and suppress others according to the inelastic structure factor discussed above. Usually only high symmetry directions are mapped out in this way. For this body-centered tetragonal, we have mapped some of the lower Δ, Λ, and Σ branches which are along the [100], [001] and [110] directions.

Dissertation Organization

The first chapter gives a brief overview of the system discussed in this dissertation. Chapters 2-5 and Appendix B of this dissertation consist of papers that are published, or have been submitted, which show experimental data regarding

the phonon softening of $LuNi_2B_2C$. The papers are in chronological order and show how the problem has progressed over time. Each of these papers has a list of references pertaining to that particular paper, which are located at the end of each chapter. The author's name is first on the last three papers, and second on the other two papers; the author played a significant role in the experimentation, data interpretation, and compiling of all five papers. At the time this dissertation was completed, the paper that is chapter 4 of this dissertation has not been approved by Physical Review B for publication yet. In addition, the paper given in appendix B is a rough draft of a proposed paper that should be submitted shortly after the completion of this dissertation.

Chapter 6 will contain a summary of the conclusions up to date. Appendix A will consist of a brief derivation of $\chi(q)$ which is talked about in the introduction of the dissertation. Appendix B will contain a Born-von Kármán model fit to the experimental $LuNi_2B_2C$ data and a comparison with experimental data. Appendix C will contain a brief summary of the work done on $LuNi_2B_2C$ as well as a complete listing of experimental data taken on the crystals which may be needed later for theoretical models of this system. Appendix D will outline a brief introduction covering some of the field theory used in the theoretical work for this

thesis. The bibliography at the end of the dissertation will contain references cited in Chapters 1, Chapter 6, and Appendices A, C, and D.

CHAPTER 2. SOFT PHONONS IN SUPERCONDUCTING $LuNi_2B_2C$

A paper published in *Physical Review B*[1]

P. Dervenagas, M. Bullock, J. Zarestky, P. Canfield,
B. K. Cho, B. Harmon, A. I. Goldman, and C. Stassis

Ames Laboratory and Department of Physics and Astronomy
Iowa State University, Ames, IA 50011

Abstract

Inelastic neutron scattering techniques have been used to measure the low-lying phonon dispersion curves of superconducting $LuNi_2B_2C$ along the [ξ00] and [00ξ] symmetry directions. The most important result of this experiment is that the phonon frequencies of the acoustic and first optical Δ_4 [ξ00] branches in the vicinity of the zone boundary point G_1 decrease with decreasing temperature. Actually these two branches exhibit pronounced dips at low temperatures, close to G_1. This shows that the electron phonon interaction is quite strong and causes an incipient lattice instability, a behavior typical of strongly coupled conventional

---

[1] Reprinted with permission from *Phys. Rev. B* **52** R9839 (1995).

superconductors. Furthermore, the phonon anomalies occur at wave vectors close to those of the incommensurate magnetically ordered structures observed in the magnetic compounds of this family, which suggests that both the magnetic ordering and the incipient lattice instabilities are influenced by common nesting features of the Fermi surfaces of the rare-earth nickel boride carbides.

Introduction

The quaternary intermetallic compounds of the recently discovered[1-4] family of rare-earth nickel boride carbides, $RENi_2B_2C$ (where RE stands for a rare-earth element), have very interesting physical properties. The structure[3] of these compounds is body-centered tetragonal (space group I4/mmm) and consists of RE-C layers separated by Ni_2B_2 sheets. Many of these compounds are superconducting with the highest superconducting temperatures, 16.6 K and 15.6 K, observed[2-5] for the Lu and Y compounds, respectively. Particularly interesting is that superconductivity is not only observed for non-magnetic rare-earth elements but also for magnetic rare-earth elements such as Tm, Er, Ho[2-5] and most recently Dy[6,7]; the Tm, Ho, Er, and Dy compounds are superconducting with superconducting temperatures of 10.8 K, 8 K, 10.5 K, and 6.2 K, respectively, whereas the Gd and Tb compounds are not

superconducting at least down to approximately 2 K. This family of intermetallic compounds is, therefore, particularly well suited for a detailed study of the interplay between superconductivity and magnetism, which has been previously examined[8-11] in the $RERh_4B_4$ and $REMo_6S_8$ magnetic superconductors.

The magnetic structure of Ho, Er, and Dy compounds have been studied[7,12-15] by neutron diffraction techniques and that of $GdNi_2B_2C$ by resonant magnetic X-ray scattering.[16] In $DyNi_2B_2C$ and below 4.7 K in $HoNi_2B_2C$ a simple antiferromagnetic structure, consisting of ferromagnetically aligned basal-plane layers with the magnetic moments of two consecutive layers pointing in opposite directions, has been observed. In the Ho compound, two incommensurate modulations of the moments were observed between 4.7 and 6 K, one with wave vector along $\vec{c}^*$, and the other with wave vector along $\vec{a}^*$. The latter modulation has also been observed in the Er and Gd compounds. The above experimental results suggest[7,12-15] that there are common Fermi surface nesting features along $\vec{a}^*$ and/or $\vec{c}^*$ which cause the magnetic ordering of the rare-earth magnetic moments via the RKKY mechanism.

Electronic band structure calculations[17-19] suggest that these materials are conventional superconductors with a relatively high density of states at the Fermi level. These calculations show that there is a rather complex set of bands

crossing E_F which are strongly coupled to the phonons and may be responsible for the superconducting properties of these compounds. More recently, Mattheiss, Siegrist, and Cava suggested[20] that superconductivity in these systems can be attributed to a conventional electron-phonon mechanism that couples the s-p like conduction electrons to a high-frequency boron A_{1g} phonon mode in which the boron atoms move along the c-axis relative to the other atoms. The energy of the Raman active boron A_{1g} mode was calculated[17] by Pickett and Singh to be 106 meV(=850 cm^{-1}), a value in good agreement with Raman scattering measurements.[21,22] Furthermore, Pickett and Singh obtained an estimate of 20 meV for the average phonon frequency by using resistivity data to estimate the electron-phonon coupling parameter ($\lambda \simeq 2.6$). Since this estimate of an average phonon energy is considerably lower than the energy of the boron A_{1g} mode, they suggest that superconductivity in these compounds may involve soft modes or strong contributions from the heavier atoms.

More recently, Rhee, Wang, and Harmon[23] performed a calculation (without matrix elements) of the generalized electronic susceptibility $\chi(q)$ of $LuNi_2B_2C$ based on the normal state electronic band structure of this compound. Peaks in the calculated $\chi(q)$ occur near wave vectors corresponding to those observed for the incommensurate magnetic structures observed in $HoNi_2B_2C$. Of particular interest is that the

sharp peak in the calculated $\chi(q)$ along $\bar{a}^*$ is due to strong Fermi surface nesting and occurs at a wave vector of approximately 0.6, which is close to the values of the incommensurate magnetic modulations along $\bar{a}^*$ observed in the Ho, Er, and Gd compounds (0.585, 0.553, and 0.553, respectively). If such a strong nesting feature is indeed present at the Fermi surface of $LuNi_2B_2C$, one also would expect strong Kohn anomalies in the phonon dispersion curves of this compound.

It is clear from the above discussion that experimental studies of the lattice dynamical properties of these compounds may lead to a better understanding of their properties. No detailed experimental study of the phonon dispersion curves of these compounds has been performed to date, since the presently available crystals are not of sufficient size for inelastic neutron scattering experiments. However, by mounting two crystals together, we were able to measure several low-lying phonon dispersion curves of the Lu compound. In this report we present the results of these experiments.

Experimental

Single crystals of $LuNi_2B_2C$ were grown at the Ames Laboratory by the high-temperature flux technique as

described elsewhere.[24] The crystals obtained are platelets with the c-axis perpendicular to their flat surface. Since the size of the crystals (approximately 5 x 5 x 0.5 mm^3) is relatively small for inelastic neutron scattering, a composite crystal, consisting of two of these crystals, was used in the present experiments. The two crystals were mounted together and their alignment was adjusted until their Bragg reflections were found to coincide to within the instrumental resolution.

The experiments were performed using the HB1A, HB2, and HB3 triple-axis spectrometers at the High Flux Isotope Reactor (HFIR) of the Oak Ridge National Laboratory. Pyrolitic graphite reflecting from the (002) planes was used as both monochromator and analyzer in the HB2 and HB3 spectrometers and the data were collected using fixed scattered neutron energies of 14.7 and 30.5 meV. The HB1A spectrometer is a constant incident energy (14.7 meV) instrument utilizing a double pyrolitic graphite monochromator (reflecting from the (002) planes). The collimation before the sample was either 20 or 40 minutes of arc and that after the sample was 40 minutes of arc. Pyrolitic graphite filters were used in all spectrometers to attenuate higher-order contaminations.

All data were collected with the crystal oriented so that the scattering plane coincides with the a-c crystal

plane. Measurements of the phonon dispersion curves were performed along the [ξ00] and [00ξ] high symmetry directions. The measurements along the [ξ00] direction were extended beyond the zone boundary point G_1 $\left(at\frac{\pi}{a}\left(1+\frac{a^2}{c^2}\right)\right)$ to (2π/a, 0, 0) which is the same point as the zone boundary point Z along the [00ξ] direction. While most measurements were performed at room temperature, the temperature dependence of the phonon frequencies of the interesting Δ_4 branches along the [ξ00] direction was determined by measurements at 120, 60, 25, 10, and 2 K. A selected number of phonon frequencies of the other branches were also measured at 10 K to assess whether they exhibit anomalous behavior.

The measured frequencies were assigned to the various branches by comparing the measured intensities of the corresponding neutron groups with calculations of intensities based on Born-von-Kármán force constant models; the parameters of the force-constant models were determined by fitting the neutron scattering data along with the frequencies of the measured[21,22] Raman active modes. The way we have chosen to satisfy the compatibility relations at the zone boundary point Z is only one of several alternatives, since the phonon frequencies belonging to different representations are so close to each other in the vicinity of

Z that the corresponding neutron groups cannot be sufficiently resolved with the resolution of the present experiment.

The lowest lying acoustic and optical branches were both obtained by measurements from the (008) reciprocal point, i.e., with a configuration appropriate for transverse branches with polarization along the c-axis. By symmetry, the acoustic branch with this polarization belongs to the Δ_4 representation. Based on the analysis of the data using a Born-von-Kármán force constant model (see previous paragraph), the optical branch was also assigned to the Δ_4 [ξ00] representation. For small wave vectors, both Δ_4 branches are purely transverse with atomic displacements along the c-axis. For the acoustic branch all atoms move in phase, whereas in the optical branch the motion of the Ho atom is out of phase with that of the other atoms. For larger values of the wave vector the Ho and C displacements remain transverse, while the Ni and B atoms develop a longitudinal component.

Results and Discussion

At room temperature, the phonon frequencies of the acoustic and optical branches, with zone-center energies at approximately 14, 15, and 24 meV, were measured. The room

temperature acoustic and lowest lying optical branches are plotted in Fig. 2.1. The highest measured energy at the zone center ($\simeq$ 24 meV) is in good agreement with the experimentally determined[21,22] lowest Raman active Ni-B_{1g} mode. A complete analysis of these measurements in terms of lattice dynamical models will be published elsewhere.

The most interesting result of these experiments is the temperature dependence of the observed phonon frequencies. The frequencies of selected phonons on all the measured branches, except the Δ_4 [ξ00], show no significant change with temperature. The phonon frequencies of the acoustic and first optical Δ_4 [ξ00] branches in the vicinity of the zone boundary point G_1, on the other hand, decrease with decreasing temperature. Actually, these two branches exhibit pronounced dips at low temperatures close to G_1 (Fig. 2.2). This is quite a unique case of soft phonon behavior: the softening occurs over the same region of wave vectors for two (Δ_4) branches that cannot cross by symmetry.

The observed phonon softening shows that the electron-phonon interaction is quite strong in this compound and causes an incipient lattice instability, a behavior which is typical of conventional superconductors with relatively high superconducting transition temperatures. This observation provides experimental support for the argument, based on band theoretical calculations,[17-19] that this compound is a

conventional superconductor. The strong electron-phonon interaction is presumably responsible both for the relatively high T_c of this compound as well as the observed incipient lattice instability.

As mentioned in the Introduction, Pickett and Singh argued[17] that soft phonon modes, as those observed in this experiment, may be involved in determining the superconducting properties of this compound. However, the importance of the observed soft phonons in determining T_c relative to that of the boron A_{1g} mode in the model[19] of Mattheis, Siegrist, and Cava cannot be presently ascertained without comparing the experimental results with detailed lattice dynamical calculations incorporating the electron phonon interaction.

The calculated[23] (without matrix elements) generalized electronic susceptibility of $LuNi_2B_2C$ along [ξ00] exhibits a pronounced peak close to G_1 due to a strong nesting feature of the Fermi surface of this compound. This nesting feature may be responsible for the observed incommensurate magnetic ordering wave vectors in the magnetic rare-earth nickel boride carbides. The same Fermi surface nesting feature may be responsible for the strong anomalies observed in the present experiment for the Δ_4 [ξ00] phonon modes close to G_1. Therefore, it appears that in the magnetic compounds of this family we may have the interesting situation where, due to

the nesting of the Fermi surface, phonon softening and magnetic ordering are competing to decrease the energy of the system. Therefore, the electron-phonon and RKKY interactions in the magnetic superconducting systems are extremely interesting and further experimental and theoretical investigations will be required to establish a detailed understanding of the low temperature properties of these materials. An experimental study of the phonon dispersion curves of $HoNi_2B_2C$ is presently in progress in this laboratory.

Acknowledgments

The authors are grateful to Professor W. Weber for communicating to us his preliminary lattice dynamical calculations that incorporate the effect of the electron phonon interaction. Ames Laboratory is operated by the U.S. Department of Energy by Iowa State University under Contract No. W-7405-Eng-82. This work was supported by the Director for Energy Research, Office of Basic Energy Sciences.

References

1. R. Nagarajan, C. Maxamundar, Z. Hossain, S. K. Dhar, K V. Golparrishnan, L. C. Gupta, C. Godart B. D. Padalia, and R. Vijazarahgavan, *Phys. Rev. Lett.* **72**, 274 (1994).
2. R. J. Cava, H. Takagi, H. W. Zandbergen, J. J. Krajewski, W. F. Peck, Jr., T. Siegrist, B. Batlogg, R. B. van Dover, R. J. Felder, K. Mizuhashi, J. O. Lee, H. Eisaki, and S. Uchida, *Nature* **367**, 252 (1994).
3. T. Siegrist, H. W. Zandbergen, R. J. Cava. J. J. Krajewski, and W. F. Peck, Jr., *Nature* **367**, 254 (1994).
4. R. Cava, H. Takagi, B. Batlogg, H. W. Zandbergen, J. J. Krajewski, W. F. Peck, Jr., R. B. van Dover, R. J. Felder, T. Siegrist, K. Mizuhashi, J. O. Lee, H. Eisaki, S. A. Cater, and S. Uchida, *Nature* **367**, 146 (1994).
5. H. Eisaki, H. Takagi, R. J. Cava, K. Mizuhashi, J. O. Lee, B. Batlogg, J. J. Krajewski, W. F. Peck, Jr., and S. Uchida, *Phys. Rev. B* **50**, 647 (1994).
6. B. K. Cho, P. C. Canfield, and D. C. Johnston, *Phys. Rev. B* (to be published).
7. P. Dervenagas, J. Zarestky, C. Stassis, A. I. Goldman, P. C. Canfield, B. K. Cho, *Physica B* **212**, 1 (1995).
8. G. K. Shenoy, B. D. Dunlap, and F. Y. Fradin (eds.), Proc. Int. Conf. on Ternary Superconductors (North-Holland, Amsterdam, 1981).

9. M. B. Maple and O. Fischer (eds.), Superconductivity in Ternary Compounds, Vols. I and II, Topics in Current Physics (Springer, Berlin, Heidelberg and New York, 1982).

10. S. K. Sinha, G. W. Crabtree, D. G. Hinks, and H. A. Mook, *Phys. Rev. Lett.* **48**, 950 (1982).

11. S. K. Sinha, H. A. Mook, O. A. Pringle, D. G. Hinks, in: Superconductivity in Magnetic and Exotic Materials; Proc. 6th Taniguchi Internat. Symp. Kashikojima, Japan, November 14-18, 1983, eds, T. Matsubara and A. Kotani, (Springer-Verlag, New York, 1984) pp. 14-28.

12. A. I. Goldman, C. Stassis. P. C. Canfield, J. Zarestky, P. Dervenagas, B. K. Cho, D. C. Johnston, and B. Sternlieb, *Phys. Rev. B* **50**, 9668 (1995).

13. T. E. Grigereit, J. W. Lynn, Q. Huang, A. Santoro, R. J. Cava, J. J. Krajewski, W. F. Peck, Jr., *Phys. Rev. Lett.* **73**, 2756 (1994).

14. J. Zarestky, C. Stassis, A. I. Goldman, P. C. Canfield, P. Dervenagas, B. K. Cho, and D. C. Johnston, *Phys. Rev. B* **51**, 678 (1995).

15. S. K. Sinha, J. W. Lynn, T. E. Grigereit, Z. Hossain, L. C. Gupta, R. Nagarajan, and C. Godart, *Phys. Rev. B* **51**, 681 (1995).

16. C. Detlefs, A. I. Goldman, J. P. Hill, D. Gibbs, C. Stassis, P. C. Canfield, and B. K. Cho (to be published).

17. W. E. Pickett and D. J. Singh, *Phys. Rev. Lett.* **72**, 3702 (1994).

18. L. F. Mattheiss, *Phys. Rev. B* **49**, 13,279 (1994).

19. R. Coehoorn, *Physica C* **228**, 5671 (1994).

20. L. F. Mattheiss, T. Siegrist, and R. J. Cava, *Sol. State Commun.* **91**, 587 (1994).

21. V. G. Hadjiev, L. N. Bozukov, M. G. Baychev, *Phys. Rev. B* **50**, 16,726 (1994).

22. H. Lee, H. Park, H. Shin, I. Yang, W. C. Lee, B. K. Cho, P. C. Canfield, and D. C. Johnston (to be published).

23. J. Y. Rhee, X. Wang, and B. N. Harmon, *Phys. Rev. B* **51**, 15,585 (1995). Inadvertently, incorrect k_z values for the Fermi surface cross-sections were listed in this reference. The correct k_z values are 0.0, 0.2, 0.35, and 0.45 in units of $2\pi/c$

24. M. Xu, P. C. Canfield, J. E. Ostenson, D. K. Finnemore, B. K. Cho, Z. R. Wang, and D. C. Johnston, *Physica C* **227**, 321 (1994).

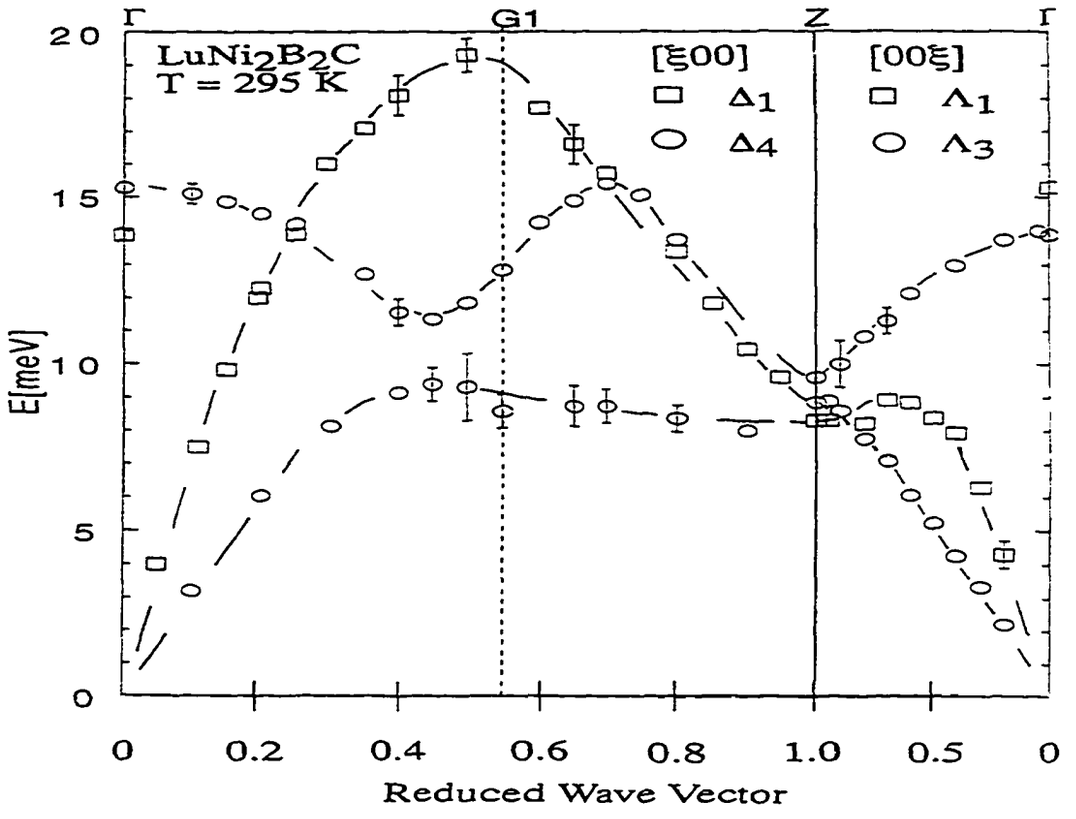

Figure 2.1: Room temperature acoustic and lowest lying optical phonon dispersion curves of $LuNi_2B_2C$ along the [ξ00] and [00ξ] symmetry directions. The lines are intended as guides to the eye. The size of the symbols is a measure of the estimated uncertainties in the measured frequencies.

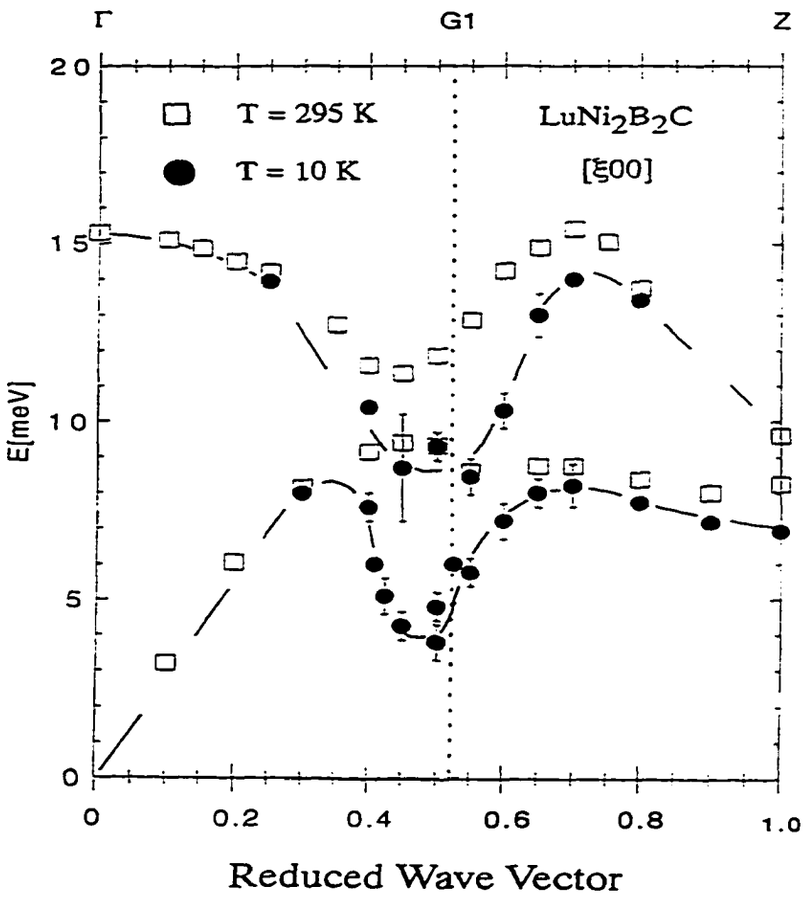

Figure 2.2: The Δ_4 [ξ00] branches at 295 K and 10 K. The lines through the 10 K points are intended as guides to the eye.

CHAPTER 3. PHONON MODE COUPLING IN SUPERCONDUCTING $LuNi_2B_2C$

A paper published in Physical Review B[1]

C. Stassis, M. Bullock, J. Zarestky, P. Canfield,

A. I Goldman

Ames Laboratory and Department of Physics and Astronomy

Iowa State University, Ames, IA 50011

G. Shirane and S. M. Shapiro

Brookhaven National Laboratory, Upton, NY 11973

Abstract

Recently, Kawano et al. reported that a new phonon-like excitation, localized in q and ω, appears below T_c in the superconducting compound YNi_2B_2C. This interesting observation led us to perform a series of new experiments on the previously studied $LuNi_2B_2C$ superconducting compound covering a large range of q and ω. We demonstrate that there is no new excitation and that the lowest lying excitations can be associated with the $\Delta_1[\xi 00]$ acoustic and optical phonon branches which exhibit pronounced dips at low

[1]Reprinted with permission from *Phys. Rev. B* **55** R8678 (1996).

temperatures for wavevectors close to the Fermi surface nesting vector, $\vec{\xi}_m$, characteristic of these compounds. Above T_c, as the temperature decreases the frequencies of both modes in the vicinity of $\vec{\xi}_m$ decrease and there is a shift of intensify from the upper to the lower mode, an effect characteristic of mode coupling. Below T_c, there is a dramatic decrease in the line width of the acoustic mode due to the opening of the superconducting gap.

Introduction

The rare-earth nickel boride carbides[1-4] (RNi_2B_2C; R=rare-earth) have very interesting properties. Their crystal structure,[3] body-centered tetragonal (space groups I4/mmm), resembles that of the high-T_c superconductors and consists of R-C layers separated by Ni_2B_2 sheets (typically $a \cong 3.5\text{Å}$ and $c \cong 3a$). Many of these compounds (R=Lu, Y, Tm, Er, Ho, Dy), including several containing magnetic rare-earth elements, have relatively high superconducting transition temperatures[2-6] ($T_c \cong 16.5\text{K}$ for the Lu, and $T_c \cong 15.5$ for the Y compound).

The magnetic structures of these compounds have been studied extensively by neutron and x-ray scattering techniques.[7] The superconducting Er[8,9] and Ho[10,11] compounds and the non-superconducting Tb[12] and Gd[13] compounds all order

in an incommensurate magnetic structure characterized by a propagation vector $\vec{\xi}_m=(\xi_m, 0, 0)$ with $\xi_m \cong 0.55$ for all of these compounds. This observation, and band theoretical calculations[14] of the generalized electronic susceptibility $\chi(\vec{q})$ of $LuNi_2B_2C$, led to the suggestion that a common Fermi surface nesting, characterized by a nesting vector $\vec{\xi}_m$, exists in these compounds and it is responsible for the ordering of the rare-earth moments via the RKKY mechanism. The existence of such a nesting suggested that strong Kohn anomalies should be observed in the dispersion curves of these compounds for wavevectors close to the nesting wavevectors $\vec{\xi}_m$. Recently, Dervenagas et al.[15] measured the phonon dispersion curves of the non-magnetic Lu compound ($T_c \cong 16.5K$) along the $[\xi 00]$ and $[00\ \zeta]$ symmetry directions. They found that indeed the frequencies of the lowest lying acoustic and optic $\Delta_4[\xi 00]$ near ξ_m decrease with decreasing temperature and exhibit strong dips at low temperatures.

More recently, Kawano et al.[16] studied the temperature dependence of the phonons close to ξ_m in the non-magnetic Y compound ($T_c \cong 15K$). They reported that at $\xi=0.525$ the frequency of the acoustic $\Delta_4[\xi 00]$ branch decrease with decreasing temperature, as in the case of the Lu compound, but that the frequency of the corresponding optical mode remain practically unchanged. In addition, they reported that a "new" peak appears below T_c at 4 meV and at the same

wavevector (ξ=0.525). This interesting observation led us to perform new experiments on $LuNi_2B_2C$ in order to understand the appearance of this new excitation.

The experiments were performed on a composite crystal consisting of two 4x4x0.5 mm^3 single crystals. The two crystals were oriented within 0.8 decrees on a single holder and placed in an He-gas filled aluminum can in a low temperature refrigerator capable of regulating the temperature between 3.5 and 300K better than ±0.1K. The crystal was mounted with the [010] direction perpendicular to the scattering plane and most measurements were made in the Brillouin zone centered at (0,0,8). The experiments were performed using the H-7 and H-8 triple-axis spectrometers at Brookhaven National Laboratory's High Flux Beam Reactor. Pyrolytic graphite (PG), reflecting from the (002) planes was used as monochromator and analyzer, and a 75mm thick PG filter was used after the sample to eliminate higher order contamination. Most of the data were collected using a fixed final neutron energy of 14.7meV and a collimation of 40-40-40-80 minutes of arc in the standard positions on the spectrometer.

In the present investigation we studied in detail the temperature dependence of the two lowest lying transverse-like acoustic and optical phonon branches propagating along the [ζ00] direction (Fig. 3.1). These two branches belong to

the same Δ_4 representation and, for small wavevectors, are purely transverse with atomic displacements along the c-axis; for the acoustic branch all atoms move in phase, whereas for the optical branch the motion of the Lu atoms is out of phase with that of the other atoms. For wavevectors well into the Brillouin zone the Lu and C displacements remain transverse while the Ni and B atoms develop a longitudinal component. Since the two modes belong to the same irreducible representation, they cannot cross in energy and, therefore must interact strongly. In fact, it can be seen (Fig. 3.1) that at room temperature these two branches approach each other and then are "repelled" near $\xi_m \equiv 0.5$. At this temperature the two modes are well separated at $\xi = 0.4$ (top panel of Fig. 3.2) but as ξ approaches ξ_m the two modes are so close in energy that it is difficult to resolve them. At ξ=0.475 the acoustic mode is barely visible as a shoulder near 9.0 meV (top panel of Fig. 3.2). As the temperature decreases the frequencies of both modes decrease (Fig. 3.2) and there is a shift of intensity from the upper to the lower mode, an effect characteristic of mode interaction. At 120K the ξ=0.475 optical mode is just a shoulder to the peak corresponding to the acoustic branch, almost a complete reversal from the room temperature spectrum. As the temperature is further decreased the frequencies of the modes close to ξ=0.5 continues to decrease as well as the transfer

of intensity from the upper to the lower mode. As a result already at 30K, well above T_c, only a broad peak is observed (see top panel of Fig. 3.3) and it is difficult to establish the energies of the individual acoustic and optical modes. This type of mode coupling is quite common and has been observed in compounds undergoing structural phase transitions.[17] The situation is more complicated for $LuNi_2B_2C$, since the observed pronounced phonon anomalies are due to the strong electron-phonon interaction via the nesting of the Fermi surface. The softening of these modes in the present case is due to the sharpening of the Fermi surface nesting feature as the temperature decreases. Anharmonic effects[17] may play some role as the compound approaches (but never achieves) a phase transformation at low temperatures.

At 15K, just below T_c, the spectrum is practically unchanged from that obtained at 30K. However as the temperature is further decreased below T_c a dramatic change in the spectrum is observed (lower panels of Figs. 3.2 and 3.3). The spectrum consists of a sharp peak at approximately 4.5 meV with a broad weak shoulder in the higher energy side. The position and width of the lower peak remain unchanged below approximately 14K and its peak intensity (Insert of Fig. 3.3) follows approximately the same temperature dependence as the excitation studied by Kawano et al.[14] The energy of this lower excitation varies continuously as ξ

varies from 0.4 to 0.6 between the energies observed at these points for the acoustic branch. Furthermore by measurements along the [00 ζ] direction we showed that the dispersion of this excitation is also continuous along a direction perpendicular to [ξ00] (Fig. 3.4). We therefore conclude that the lower mode must be associated with the Δ_4[ξ00] acoustic branch and the upper mode with the optical branch. In contrast to the situation above T_c, these two modes can be resolved at temperatures below T_c because of the dramatic decrease in the width of the acoustic mode. This change is due to the opening of the superconducting gap below T_c. The acoustic mode cannot decay by breaking Cooper pairs, since its energy is lower than the superconducting gap 2Δ, and therefore its lifetime is increased (line width narrowing) compared to that at temperatures above T_c. Similar behavior was observed[18, 19] many years ago in superconducting Nb and Nb_3Sn. The dispersion curves of the acoustic and optical modes below T_c (T=4.0K) is shown in the right hand side of Fig. 3.1. Notice the abrupt decrease in the energy of these modes in the vicinity of ξ=0.4 which makes it difficult to precisely determine the dispersion curves in this region.

In summary, in $LuNi_2B_2C$ we observe a unique case of phonon softening of two branches (one acoustic and one optic) which belong to the same (Δ_4) representation and therefore cannot cross in energy. Because of the strong electron-

phonon interaction these branches exhibit pronounced Kohn anomalies for wavevectors close to the Fermi surface nesting wavevector $\xi_m \cong (0.5,0,0)$. The energies of the modes with wavevectors close to ξ_m decrease with decreasing temperature and intensity is transferred from the higher to the lower in energy mode, a behavior typical of coupled modes. Already at temperatures above T_c these modes are so strongly coupled that the two peaks cannot anymore be resolved. At temperatures below T_c the peaks corresponding to these two modes can again be resolved because of the dramatic decrease in the width of the lower peak due to the opening of the superconducting gap. This interpretation is to be contrasted to the "localized - q" picture[21] of Kawano et al[16] based on the assumption that a new excitation appears below T_c. Finally, we should point out that it appears that the opening of the superconducting gap does not affect appreciably the Fermi surface nesting in this compound as one would have expected.[20] Actually, it is difficult to say at this stage whether there is a change in the frequencies or line widths of the peaks as the temperature is decreased below T_c. A preliminary analysis of the data based on the formulae[17] used to analyze the corresponding case in ferroelectrics indicates that there is an additional softening of the branches as the temperature is decreased below T_c. Further analysis of the data and new

experiments are presently underway to study this and other features of these modes in the vicinity of T_c.

We thank H. Kawano for sending us her unpublished data and informative discussions. Ames Laboratory is operated for the DOE by Iowa State University under Contract No. W-7405-ENG-82. The work at Brookhaven National Laboratory was supported by the Department of Energy, Division of Materials Sciences under Contract No. DE-AC02-76CH00016.

References

1. R. Nagarajan, C. Mazumdar, Z. Hossain, S.K. Dhar, K. V. Gopalakrishnan, L. C. Gupta, C. Godar, T. B. D. Padalia, and R. Vijayaraghavan, *Phys. Rev. Lett.* **72**, 274 (1994).
2. R. J. Cava, H. Takagi, H. W. Zandbergen, J. J. Krajewski, W. F. Peck, Jr., T. Siegrist, B. Batlogg, R. B. van Dover, R. J. Felder, K. Mizuhashi, J. O. Lee, H. Eisaki, and S. Uchida, *Nature* **367**, 252 (1994).
3. T. Siegrist, H. W. Zandbergen, R. J. Cava, J. J. Krajewski, and W. F. Peck, Jr., *Nature* **367**, 254 (1994).
4. R. Cava, H. Takagi, B. Batlogg, H. W. Zandbergen, J. J. Krajewski, W. F. Peck, Jr., R. B. van Dover, R. J. Felder, T. Siegrist, K. Mizuhashi, J. O. Lee, H. Eisaki, S. A. Cater, and S. Uchida, *Nature* **367**, 146 (1994).

5. H. Eisaki, H. Takagi, R. J. Kaura, K. Mizuhashi, J. O. Lee, B. Batlogg, J. J. Krajewski, W. F. Peck, Jr., and S. Uchida, *Phys. Rev. B* **50**, 647 (1994).

6. B. K. Cho, P. C. Canfield, and D. C. Johnston, *Phys. Rev. B* **52**, R3844 (1995).

7. C. Stassis and A. I. Goldman in Proceedings of Twenty First Rare Earth Conference, Duluth, Minnesota (1996) (to be published).

8. J. Zarestky, C. Stassis, A. I. Goldman, P. C. Canfield, P. Dervenagas, B. K. Cho, and D. C. Johnston, *Phys. Rev. B* **51**, 678 (1995).

9. S. K. Sinha, J. W. Lynn, T. E. Grigereit, Z. Hossain, L. C. Gupta, R. Nagarajan, and C. Godart, *Phys. Rev. B* **51**, 681 (1995).

10. A. I. Goldman, C. Stassis, P. C. Canfield, J. Zarestky, P. Dervenagas, B. K. Cho, D. C. Johnston, *Phys. Rev. B* **50** 9668 (1994).

11. T. Vogt, A. Goldman, B. Sternlieb, and C. Stassis, *Phys. Rev. Lett.* **75**, 2628 (1995).

12. P. Dervenagas, J. Zarestky, C. Stassis, A. I. Goldman, P. C. Canfield, B. K. Cho, *Phys. Rev. B* **53,** 8506 (1996).

13. C. Detlefs, A. I. Goldman, C. Stassis, P. Canfield, B. K. Cho, J. P. Hill, D. Gibbs, *Phys. Rev. B* **53**, 6355 (1996).

14. J. Y. Rhee, X. Wang, and B. N. Harmon, *Phys. Rev. B* **51**, 15, 585 (1995).

15. P. Dervenagas, M. Bullock, J. Zarestky, P. Canfield, B. K. Cho, B. Harmon, A. I. Goldman, C. Stassis *Phys. Rev. B* **52**, 9839 (1995).

16. K. Kawano, H. Yoshizawa, H. Takeya and K. Kadownki, *Phys. Rev. Lett.* (to be published).

17. J. Harada, J. D. Axe, G. Shirane, *Phys. Rev. B* **4**, 155 (1971).

18. J. D. Axe and G. Shirane, *Phys. Rev. Lett.* **30**, 214 (1973); *Phys. Rev. B* **8**, 1965 (1973).

19. M. Shapiro, G. Shirane, J. D. Axe, *Phys. Rev. B*, **12**, 4899 (1975).

20. See for instance T. V. Ramakrishnan and C. M. Varma, *Phys. Rev. B*, **24**, 137 (1981).

21. We understood "localized" as a narrow range of q between 0.5 and 0.55. Recently we were informed by Dr. Kawano that the word localized is used as an isolated, not as a narrow q branch.

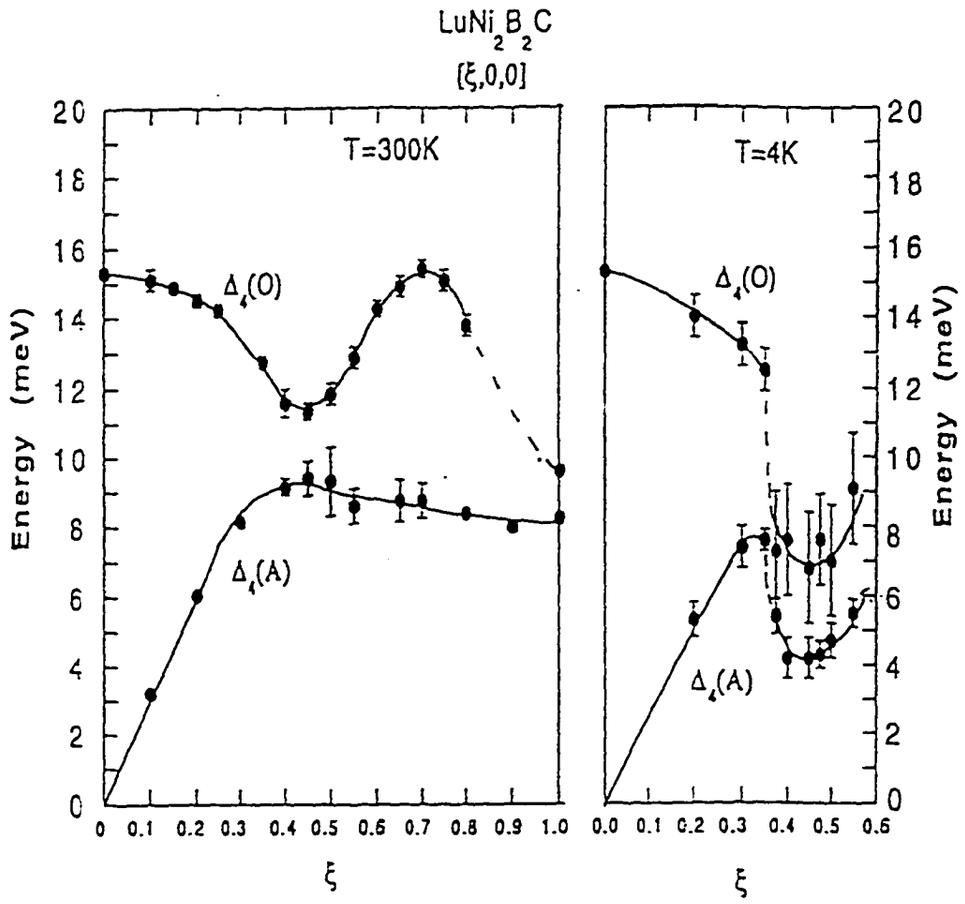

Fig. 3.1: Dispersion of the $\Delta_1[\xi 00]$ acoustic and optical branches at room temperature and 4.2K.

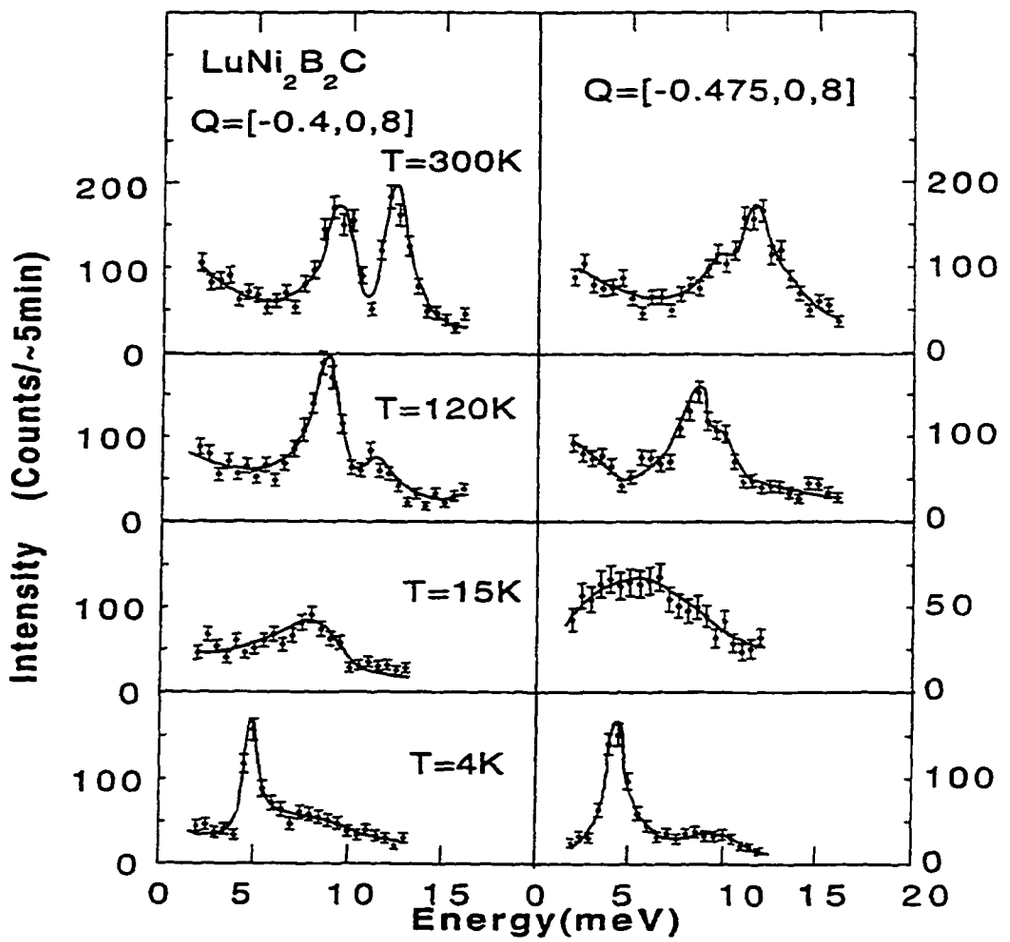

Fig. 3.2: The ξ=0.4 and ξ=0.475 spectra at some selected temperatures.

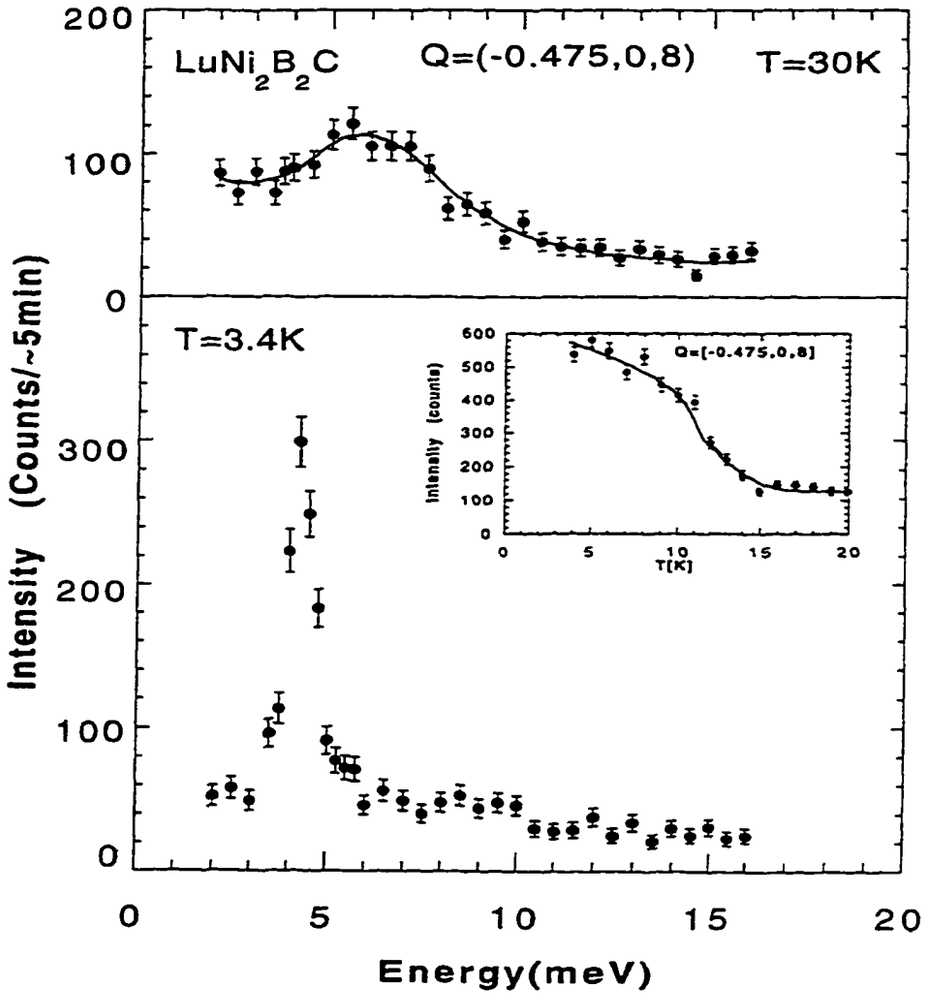

Fig. 3.3: The ξ=0.475 spectra at 30 and 3.4K. The temperature dependence of the intensity of this acoustic mode below T_c is given in the inset.

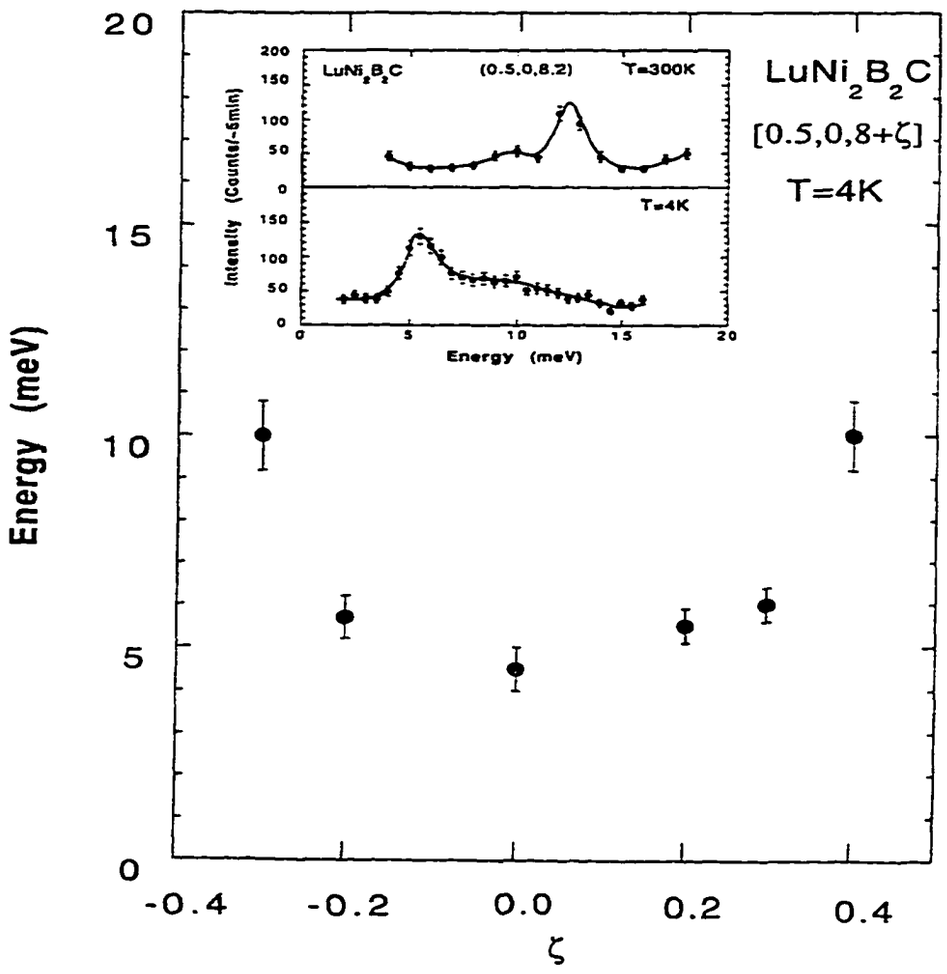

Fig. 3.4: ζ dependence of the (0.5, 0, 8 +ζ) mode. The inset shows the softening of the (0.5, 0, 8.2) mode between 300 and 4K (see text).

CHAPTER 4. LOW-ENERGY PHONON EXCITATIONS IN SUPERCONDUCTING $RENi_2B_2C$ (RE=Lu, Y)

A paper submitted to Physical Review B

M. Bullock, J. Zarestky, C. Stassis, A. Goldman, P. Canfield
Ames Laboratory and Department of Physics and Astronomy
Iowa State University, Ames, IA 50011

Zentaro Honda and Gen Shirane*
The Institute of Physical and Chemical Research (RIKEN),
Wako, Saitama 351-01, Japan

S. M. Shapiro
Brookhaven National Laboratory
Upton, NY 11973-5000

Abstract

Inelastic neutron scattering techniques have been used to study the low energy phonon excitations in superconducting $RENi_2B_2C$ (RE=Lu, Y) to further characterize the anomalous features observed by Kawano et al. (*Phys. Rev. Lett.*, **77**, 4628 (1996)) for RE=Y and Stassis et al. (*Phys. Rev. B*, **55**, R8678 (1997)) for RE=Lu, when these systems enter the superconducting ground state. We find that above T_c the

frequencies of the $\Delta_4[\xi 00]$ lowest-lying acoustic and optic phonon modes decrease with decreasing temperature, for $\vec{\xi}$ close to the nesting vector $\vec{\xi}_m$. In addition there is a shift of intensity from the upper to the lower mode, an effect characteristic of mode coupling. The observed intensity transfer between these modes above T_c can be described satisfactorily in both compounds by a coupled-mode model. Below T_c the observed spectrum changes dramatically: it consists of a sharp peak at approximately 4 meV with a broad weak shoulder at higher energies. The experimental results unambiguously show that this dramatic change is due to the onset of superconductivity in these compounds. In this temperature region, the results are in qualitative agreement with recent theoretical calculations.

Introduction

The physical properties of the rare-earth nickel boride carbides ($RENi_2B_2C$; RE = rare earth) are of considerable interest.[1-4] Their crystal structure[3] is body-centered tetragonal (space group I4/mmm), with $a \cong 3.5\text{Å}$ and $c \cong 3a$, and consists of RE-C layers separated by Ni_2B_2 sheets. Many of these compounds are superconductors with relatively high superconducting temperatures. Among these superconductors, the non-magnetic Lu and Y compounds exhibit[2-5] the highest

superconducting temperatures, 16.5K and 15.5K, respectively. Of particular interest is that in several of these compounds (RE=Tm, Ho, Er, and Dy) superconductivity coexists with magnetic order.[2-7]

To obtain some insight into the subtle interplay between superconductivity and magnetism, the magnetic structures of these compounds have been studied extensively by neutron and x-ray scattering techniques on both single crystal and powder specimens.[3,9] Of particular relevance to the present study is that the superconducting Er[10,11] and Ho[12,13] compounds as well as the non-superconducting Tb[14] and Gd[15] compounds all order in an incommensurate magnetic structure characterized by a propagation vector $\vec{\xi}_m = (\xi_m, 0, 0)$, with $\xi_m \cong 0.55$ for all of these compounds. This observation is particularly important, since band theoretical calculations[16] of the generalized electronic susceptibility of $LuNi_2B_2C$ show that there is strong Fermi surface nesting in this compound with a nesting vector close to $\vec{\xi}_m$. These results indicate that there is a common Fermi surface nesting in these compounds, characterized by a nesting vector $\vec{\xi}_m$, which is responsible for the ordering of the rare-earth moments via the RKKY mechanism. The existence of such a nesting suggests that strong Kohn anomalies should be observed in the dispersion curves of these compounds for wave vectors close to $\vec{\xi}_m$. In addition, electronic band structure calculations[17-20] suggest

that these materials are conventional superconductors with relatively high electronic density of states at the Fermi level, E_F, and that there is a complex set of bands crossing E_F which are strongly coupled to the phonons and may be responsible for the superconducting properties of these compounds. Therefore, it appears that this family of compounds is ideal for the study of the subtle competition between lattice instabilities, superconductivity, and magnetic ordering.

Dervenagas et al.[21] measured the low-lying phonon dispersion curves of the Lu compound ($T_C \cong 16.5K$) along the $[\xi 00]$ and $[00\zeta]$ symmetry directions and they found that the frequencies of the lowest lying modes near $\vec{\xi}_m$ decrease with decreasing temperature and, as a result, the corresponding branches exhibit strong dips in the vicinity of this point at low temperatures. A similar study in the isomorphous Y compound was performed by Kawano et al.[22] The softening of these modes is so significant that it was observed in phonon-density of states measurements by Gompf et al.[23] as well as in the point-contact spectra of these compounds by Yanson et al.[24] In addition Kawano et al.[22] performed a detailed study of the low-lying excitations in the Y compound as a function of temperature and magnetic field. They observed a dramatic change in the spectrum associated with the onset of superconductivity which includes a sharp feature at

approximately 4 meV which they attributed to a "new" excitation. This interesting observation led us to perform a systematic study of these excitations as a function of temperature on the Lu and Y compounds. We already presented a brief account.[25] of the results obtained in the experiments on the Lu compound. In this paper we present a more detailed account of these experiments as well as a comparison of the Lu and Y compound.

Experimental Details

The single crystals of $LuNi_2B_2C$ and YNi_2B_2C used in the present experiment were grown at the Ames laboratory by the high-temperature flux technique as described elsewhere.[26] The as grown crystals are platelets with the c-axis perpendicular to their flat surface. Since the size of the crystals is relatively small (approximately 5 X 5 X $0.5mm^3$) for inelastic neutron scattering, most of the measurements on $LuNi_2B_2C$ were performed on a composite crystal, consisting of two crystals (mounted on a single holder) oriented to within 0.8 degrees. Since the effect of the misorientation of the two $LuNi_2B_2C$ crystals is most pronounced for ξ between 0.375 and 0.425, where the abrupt decrease in the phonon frequencies occurs (see Fig. 1, Ref. 21), measurements in this region were performed with only one of the two $LuNi_2B_2C$

crystals. All measurements on YNi_2B_2C were performed on a single crystal of this compound.

The measurements between 300 and 3.5K were performed with the crystal placed in an He-gas filled aluminum can in a low temperature refrigerator capable of regulating the temperature in this region to within 0.1K. The measurements on the YNi_2B_2C compound were extended up to 485K and for these measurements the crystal was mounted in a high temperature furnace. For all measurements on these compounds the crystal was mounted with the [010] crystallographic direction perpendicular to the scattering plane.

The neutron scattering experiments were performed using the variable incident neutron energy triple-axis spectrometers H-7 and H-8 at Brookhaven National Laboratory's High Flux Beam Reactor and the constant incident neutron energy (14.7 meV) HB1A triple-axis spectrometer at the Oak Ridge National Laboratory's High Flux Isotope Reactor. Pyrolitic graphite (PG), reflecting from the (002) planes, was used as monochromator and analyzer and a PG filter was used to eliminate higher order contamination. On the H-7 and H-8 spectrometers most of the data were collected using a fixed final neutron energy of 14.7 meV. The HB1A constant incident energy spectrometer was mainly used to study the temperature dependence (between 150K and 485K) of the low-lying modes, in the vicinity of $\vec{\xi}_m$, of the YNi_2B_2C compound.

Most of the data were collected with a collimation of 40-40-40-80 minutes of arc in the standard positions on the spectrometers.

Experimental Results and Discussion

The phonon modes with frequencies below approximately 40 meV were studied systematically on the $LuNi_2B_2C$ compound at room temperature.[21, 27] Less extensive measurements were also made on the Y compound. The measured phonon frequencies were assigned to the various branches by comparing the measured intensities with calculations based on Born-von Kármán force-constant models. In the present investigation we studied in detail the temperature dependence of the $[\xi 00]$ acoustic and lowest lying optic branches of $LuNi_2B_2C$ and YNi_2B_2C in the vicinity of the nesting vector $\vec{\xi}_m$, which is close to the zone boundary point $G_1\left(a\iota\frac{\pi}{a}(1+\frac{d^2}{c^2})\right)$ along this direction. By symmetry, the $[\xi 00]$ acoustic branch belongs to Δ_4 representation. Based on the analysis of the data using Born-von Kármán models, the lowest lying optical branch along this direction was also assigned to the Δ_4 representation. No other branches of the same symmetry are close to these two branches. These calculations show that

for small wave vectors these branches are purely transverse with atomic displacements parallel to the c-axis; the displacements for all atoms in the acoustic modes are, of course, in phase, whereas in the optic modes the motion of the Lu atoms is out of phase with that of the other atoms. For larger wave-vectors the displacements of the Lu and C atoms remain transverse but the Ni and B atoms develop a longitudinal component.

The temperature dependence of the two lowest lying Δ_4 modes were studied by measurements in the Brillouin zones centered at (0,0,8) and (1,0,7). Figure 4.1 shows the dispersion of the Δ_4 optic (O) and acoustic (A) modes in the Lu and Y compounds at room temperature. The mass of Lu being nearly twice as large as that of Y, the energies of the modes are lower in $LuNi_2B_2C$ than in YNi_2B_2C. For $\xi<\xi_m$, both modes of the Lu compound are observed by measurements in the (008) Brillouin zone, whereas in the Y compound the optical mode is more easily observed by measurements in the (107) Brillouin zone. For $\xi>\xi_m$ the intensity of the acoustic and optical mode in the Lu and Y compounds, respectively, are very weak, and this is indicated by dotted lines in Fig. 4.1. In the vicinity of $\xi=\xi_m$, measurements in the (008) zone on the Y compound show, in addition to the acoustic mode, a peak at approximately 14 meV which was also observed by Kawano et

al.[22] and could be assigned to the optical branch (see discussion below).

Figure 4.2 shows the spectra of the interacting optic and acoustic mode in the vicinity of ξ_m at temperatures much higher than T_c. In the Y compound it is necessary to perform measurements at temperatures higher than room temperature in order to see clearly the mode interaction. At these high temperatures the optic mode (higher frequency mode) in both compounds is more intense than the acoustic mode. As T decreases the energy of the modes decrease and there is a transfer of intensity from the optic to the acoustic mode. For T< 150K the two modes cannot be resolved and a broad feature is observed in the Lu compound. In the Y compound, a small peak at approximately 14 meV can be seen at temperatures below 150K (see lowest panel of Fig. 4.2b). As we mentioned earlier, this small peak was observed also by measurements in the (008) zone in the present experiments as well as those by Kawano et al.[22] The intensity of this peak at 150K is, however, approximately 60% lower than that expected from the intensity at 295K (see Fig. 4.2b). We believe that this peak is either the remnant of the optical mode or belongs to the Δ_1 representation, a possibility indicated by Born-von Kármán calculations.

The observed mode behavior above T_c both compounds is quite similar to that observed in materials with soft optic

modes interacting with acoustic modes of the same symmetry. In the latter case their anticrossing behavior was formulated as a problem of mode coupling via anharmonic forces.[27,28] The scattered neutron intensity in the coupled-mode problem is given by formula A.1 of the Appendix, and the effect of mode coupling for two different coupling constants is shown in Fig. 4.A.1. The first three top panels of Fig. 4.3 compare the spectra calculated using this simple model (see Appendix) with the observed spectra of $LuNi_2B_2C$ at temperatures well above T_c. In these calculations (see formula A1 of the Appendix) the inelastic structure factors ($F_{1,2}$) of the two modes and the coupling constant (λ) are kept constant and only the linewidths (Γ_1,Γ_2) and frequencies (Ω_1,Ω_2) are adjusted to fit the experimental data. The left panels compare the measured and calculated spectra at (0.45, 0, 8) and the right panels those at (0.45, 0, 8.4) obtained for ζ=0.4 along a direction ([00 ζ]) which is perpendicular to [ξ00]. For $T>T_c$ the model provides an adequate fit to the data in both cases. In particular it reproduces the merging of the two peaks at T=60K for the (0.45, 0, 8) mode as well as the two distinct peaks observed at (0.45, 0, 8.4) at all temperatures above T_c. It is probably of some interest to notice that the drastic change in the spectra occurring at temperature below T_c (see below) can be simulated in this simple model by a change in the width ($\Gamma_{1,2}$) of the two

interacting modes, (this change being the largest for ζ=0) as shown in the lowest panels of Fig. 4.3. We would like to emphasize that the calculated curves in the lowest panels of Fig. 4.3 are not fits to the data, since below T_c no meaningful fits can be obtained (because of the large number of parameters involved); they were obtained by making appropriate choices for the widths, ($\Gamma_{1,2}$), so that these curves resemble the experimental profiles. It should also be pointed out that even above T_c the actual situation is much more complicated than the coupled-mode model, since the observed phonon anomalies in the Lu and Y compounds are due to the strong electron-phonon interaction via the nesting of the Fermi surface. As a result, the softening of these modes in the present case is mainly due to the sharpening of the Fermi surface nesting feature as the temperature decreases. In addition, anharmonic effects may play some role as the compounds approach (but never achieve) a phase transformation at low temperatures.

As the temperature decreases below T_C, a spectacular change in the spectra is observed as was first reported by Kawano et al.[22] for YNi_2B_2C and Stassis et al.[25] for $LuNi_2B_2C$. Figure 4.4 shows our measurements on both compounds measured in the vicinity of T_C and well below T_C. In the vicinity of T_c, the Δ_4 optical and acoustic modes cannot be resolved and only a relatively broad feature is

observed (See Fig. 4.4). Well below T_C the spectra are remarkably different. They consist of a sharp peak at approximately 4.5 meV with a weak shoulder at the higher energy side. Figure 4.5 illustrates the behavior of this sharp peak in $LuNi_2B_2C$ as a function of temperature (Fig. 4.5a) and ξ measured along [ξ00] (Fig. 4.5b). The width and position of this sharp peak remain practically unchanged below T_C, its intensity decreases with increasing temperature, and it is practically indistinguishable from the background at a temperature close to T_C (Fig. 4.5a). Although the full width at half maximum (FWHM) of this peak remains practically unchanged for ξ between 0.4 and 0.55, its intensity is maximum in the vicinity of ξ=0.475 (Fig. 4.5b). The energy of this sharp lower mode is minimum at approximately this wave vector (ξ=0.475), and varies continuously with ξ between 0.4 and 0.6 between the energies observed at ξ=0.4 and ξ=0.6 for the Δ_4 acoustic branch. Figure 4.6 compares the dispersion along the [00ζ] direction of the sharp peak and weak shoulder observed at low temperatures (right panel) with that of the Δ_4 modes at room temperature (left panel). The energies of the modes observed at 4K (right panel) vary continuously with ζ, and as ζ increases the shoulder at the high energy side becomes more well defined and, as a result, the two modes are clearly visible (Fig. 4.3). In particular, the study of the ζ

dependence of the phonon modes clearly demonstrates that the single unresolved peak obtained, after the merging of the optical and acoustic modes, consists indeed of two phonon modes down to temperatures close to T_c (see third panel from top of Fig. 4.3). From this continuity of the modes we conclude that the sharp peak must be associated with the acoustic mode and the barely visible shoulder with the optical mode. Notice (Fig. 4.6) that between 300K and 4K the energies of both modes decrease by almost a factor of two. The interpretation presented here is different from that proposed by Kawano et al.[22] who associated the sharp peak observed at low temperatures with a "new" phonon-like excitation which appears below T_c.

The experimental results clearly show that the origin of the dramatic change in the phonon spectra is the onset of superconductivity in these compounds. One of the direct effects of the superconducting gap opening is well understood and has been observed[29,30] many years ago in superconducting Nb and Nb_3Sn. A phonon mode with energy lower than the superconducting gap 2Δ cannot decay by breaking Cooper pairs and therefore its lifetime is increased (line width narrowing) compared to its lifetime above T_C. In addition, because of the singularity at $\omega \cong 2\Delta$ in the polarizability of superconducting electrons, there is a shift in the phonon frequencies as well as a change in the phonon spectra as the

temperature is decreased below T_c.[31-33] Both the energy shifts and the phonon shapes depend on the position of the normal phonon frequency, ω_n, with respect to the superconducting gap 2Δ. It is interesting to note that for normal phonon frequencies close to $2\Delta(T)$ phonon shapes similar to the ones observed in the present experiment have been predicted.[31,32] Actually, recent calculations by Allen et al.[33] yield phonon spectra almost identical to the low temperature spectra shown in Fig. 4.4.

The above theoretical approaches[31-33] are independent of the phonon wave vector whereas in the present experiments the anomalous phonon behavior is observed for phonon wave vectors close to the nesting vector $\vec{\xi}_m$. Recently, however, Kee and Varma[34] found that the electronic polarizability for an extremum vector of the Fermi surface exhibits a pole for frequencies close to 2Δ. For a phonon with normal state frequency above 2Δ this leads to a delta function at ω slightly below 2Δ and a peak centered around the normal state phonon frequency. Their spectra (see Fig. 2 of Ref. 34) when convoluted with the instrumental resolution are similar to those observed below T_c in the present experiments. The frequency of the observed sharp peak, on the other hand, does not follow the BCS temperature dependence of the superconducting gap as the Kee-Varma theory[34] predicts. Also it should be pointed out that the theory assumes that the

opening of the superconducting gap does not affect appreciably the Fermi surface nesting in these compounds as one would have expected.[35]

In summary, in both compounds we observe a case of phonon softening of two branches, one acoustic and one optic, which belong to the same representation and therefore cannot cross by symmetry. Above T_C the observed anticrossing behavior of these branches is similar to a coupled-mode problem, and such a model gives a satisfactory explanation of the observed phonon profiles. Below T_C, the dramatic change in the observed spectra can be qualitatively understood in terms of the well known line width-narrowing and frequency shift associated with the opening of the superconducting gap[31-34]. More experimental and theoretical work is necessary, however, to relate the observed temperature dependence of the lowest lying mode to the superconducting properties of these compounds.

Appendix

The temperature dependent behavior of the phonon modes of two branches which cannot cross by symmetry can be modeled as a mode-coupling problem by attributing the observed temperature dependence to anharmonic forces. The most convenient, for our purpose, formulation of the problem of

two phonon modes interacting via anharmonic forces is that given by Harada et al.[28] which was used to explain the asymmetric phonon profiles observed in ferroelectric $BaTiO_3$. The intensity distribution for two interacting modes, with frequencies Ω_1, Ω_2 and widths Γ_1, Γ_2, is given, for neutron energy loss, by

$$I \sim (n(\omega)+1)\frac{\omega}{\left(A^2+\omega^2B^2\right)}\left\{\left[\left(\Omega_2^2-\omega^2\right)B-\Gamma_2 A\right]F_1^2+2\lambda BF_1F_2+\left[\left(\Omega_1^2-\omega^2\right)B-\Gamma_1 A\right]F_2^2\right\} \qquad (A1)$$

where

$$A = (\Omega_1{}^2-\omega^2)(\Omega_2{}^2-\omega^2) - \omega^2\Gamma_1\Gamma_2$$

$$B = \Gamma_1(\Omega_2{}^2-\omega^2) + \Gamma_2(\Omega_1{}^2-\omega^2) .$$

In formula A1,

$$n(\omega) = \{\exp(\omega/kT) - 1\}^{-1},$$

$F_{1,2}$ are the structure factors of mode 1 and 2, and λ is the coupling strength between the two modes.

Figure 4.A1 (a) shows the calculated spectra, at 300K, of two coupled modes for the case $\lambda=0$ (no coupling) and $\lambda=10$. The two modes were taken to be well separated in energy and with line widths much smaller than their energies. The inelastic structure factors were appropriately chosen in order to make the intensities of the two modes almost equal in the absence of coupling ($\lambda=0$). As the coupling is turned on ($\lambda=10$), there is considerable transfer of intensity from

the upper to the lower mode. Since such transfer of intensity between modes is observed for $T>T_C$ in both the Y and Lu compounds (Fig. 4.2), it is clear that this simple coupled-mode model can be used to simulate the behavior of the Δ_4 modes above T_C. Figure 4.3 shows that this is indeed the case.

Figure 4.A1(b) shows that, by choosing the energies and widths so that there is considerable overlapping of the two modes, one can obtain spectra qualitatively similar to those observed in both the Y and Lu compounds at temperatures below T_C (Fig. 4.4). The onset of superconductivity can therefore be simulated in this model by a change in the widths of the two interacting modes. Notice, however, that this change in the widths may be quite large (see Fig. 4.3).

Acknowledgments

The authors are grateful to Drs. C. Varma, P. Allen, and S. K. Sinha for many stimulating discussions. Ames Laboratory is operated by the U.S. Department of Energy by Iowa State University under Contract No. W-7405-Eng-82. The work at Brookhaven National Laboratory was supported by the Department of Energy, Division of Materials Sciences under

Contract No. DE-AC02-76CH00016. Some of the experiments were performed at Oak Ridge National Laboratory which is supported by the Department of Energy, Division of Materials Sciences under Contract No.DE-AC05-96OR22464.

References

*Present address: Brookhaven National Laboratory, Physics Dept., Bldg. 510B, P. O. Box 5000, Upton, NY 11973-5000.

1. R. Nagarajan, C. Maxamundar, Z. Hossain, S. K. Dhar, K V. Golparrishnan, L. C. Gupta, C. Godart, B. D. Padalia, and R. Vijazarahgavan, *Phys. Rev. Lett.* **72**, 274 (1994).
2. R. J. Cava, H. Takagi, H. W. Zandbergen, J. J. Krajewski, W. F. Peck, Jr., T. Siegrist, B. Batlogg, R. B. van Dover, R. J. Felder, K. Mizuhashi, J. O. Lee, H. Eisaki, and S. Uchida, *Nature* **367**, 252 (1994).
3. T. Siegrist, H. W. Zandbergen, R. J. Cava, J. J. Krajewski, and W. F. Peck, Jr., *Nature* **367**, 254 (1994).
4. R. Cava, H. Takagi, B. Batlogg, H. W. Zandbergen, J. J. Krajewski, W. F. Peck, Jr., R. B. van Dover, R. J. Felder, T. Siegrist, K. Mizuhashi, J. O. Lee, H. Eisaki, S. A. Cater, and S. Uchida, *Nature* **367**, 146 (1994).
5. H. Eisaki, H. Takagi, R. J. Cava, K. Mizuhashi, J. O. Lee, B. Batlogg, J. J. Krajewski, W. F. Peck, Jr., and S. Uchida, *Phys. Rev. B* **50**, 647 (1994).

6. B. K. Cho, P. C. Canfield, and D. C. Johnston, *Phys. Rev. B* **52**, 3844 (1997).

7. P. Dervenagas, J. Zarestky, C. Stassis, A. I. Goldman, P. C. Canfield, B. K. Cho, *Physica B* **212**, 1 (1995).

8. C. Stassis and A. Goldman, *J. Alloys and Comp.* **250**, 603 (1997).

9. J. Lynn, *J. Alloys and Comp.* **250**, 552 (1997).

10. J. Zarestky, C. Stassis, A. I. Goldman, P. C. Canfield, P. Dervenagas, B. K. Cho, and D. C. Johnston, *Phys. Rev. B* **51**, 678 (1995).

11. S. K. Sinha, J. W. Lynn, T. E. Grigereit, Z. Hossain, L. C. Gupta, R. Nagarajan, and C. Godart, *Phys. Rev. B* **51**, 681 (1995).

12. A. I. Goldman, C. Stassis, P. C. Canfield, J. Zarestky, P. Dervenagas, B. K. Cho, D. C. Johnston, *Phys. Rev. B* **50** 9668 (1994).

13. T. Vogt, A. Goldman, B. Sternlieb, and C. Stassis, *Phys. Rev. Lett.* **75**, 2628 (1995).

14. P. Dervenagas, J. Zarestky, C. Stassis, A. I. Goldman, P. C. Canfield, B. K. Cho, *Phys. Rev. B* **53,** 8506 (1996).

15. C. Detlefs, A. I. Goldman, C. Stassis, P. Canfield, B. K. Cho, J. P. Hill, D. Gibbs, *Phys. Rev. B* **53**, 6355 (1996).

16. J. Y. Rhee, X. Wang, and B. N. Harmon, *Phys. Rev. B* **51**, 15585 (1995).

17. W. E. Pickett and D. J. Singh, *Phys. Rev. Lett.* **72**, 3702 (1994).

18. L. F. Mattheiss, *Phys. Rev. B* **49**, 13279 (1994).

19. R. Coehoorn, *Physica C* **228**, 5671 (1994).

20. L. F. Mattheiss, T. Siegrist, and R. J. Cava, *Sol. State Commun.* **91**, 587 (1994).

21. P. Dervenagas, J. Zarestky, C. Stassis, A. I. Goldman, P. C. Canfield, B. K. Cho, *Phys. Rev. B* **53,** 8506 (1996).

22. K. Kawano, H. Yoshizawa, H. Takeya, and K. Kadownki, *Phys. Rev. Lett.* **77**, 4628 (1996)

23. F. Gompf, W. Reichardt, H. Schober, B. Renker, and M. Bchgeister, *Phys. Rev. B* **55**, 9058 (1997).

24. I. K. Yanson, V. V. Fisun, A. G. M. Jansen, P. Wyder, P. C. Canfield, B. K. Cho, C. V. Tomy, and D. McK. Paul, *Phys. Rev. Lett.* **28**, 935 (1997).

25. C. Stassis, M. Bullock, J. Zarestky, P. Canfield, A. Goldman, G. Shirane, S. M. Shaprio, *Phys. Rev. B* (Rapid Communications) **55**, 8678 (1997).

26. M. Xu, P. C. Canfield, J. E. Ostenson, D. K. Finnemore, B. K. Cho, Z. R. Wang, and D. C. Johnston, *Physica C* **227**, 321 (1994).

27. J. D. Axe, J. Harada, G. Shirane, *Phys. Rev. B* **1**, 1227 (1970).

28. J. Harada, J. D. Axe, G. Shirane, *Phys. Rev. B* **4**, 155 (1971).

29. J. D. Axe and G. Shirane, *Phys. Rev. Lett.* **30**, 214 (1973); *Phys. Rev. B* **8**, 1965 (1973).

30. S. M. Shapiro, G. Shirane, J. D. Axe, *Phys. Rev. B* **12**, 4899 (1975).

31. H. G. Schuster, *Solid State Comm.* **13**, 1559 (1973).

32. R. Zeyher and G. Zwicknagl, *Z. Phys. B* **78**, 175 (1990).

33. P. B. Allen, V. N. Kostur, N. Takesue and G. Shirane *Phys Rev. B* **56**, 5552 (1997).

34. H.-Y. Kee and C. M. Varma (in press).

35. See, for instance, T. V. Ramakrishnan and C. M. Varma, *Phys. Rev. B* **24**, 137 (1981).

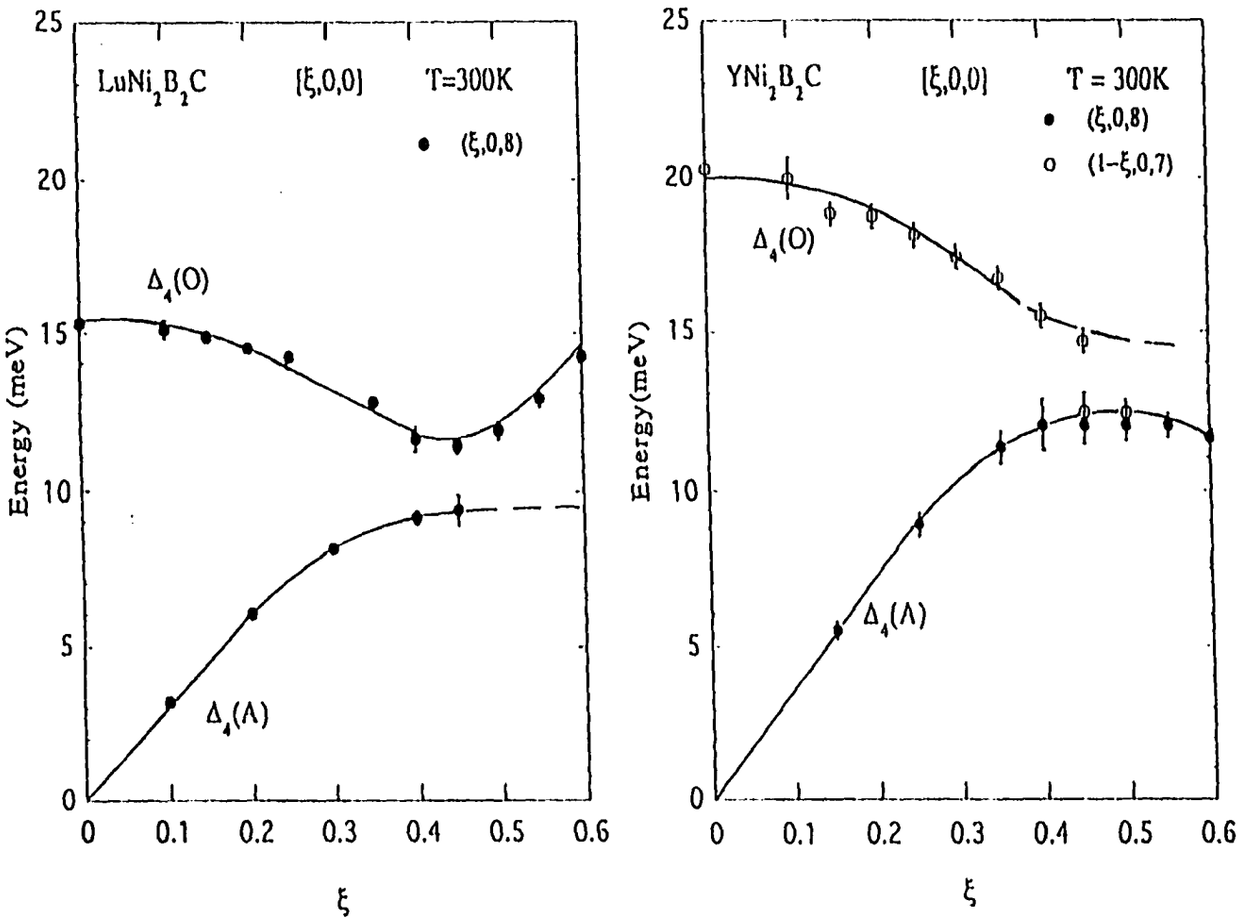

Fig. 4.1: Phonon dispersion of the two low lying Δ_4 acoustic (A) and optic (O) branches measured, at 300K, along the [ξ00] direction for $LuNi_2B_2C$ (left) and YNi_2B_2C (right). The lines are used as a guide to the eye.

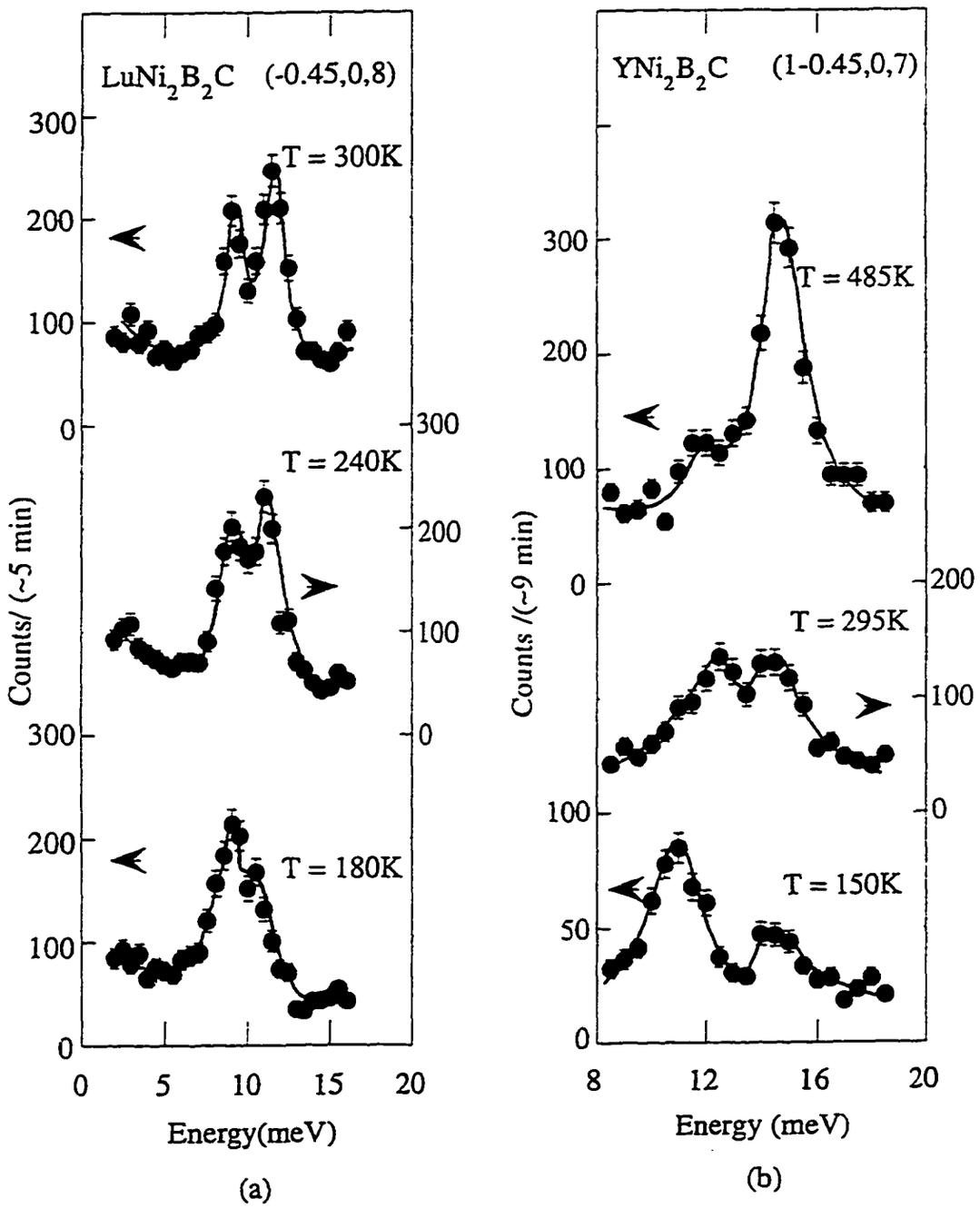

Fig. 4.2: Temperature dependence of the phonon spectra in the vicinity of ξ_m in (a) the Lu and (b) Y compounds. The lines are used as a guide to the eye.

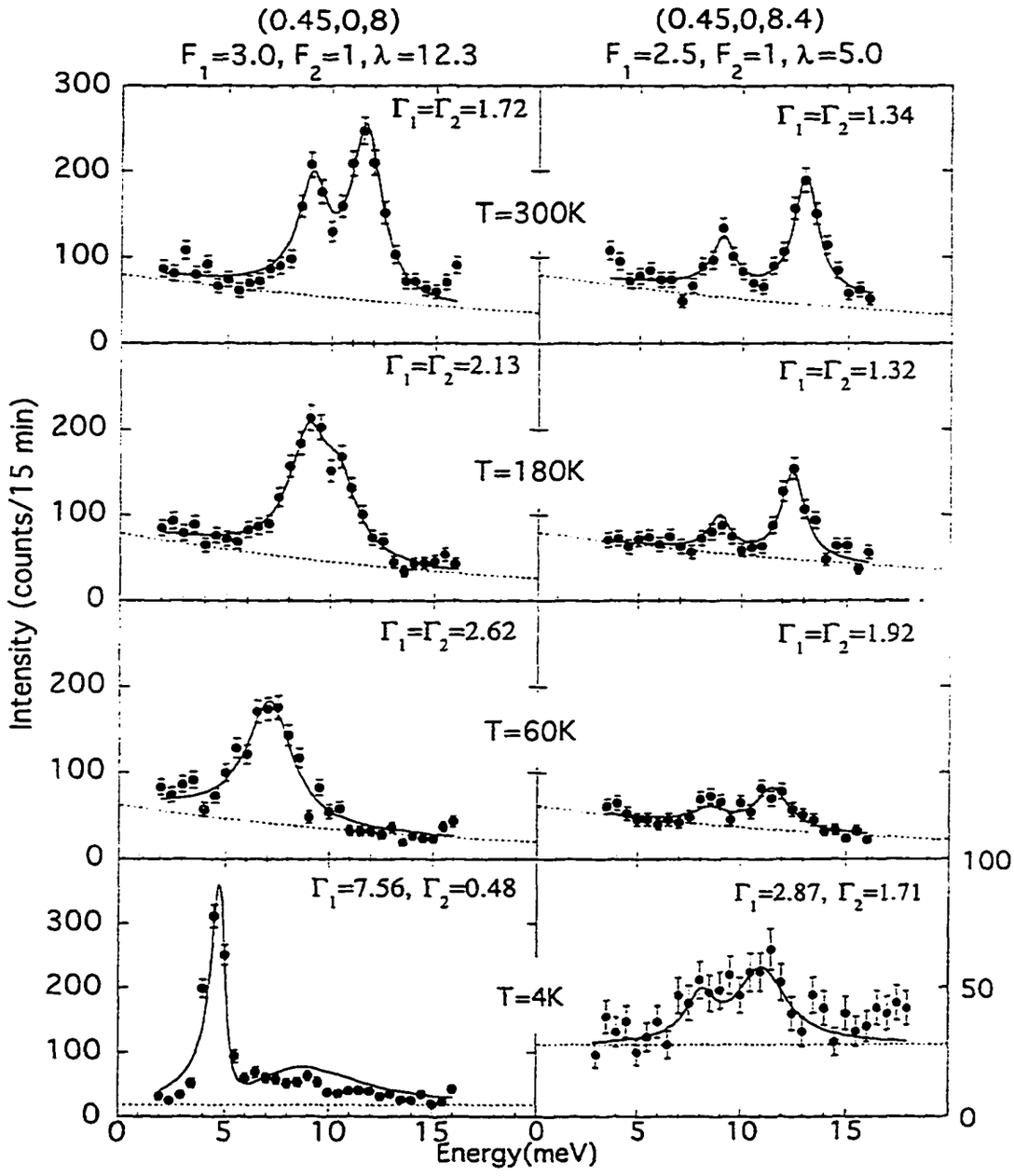

Fig. 4.3: Measured and calculated phonon profiles for several temperatures for (a) **Q**=(0.45,0,8) and (b) **Q**=(0.45,0,8.4). The calculations are based on the coupled-mode model described in the appendix.

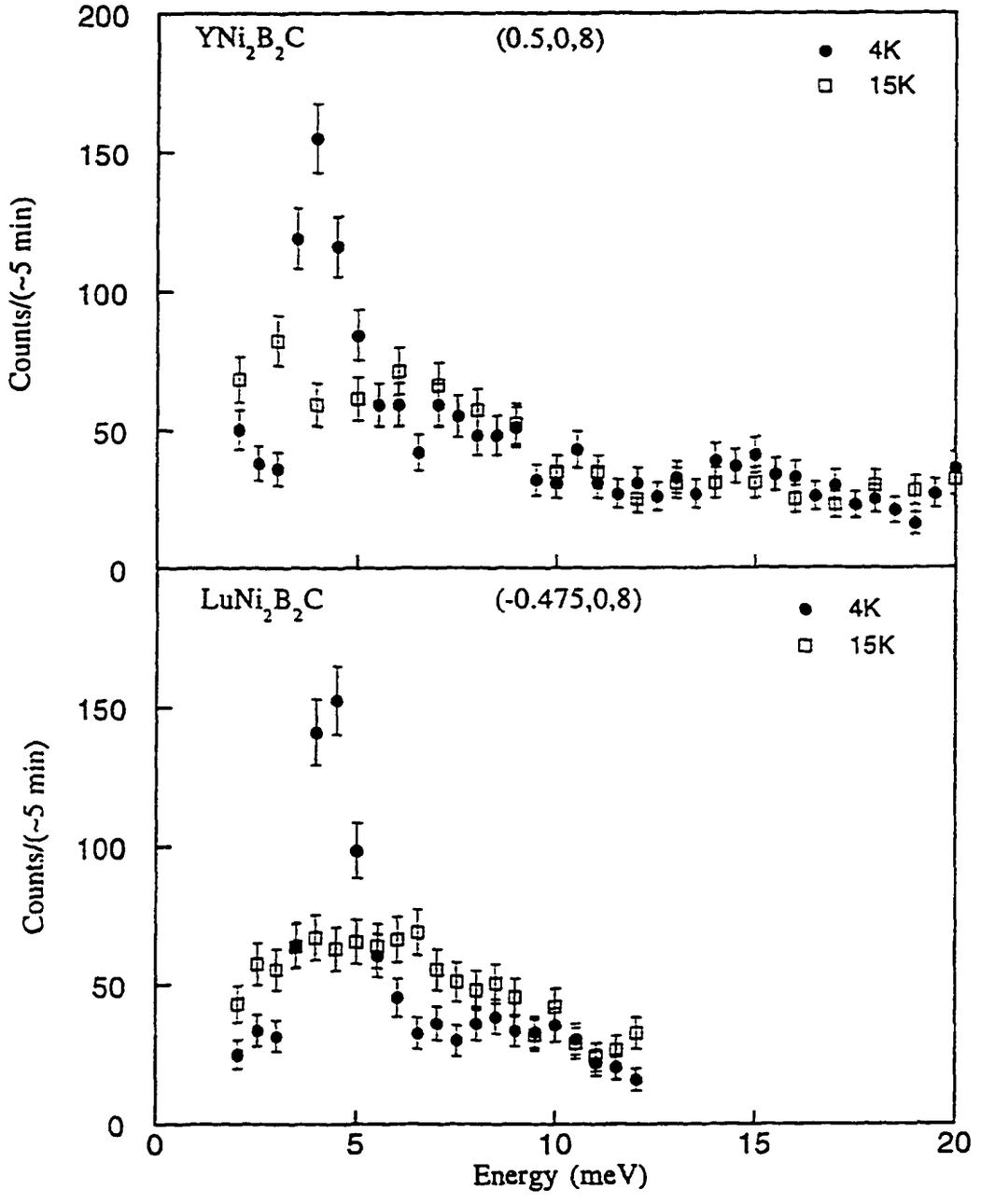

Fig. 4.4: Comparison of phonon profiles in YNi_2B_2C (top) and $LuNi_2B_2C$ (bottom) obtained very near T_c (15K) and below T_c (4K).

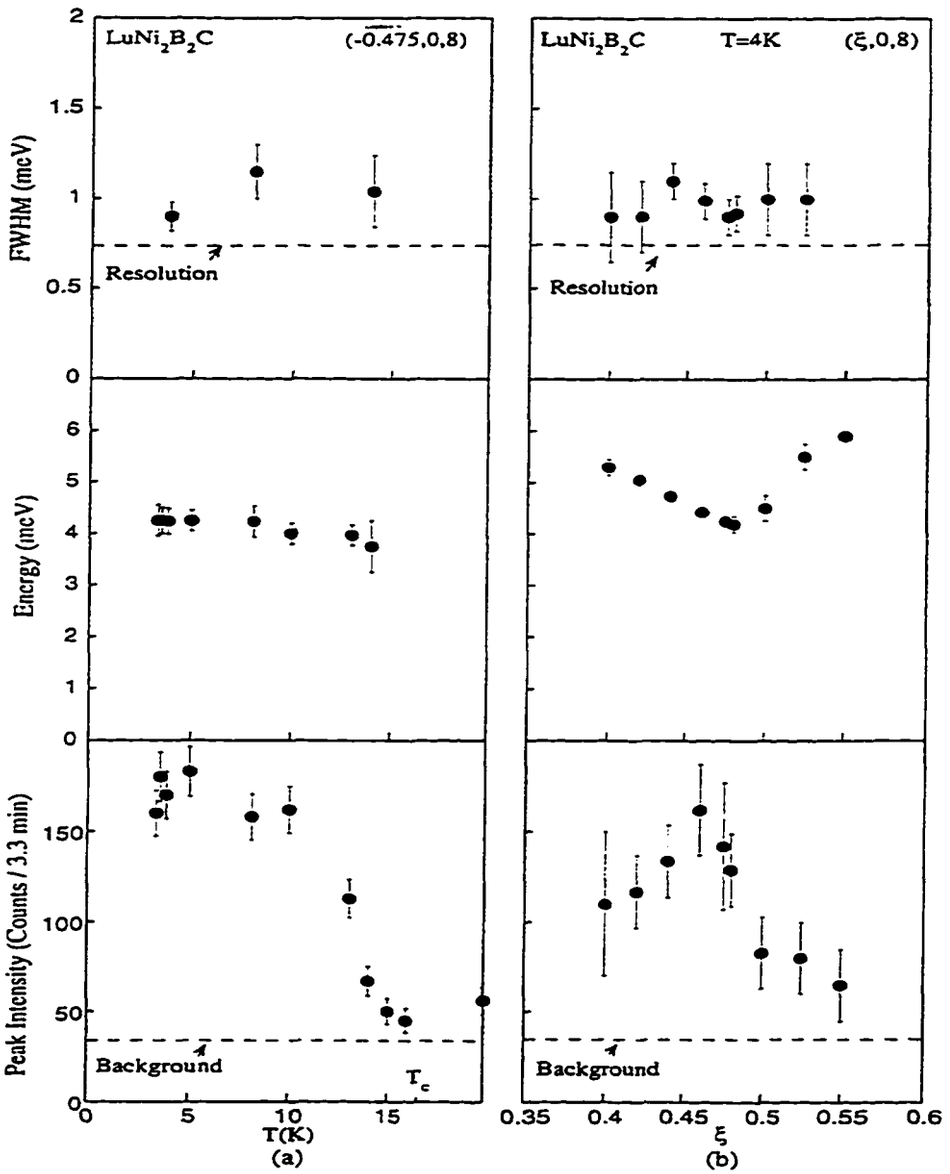

Fig. 4.5: (a) Temperature dependence of the FWHM, energy, and peak intensity of the sharp lower peak obtained at (-0.475, 0, 8); (b) ξ dependence of the FWHM, energy, and peak intensity of the lower peak observed at 4K. The lines are used as a guide to the eye.

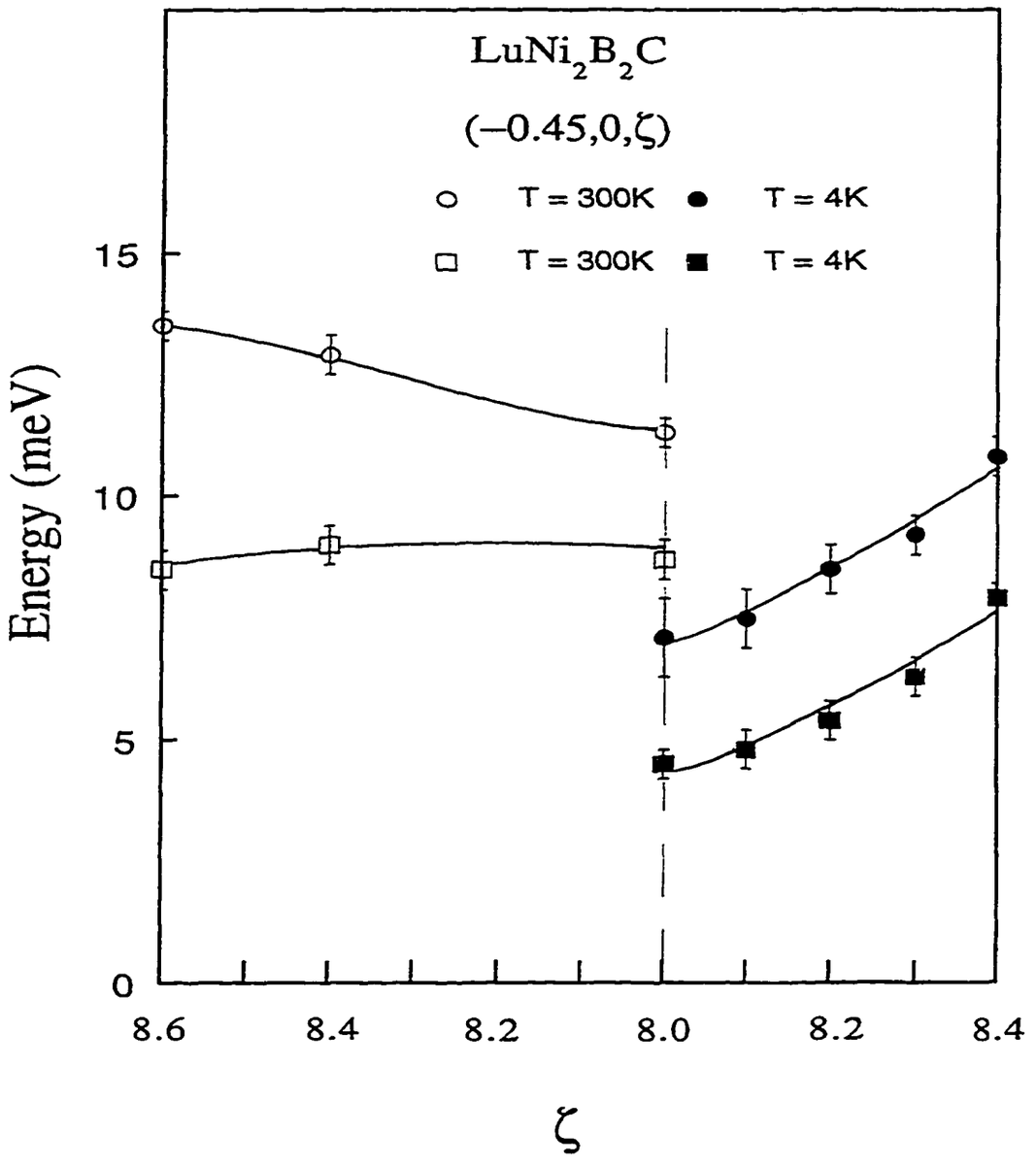

Fig. 4.6: Dispersion of the acoustic and optic Δ_4 modes measured along [00ζ] from **Q**=(-0.45,0,8) at T=300K and T=4K. The lines are used as a guide to the eye.

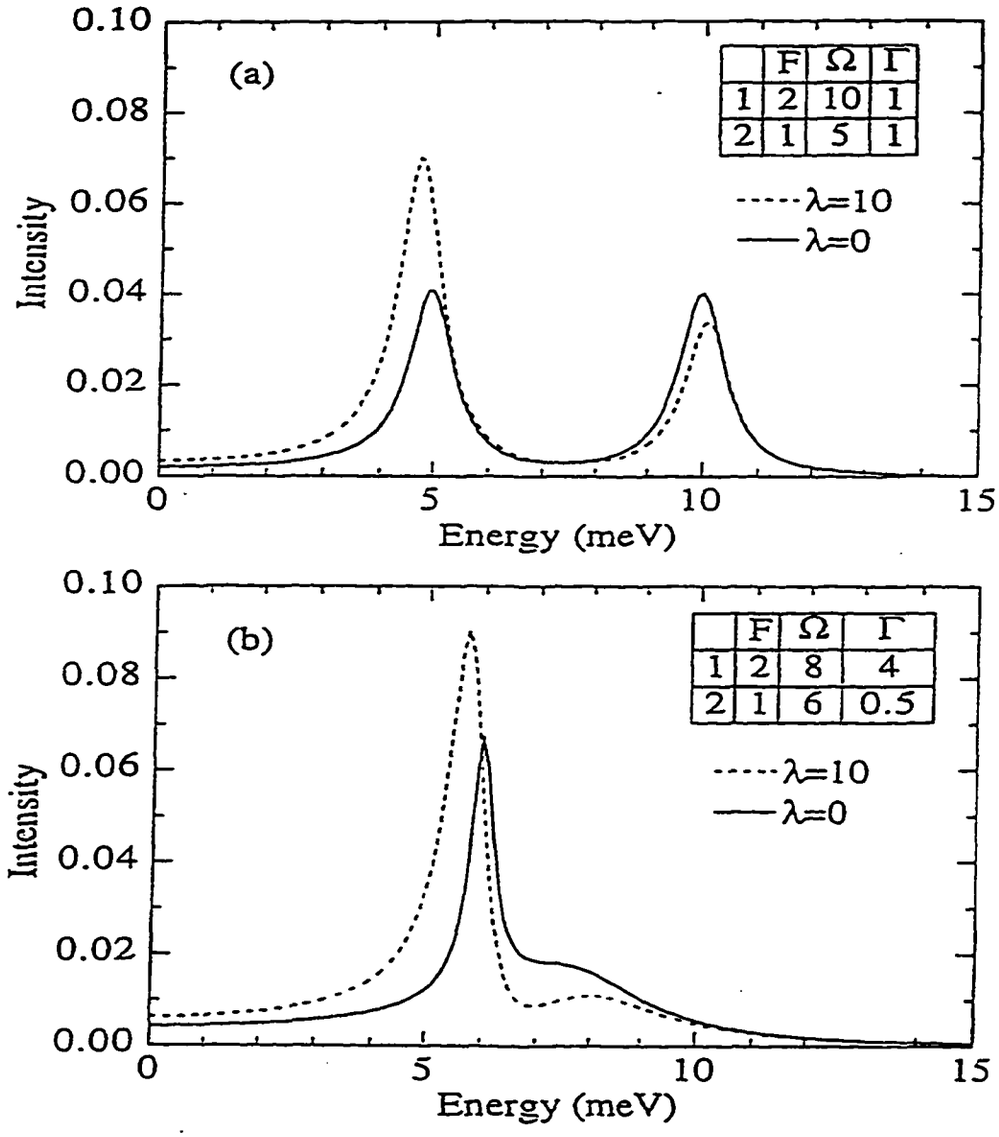

Fig. 4.A1: (a)Calculated spectra for two modes with $\Gamma << \Omega$ in the uncoupled case ($\lambda=0$) and with coupling $\lambda=10$ showing transfer of intensity from one mode to another with increased coupling; (b) Calculated spectra for two modes with considerable spectral overlap.

CHAPTER 5. INELASTIC NEUTRON STUDIES OF THE LOW ENERGY PHONON EXCITATIONS IN THE $RENi_2B_2C$ SUPERCONDUCTORS (RE=Lu,Y,Ho,Er)

A paper presented at ICNS

M. Bullock, C. Stassis, J. Zarestky, A. Goldman, P. Canfield

Ames Laboratory and Department of Physics, Iowa State University, Ames, IA 50011

G. Shirane and S. Shapiro

Brookhaven National Laboratory, Upton, NY 11973

Abstract

We studied the low-energy phonon excitations for wavevectors close to the Fermi surface nesting vector $\bar{\xi}_m \cong 0.55\bar{a}$. We find that above T_c the frequencies of the $\Delta_4[\zeta 00]$ lowest-lying optical and acoustic phonon modes decrease with decreasing temperature, for $\bar{\xi}$ close to $\bar{\xi}_m$, and there is a shift of intensity from the upper to the lower mode, an effect characteristic of coupled modes. From approximately 120K down to temperatures in the vicinity of T_c, only a single unresolved peak is observed. Below T_c the phonon spectra of the Y and Lu compounds change dramatically: they consist of

a sharp peak at approximately 4.5 meV with a weak shoulder at the higher energy side. No such sharp peak was observed below T_c in the Ho and Er compounds.

Introduction

Many of the body-centered tetragonal $RENi_2B_2C$ compounds are superconductors with relatively high superconducting transition temperatures (T_c=16.5, 15.5, 10.5, and 8.5 for the Lu, Y, Er, and Ho compounds) and in some cases (RE = Tm, Ho, Er, and Dy) superconductivity co-exists with magnetic order.[1] Of particular interest, for the present study, is that the frequencies of the lowest lying phonon modes near the nesting vector $\bar{\xi}_m$ decrease with decreasing temperature,[2,3] and a dramatic change in the phonon spectra of both Y[3] and Lu[4] compounds was observed below T_c. In this report we present a brief summary of the results obtained in a systematic study of the low-lying phonon excitations of the Lu, Y, Ho, and Er compounds.

The branches of interest are the acoustic and lowest lying optical branch in the [ξ00] direction, both belonging to the Δ_4 representation. The dispersion of these branches at room temperature, for the Y compound, is shown in Fig. 5.1. The phonon energies for the Lu, Ho, and Er are, of course, lower than in the Y compound. At room temperature

two peaks are observed for ξ up to approximately 0.45, but these peaks are not easily resolved for ξ in the vicinity of 0.5 (See Fig. 5.2).

As the temperature decreases, the energies of the modes in the vicinity of $\bar{\xi}_m$ decrease and there is transfer of intensity from the optic to the acoustic mode. For temperatures lower than approximately 120K, the two modes cannot be resolved and only a broad feature is observed. This is illustrated for the Lu compound in Fig. 5.2. In the Y compound, it was necessary to perform measurements at temperatures higher than room temperature in order to see clearly this mode interaction. As in the case of ferroelectric materials, the temperature dependence of the anticrossing behavior of the modes observed in the present experiments can be formulated as a problem of mode coupling via anharmonic forces[5].

At temperatures below approximately 120K, and down to the vicinity of T_c, the Δ_4 optical and acoustic modes close to $\bar{\xi}_m$ cannot be resolved and only a relatively broad feature is observed (see third panel of Fig. 5.2 and insert in the first panel of Fig. 5.3). Below T_c the phonon spectra for the Lu and Y change dramatically. They consist of a sharp peak at approximately 4.5 meV with a weak shoulder at the higher energy side. The width and position of this sharp peak remain practically unchanged below T_c, its intensity decreases

with increasing temperature, and it is practically indistinguishable from the background at temperatures close to T_c (see insert in the second panel of Fig. 5.3). From a study of the energies of the sharp peak and the broad shoulder as a function of ξ and ζ (along the [00ζ] direction), we concluded [5] that the sharp peak must be associated with the acoustic mode and the barely visible shoulder with the optical mode. No such sharp peak was observed in the Ho (see panel 3 of Fig. 5.3) and Er compounds at low temperatures. It should be pointed out, however, that the detailed study of the low lying phonon excitations in these magnetic superconductors is hindered by the presence of peaks corresponding to crystal electric field (CEF) levels (at approximately 10 meV in Ho and 5 meV in Er).

The experimental results show that the dramatic change in the phonon spectra of the Lu and Y compounds below T_c must be related to the abrupt change in the polarzability of the superconducting electrons at $\omega=2\Delta$. Actually, recent calculations[6,7]) yield phonon spectra almost identical to those observed in the present experiments. It should be pointed out, however, that in both approaches the theoretically predicted BCS temperature dependence of the sharp peak does not agree very well with the present experimental results.

References

1. For a brief review see: C. Stassis and A. Goldman, *J. Alloys and Comp.* (in press) and references therein.
2. P. Dervenagas, J. Zarestky, C. Stassis. A.I. Goldman, P.C. Canfield, B.K. Cho, *Phys Rev. B* **53**, 8506 (1996).
3. K. Kawano, H. Yoshizawa, H. Takeya, and K. Kadownki, *Phys. Rev. Lett.* **77**, C.V. Tomy, and D. McK. Paul, *Phys. Rev. Lett.* **28**, 935 (1997).
4. C. Stassis, M. Bullock, J. Zarestky, P. Canfield, A. Goldman, G. Shirane, S.M. Shapiro, *Phys. Rev. B* (Rapid Communications) **55**, 8678 (1977).
5. M. Bullock et al. (to be published) and references therein.
6. P.B. Allen, V.N. Kostur, N. Takesue and G. Shirane, *Phys. Rev. Lett* (in print), and references therein.
7. H.-Y. Kee and C.M. Varma (preprint).

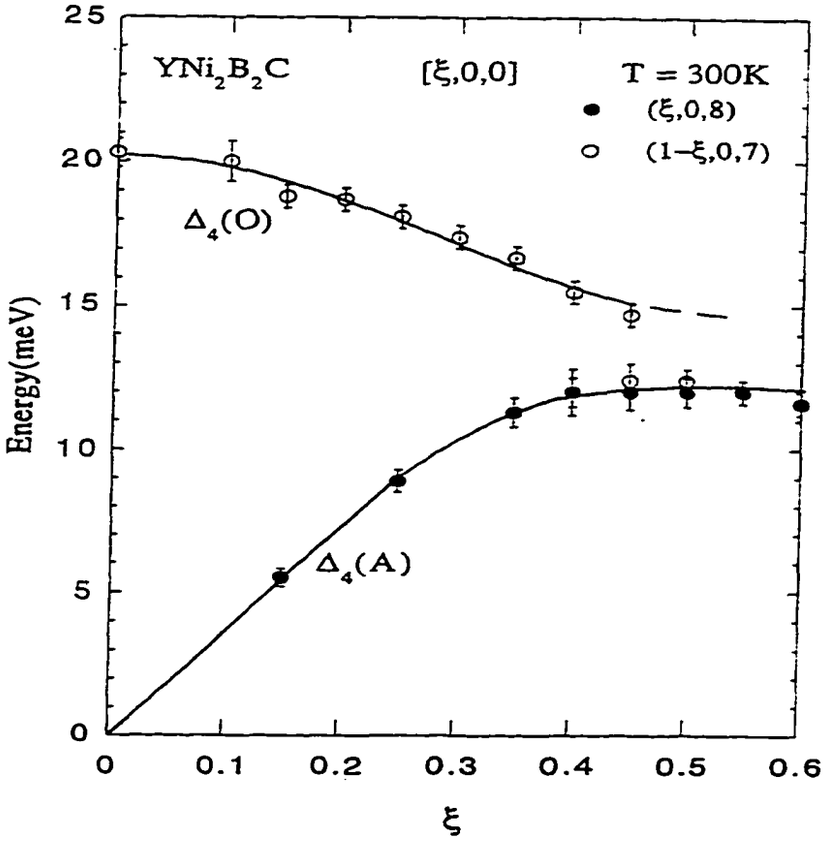

Fig. 5.1 Room temperature phonon dispersion of the Δ_4 acoustic (A) and optic (O) branches of YNi_2B_2C. For $\zeta > \zeta_m$ the intensity of the optical modes is very weak and this is indicated by a dotted line. The lines are used as a guide to the eye.

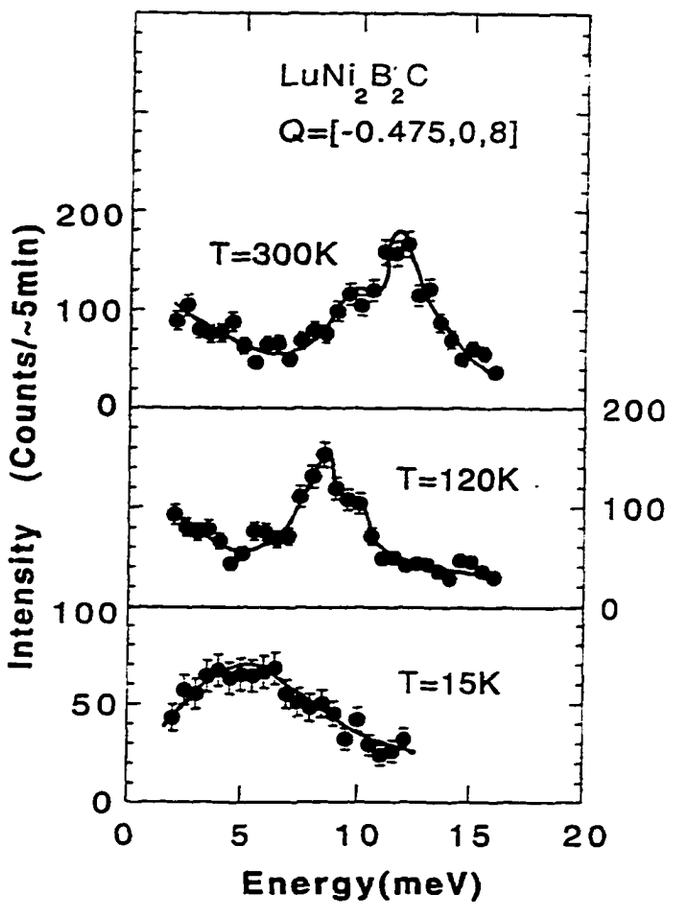

Fig. 5.2 Temperature dependence of the phonon spectra in the vicinity of ξ_m in the Lu compound, the lines are used as a guide to the eye.

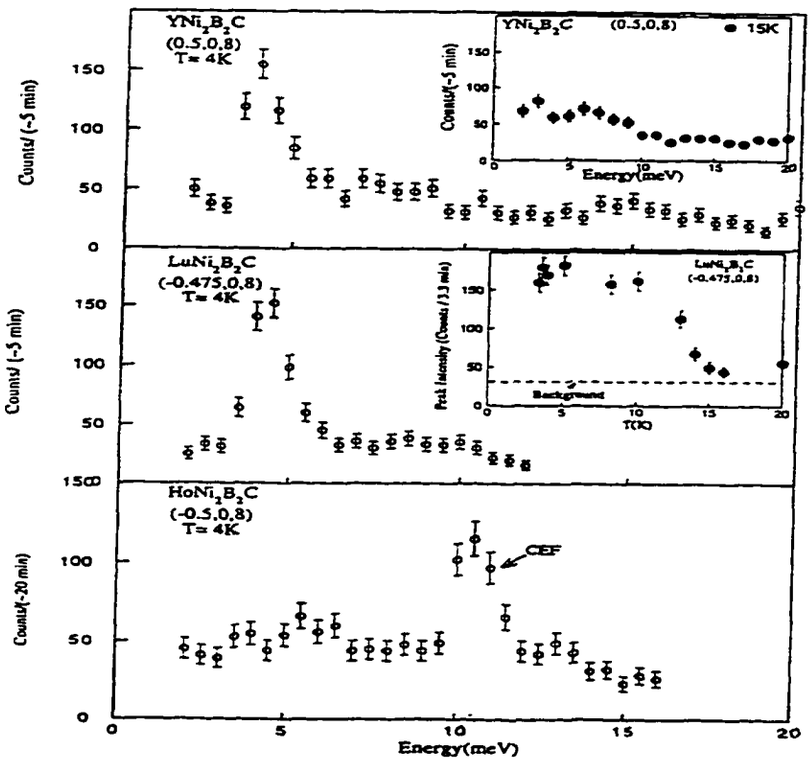

Fig. 5.3 Phonon profiles obtained below T_c for the Y, Lu and Ho compounds. Upper insert: typical phonon profile in the vicinity of T_c. Lower insert: temperature dependence of the intensity of the sharp peak (see text).

CHAPTER 6. CONCLUSION

In summary, the results obtained can be, at least, qualitatively understood both above as well as below T_c. For $T>T_c$, the softening of the two lowest Δ_1 branches can be understood in terms of two interacting modes. This is illustrated in Fig 6.1 where the results are compared with the model presented in the appendix of chapter 4[58].

For $T<T_c$, the experimental results clearly show that the origin of the dramatic change in the phonon spectra is the onset of superconductivity in these compounds. One of the direct effects of the superconducting gap opening is well understood and has been observed many years ago in superconducting Nb and Nb_3Sn[59,60]. A phonon with energy lower than the superconducting gap 2Δ cannot decay by breaking Cooper pairs and therefore its lifetime is increased (line width narrowing) compared to its lifetime above T_c. In addition, because of the singularity at $\omega \approx 2\Delta$ in the polarizability of the superconducting electrons, there is a shift in the phonon frequencies as well as a change in the phonon spectra as the temperature is decreased below T_c. Recent calculations of this change in phonon spectra by Allen et al.,[69] based on work by Schuster[71] and Zeyher et al.,[72] yield phonon spectra almost identical to those observed in this

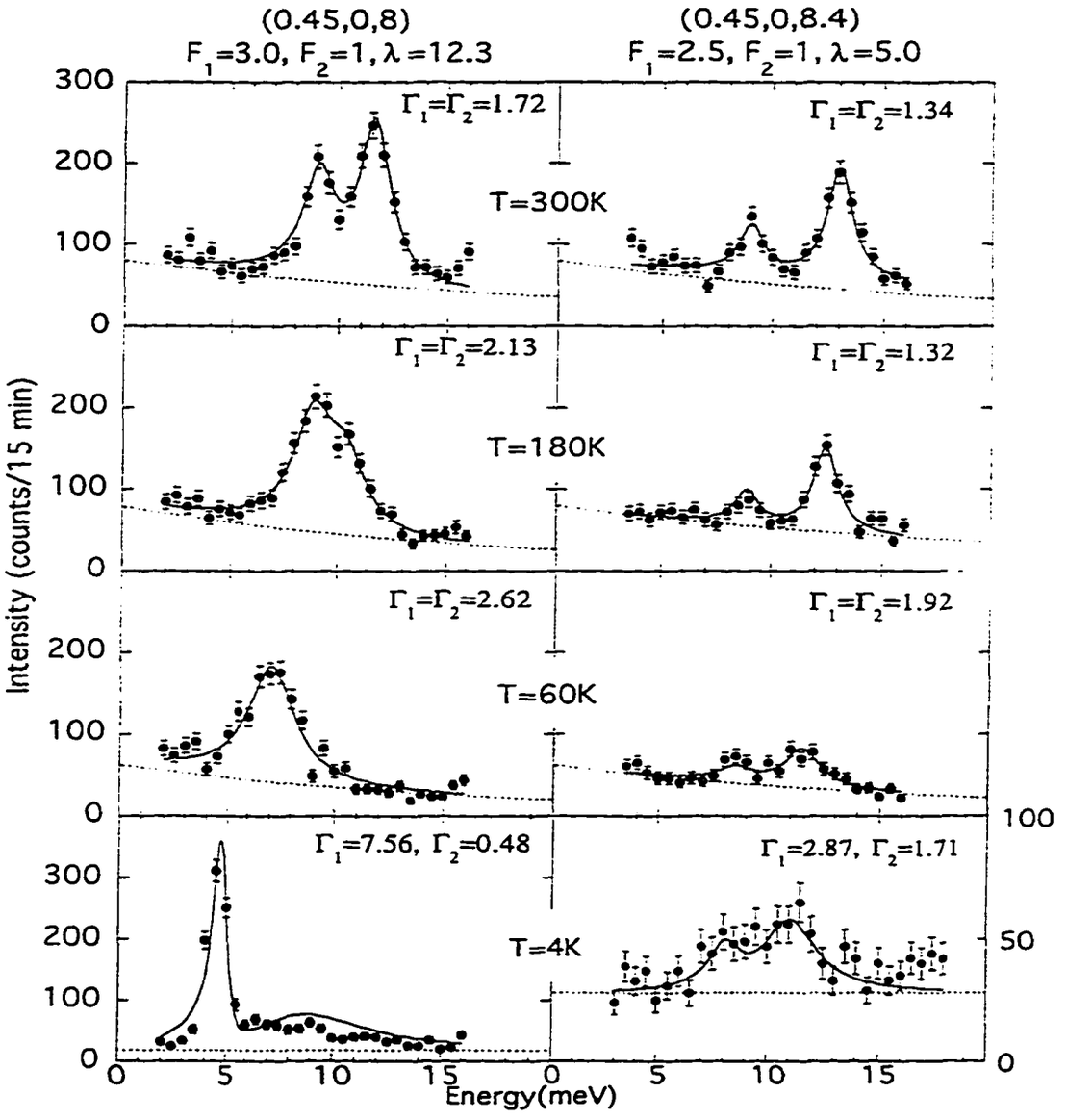

Fig. 6.1: Measured and calculated phonon profiles for several temperatures for (a) **Q**=(0.45,0,8) and (b) **Q**=(0.45,0,8.4). The calculations are based on the coupled-mode model described in the appendix of chapter 4.

dissertation. These calculations can be seen in Fig. 6.2. By looking at the right hand side, the observed spectra with instrumental resolution taken into account, we see that the spectra are very similar to the experimental phonon spectra observed at low T.

The above calculations are independent of q. Whereas in our case, the sharp feature is seen near a region that is known to have Fermi surface nesting. This suggests that these effects may be observable only when there is nesting. Kee and Varma[70] found that the electronic polarizability for an extremum vector of the Fermi surface exhibits a pole for frequencies close to 2Δ. For a phonon with normal state frequency above 2Δ this leads to a delta function in the polarizability at ω slightly below 2Δ and a peak centered around the normal state phonon frequency. The spectra, (See Fig 6.3) when convoluted with the instrumental resolution, is similar to those observed below T_c in the present experiments. The frequency of the observed sharp peak, on the other hand, does not follow the BCS temperature dependence of the superconducting gap as the Kee-Varma theory predicts.

The difference between the Kee-Varma and Allen et al. theory is due to the approximation involved in the evaluation of the electronic polarizability. Numerical calculation of the polarizability may be necessary to elucidate the difference.

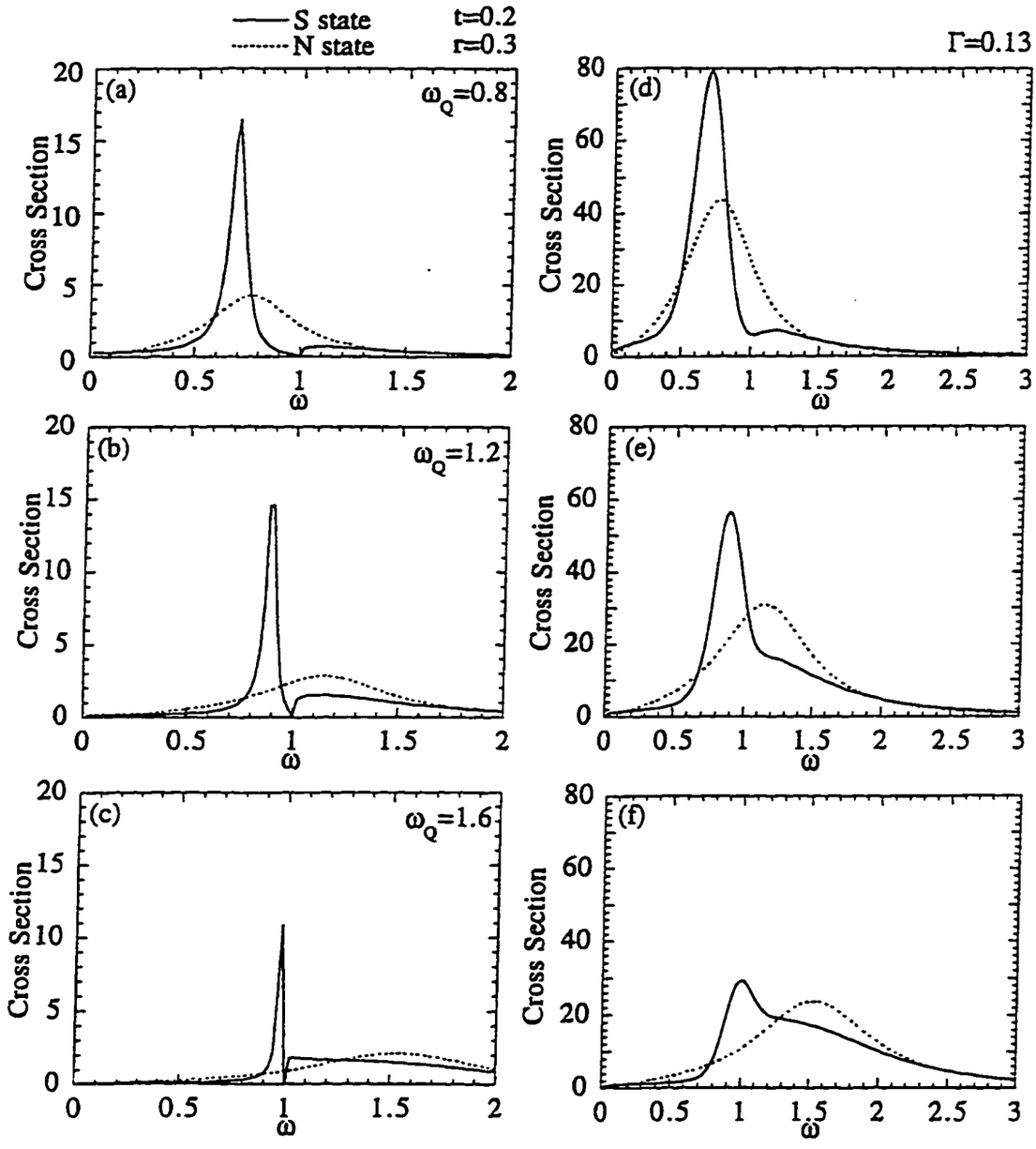

Fig. 6.2: Calculated line shapes at ω_Q=(a) 0.8, (b) 1.2, (c) 1.6 (units of 2Δ) at T/T_c=t=0.2. Panels (d)-(f) are convoluted with an instrumental broadening Γ=0.13 (units of 2Δ). (After reference Allen[69].)

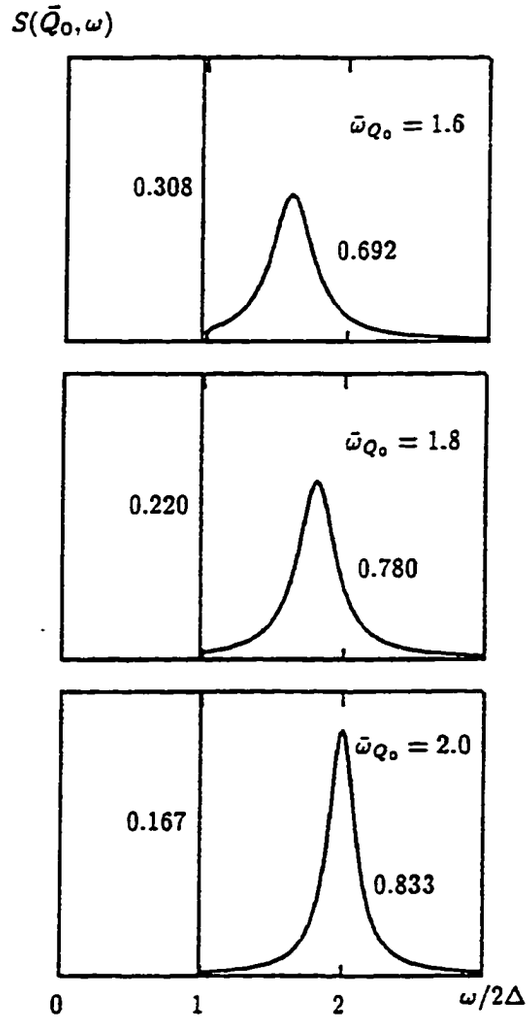

Fig. 6.3: Phonon spectral function $S(\mathbf{Q}_0,\omega)$ calculated for various ϖ_Q where $\varpi_Q = \omega_Q/2\Delta$, and $\Gamma = 2\Delta = 0.4N(0)$. (After reference Kee-Varma[70]).

Hopefully, other systems can be found that exhibit this sharp feature in the superconducting state so that this can be studied in greater detail. Since the characteristics of this sharp peak are determined by the superconducting properties of these systems, this work and future studies of these phonons may lead to the development of such measurements as a powerful technique for the study of the superconducting properties in these and other compounds.

APPENDIX A: DERIVATION OF $\chi(\mathbf{q})$

This appendix will follow the presentation of the electron-electron interaction given by Ziman.[73]

Electrons interact with other electrons via the Coulomb force. Usually we assume in materials that these interactions can be taken care of by assumptions that adjust the atomic potentials for the charge distribution of the valence electrons. Another option is to treat the gas of electons interacting via their Coulomb potential as a many-body problem. The basic effects of this interaction are now well understood.

To derive these results, we take a free-electron gas, subject to a time-dependent perturbation. Suppose that the potential seen by the elctron at r, at time t, is given by

$$\delta U(\mathbf{r},t) = Ue^{i\mathbf{q}\cdot\mathbf{r}}e^{i\omega t}e^{\alpha t}.$$

This perturbation is an oscillation, of frequency ω, wave-vector $\mathbf{q}$, that grows with a time-constant α. Perturbation acting on a state

$$|\mathbf{k}\rangle = e^{i\left(\mathbf{k}\cdot\mathbf{r}+\frac{E(\mathbf{k})t}{\hbar}\right)}$$

causes mixing of other states. This causes the wave-function to become

$$\psi_{\mathbf{k}}(\mathbf{r},t) = |\mathbf{k}\rangle + b_{\mathbf{k}+\mathbf{q}}(t)|\mathbf{k}+\mathbf{q}\rangle,$$

where the coefficients may be calculated, in first order, by perturbation theory;

$$b_{\mathbf{k}+\mathbf{q}}(t) = \frac{\langle \mathbf{k}+\mathbf{q}|\delta U|\mathbf{k}\rangle}{\mathrm{E}(\mathbf{k}) - \mathrm{E}(\mathbf{k}+\mathbf{q}) + \hbar\omega - i\hbar\alpha}$$

$$b_{\mathbf{k}+\mathbf{q}}(t) = \frac{Ue^{i\omega t}e^{\alpha t}}{\mathrm{E}(\mathbf{k}) - \mathrm{E}(\mathbf{k}+\mathbf{q}) + \hbar\omega - i\hbar\alpha}.$$

Now we will consider the change in charge density due to this change in the electron wave-functions. The electrons will see a uniform positively charged medium which will give the following change in charge denisty

$$\delta\rho(r,t) = e\sum_{\mathbf{k}}\{|\psi_{\mathbf{k}}(\mathbf{r},t)|^2 - 1\}$$

$$\delta\rho(r,t) = e\sum_{\mathbf{k}}[\{e^{-i\mathbf{k}\cdot\mathbf{r}} + b^{*}_{\mathbf{k}+\mathbf{q}}(t)e^{-i(\mathbf{k}+\mathbf{q})\cdot\mathbf{r}}\}\{e^{i\mathbf{k}\cdot\mathbf{r}} + b_{\mathbf{k}+\mathbf{q}}(t)e^{i(\mathbf{k}+\mathbf{q})\cdot\mathbf{r}}\} - 1],$$

or,

$$\delta\rho(r,t) \approx e\sum_{\mathbf{k}}\{b_{\mathbf{k}+\mathbf{q}}(t)e^{i\mathbf{q}\cdot\mathbf{r}} + b^{*}_{\mathbf{k}+\mathbf{q}}(t)e^{-i\mathbf{q}\cdot\mathbf{r}}\},$$

if we drop the term in $|b|^2$. This summation is over all occupied electron states.

We see that there appears to be two types of wave traveling in opposite directions. Since the perturbation needs to be real, we can then add the complex conjugate to our origional perturbation, which tells us that the variation in charge density follows the total perturbation

$$\delta\rho = e\sum_{\mathbf{k}}\left\{\frac{\mathrm{U}}{\mathrm{E}(\mathbf{k})-\mathrm{E}(\mathbf{k}+\mathbf{q})+\hbar\omega-\mathrm{i}\hbar\alpha}+\frac{\mathrm{U}}{\mathrm{E}(\mathbf{k})-\mathrm{E}(\mathbf{k}+\mathbf{q})-\hbar\omega+\mathrm{i}\hbar\alpha}\right\}e^{i\mathbf{q}\cdot\mathbf{r}}e^{i\omega t}e^{\alpha t}+c.c$$

To further simplify this expression, let us introduce the Fermi-Dirac function, $f_0(\mathbf{k})$ as the probablility that $|\mathbf{k}\rangle$ is occupied in the unperturbed metal. Next, we will rewrite $\mathbf{k}$ for $\mathbf{k}$-$\mathbf{q}$ as labels in the second term, this leads to

$$\delta\rho(r,t) = eU\sum_{\mathbf{k}}\left\{\frac{\mathrm{f}_0(\mathbf{k})-f_0(\mathbf{k}+\mathbf{q})}{\mathrm{E}(\mathbf{k})-\mathrm{E}(\mathbf{k}+\mathbf{q})+\hbar\omega-\mathrm{i}\hbar\alpha}\right\}e^{i\mathbf{q}\cdot\mathbf{r}}e^{i\omega t}e^{\alpha t}+c.c$$

where the sum is over all states $|\mathbf{k}\rangle$.

By Poisson's equation

$$\nabla^2(\delta\phi) = -4\pi e\delta\rho$$

we see that the charge distribution gives rise to a potential-energy field acting on the electrons. If we assume that $\delta\phi$ has the same space and time variataion as $\delta\rho$, we can then write

$$\delta\phi(\mathbf{r},t) = \phi e^{i\mathbf{q}\cdot\mathbf{r}}e^{i\omega t}e^{\alpha t}+c.c\,.$$

Combining the last 3 equations, we end up with

$$-q^2\phi = -4\pi e^2 U\sum_{\mathbf{k}}\left\{\frac{\mathrm{f}_0(\mathbf{k})-f_0(\mathbf{k}+\mathbf{q})}{\mathrm{E}(\mathbf{k})-\mathrm{E}(\mathbf{k}+\mathbf{q})+\hbar\omega-\mathrm{i}\hbar\alpha}\right\},$$

and by simplifing a little, we end up with

$$\phi = \frac{4\pi e^2}{q^2}\sum_{\mathbf{k}}\left\{\frac{\mathrm{f}_0(\mathbf{k})-f_0(\mathbf{k}+\mathbf{q})}{\mathrm{E}(\mathbf{k})-\mathrm{E}(\mathbf{k}+\mathbf{q})+\hbar\omega-\mathrm{i}\hbar\alpha}\right\}U\,.$$

This potential energy is associated with the charge redistribution created by the original potential δU. However, this new potential should have been counted as a perturbation of the electron distribution. To be consistant, we will assume that the perturbation δU already contains the term $\delta\phi$ given by

$$\delta U(\mathbf{r},t) = \delta V(\mathbf{r},t) + \delta\phi(\mathbf{r},t),$$

where $\delta V(\mathbf{r},t)$ is the external potential we applied at the start of the derivation. Combining all the expressions, we end up with

$$U = V + \left\{ \frac{4\pi e^2}{q^2} \sum_{\mathbf{k}} \frac{\mathrm{f}_0(\mathbf{k}) - f_0(\mathbf{k}+\mathbf{q})}{\mathrm{E}(\mathbf{k}) - \mathrm{E}(\mathbf{k}+\mathbf{q}) + \hbar\omega - i\hbar\alpha} \right\} U$$

or

$$U = \frac{V}{\varepsilon(\mathbf{q},\omega)},$$

where

$$\varepsilon(\mathbf{q},\omega) = 1 + \left\{ \frac{4\pi e^2}{q^2} \sum_{\mathbf{k}} \frac{\mathrm{f}_0(\mathbf{k}) - f_0(\mathbf{k}+\mathbf{q})}{\mathrm{E}(\mathbf{k}+\mathbf{q}) - \mathrm{E}(\mathbf{k}) - \hbar\omega + i\hbar\alpha} \right\}.$$

The effective potential U acting on the electrons is the applied potential V divided by the dielectric constant $\varepsilon(\mathbf{q},\omega)$. If we wish to examine screening effects for short distances, we need to look at large values of $\mathbf{q}$ and evaluate the summation. This will depend on the detailed structure of the energy surfaces $\mathrm{E}(\mathbf{k})$. For a free-electron model at absolute

zero it is not very difficult to evaluate the sum by a straightforward integration over **k**-space. This leads to the following expression

$$\varepsilon(\mathbf{q},0)=1+\frac{4\pi e^2}{q^2}\frac{n}{\frac{2}{3}E_f}\left\{\frac{1}{2}+\frac{4k_f^2-q^2}{8k_f q}\ln\left|\frac{2k_f+q}{2k_f-q}\right|\right\}$$

where k_f is the radius of the Fermi sphere. This result is interesting because at $2k_f$ the ln term is singular. This is the origin of the Kohn effect talked about in chapter 1. A phonon of wave-vector q sets up a potential with components like that for the dielectric function due to the motion of the ions. The electrons move to screen this field. This means that the ions now interact with one another via this screened field, which is inversely proportional to $\varepsilon(\mathbf{q})$. This means that the lattice frequencies will be modified depending on $\varepsilon(\mathbf{q})$. In other words, any singularity in $\varepsilon(\mathbf{q})$ will be reflected in the phonon frequency.

APPENDIX B. LATTICE DYNAMICS OF $RENi_2B_2C$ (RE=Lu, Y)

A paper to be published.

M. Bullock, B. Harmon, C. Stassis, P. Canfield

Ames Laboratory and Department of Physics and Astronomy

Iowa State University, Ames, IA 50011

Abstract

Single crystals of $RENi_2B_2C$ were used to study the lattice dynamics of the $LuNi_2B_2C$ and YNi_2B_2C compounds by standard inelastic neutron scattering techniques. The phonon dispersion curves of the lowest branches (<40 meV) were measured along the $[\xi,0,0]$, $[0,0,\zeta]$, and $[\xi,\xi,0]$ directions at room temperature. The data was then used in a Born-von Kármán force constant model to determine the entire dispersion curves, elastic constants, phonon density of states, and lattice specific heat.

Introduction

The physical properties of the rare-earth nickel boride carbides ($RENi_2B_2C$; RE = rare earth) are of considerable interest.[1,2,3,4] Their crystal structure[3] is body-centered tetragonal (space group I4/mmm), with $a \cong 3.5\text{Å}$ and $c \cong 3a$, and consists of RE-C layers separated by Ni_2B_2 sheets. Many of these compounds are superconductors with relatively high superconducting temperatures. Among these superconductors, the non-magnetic Lu and Y compounds exhibit[2,3,4,5] the highest superconducting temperatures, 16.5K and 15.5K, respectively. Of particular interest is that in several of these compounds (RE=Tm, Ho, Er, and Dy) superconductivity coexists with magnetic order.[2-7]

To obtain some insight into the subtle interplay between superconductivity and magnetism, the magnetic structures of these compounds have been studied extensively by neutron and x-ray scattering techniques on both single crystal and powder specimens.[8,9] Of particular relevance to the present study is that the superconducting Er[10,11] and Ho[12,13] compounds as well as the non-superconducting Tb[14] and Gd[15] compounds all order in an incommensurate magnetic structure characterized by a propagation vector $\vec{\xi}_m = (\xi_m, 0, 0)$, with $\xi_m \cong 0.55$ for all of these compounds. This observation is particularly important, since band

theoretical calculations[16] of the generalized electronic susceptibility of $LuNi_2B_2C$ show that there is strong Fermi surface nesting in this compound with a nesting vector close to $\vec{\xi}_m$. These results indicate that there is a common Fermi surface nesting in these compounds, characterized by a nesting vector $\vec{\xi}_m$, which is responsible for the ordering of the rare-earth moments via the RKKY mechanism. The existence of such a nesting suggests that strong Kohn anomalies should be observed in the dispersion curves of these compounds for wavevectors close to $\vec{\xi}_m$. In addition, electronic band structure calculations[17, 18, 19, 20] suggest that these materials are conventional superconductors with relatively high electronic density of states at the Fermi level, E_F, and that there is a complex set of bands crossing E_F which are strongly coupled to the phonons and may be responsible for the superconducting properties of these compounds. Therefore, it appears that this family of compounds is ideal for the study of the subtle competition between lattice instabilities, superconductivity, and magnetic ordering.

Dervenagas et al.[21] measured the low-lying phonon dispersion curves of the Lu compound ($T_c \cong 16.5K$) along the $[\xi 00]$ and $[00\zeta]$ symmetry directions and they found that the frequencies of the lowest lying modes near $\vec{\xi}_m$

decrease with decreasing temperature and, as a result, the corresponding branches exhibit strong dips in the vicinity of this point at low temperatures. A similar study in the isomorphous Y compound was performed by Kawano et al.[22] The softening of these modes is so significant that it was observed in phonon-density of states measurements by Gompf et al.[23] as well as in the point-contact spectra of these compounds by Yanson et al.[24] In addition Kawano et al.[22] performed a detailed study of the low-lying excitations in the Y compound as a function of temperature and magnetic field. They observed a dramatic change in the spectrum associated with the onset of superconductivity which includes a sharp feature at approximately 4 meV which they attributed to a "new" excitation. This interesting observation led us to perform a systematic study of these excitations as a function of temperature on the Lu and Y compounds. We already presented a brief account[25] of the results obtained in the experiments on the Lu compound, a larger summary paper[26] on both Y and Lu, and a conference paper[27] given at the ICNS 97. In this paper we present detailed room temperature Born-von Kármán model fits to the Lu and Y compounds.

Experimental Details

The single crystals of $LuNi_2B_2C$ and YNi_2B_2C used in the present experiment were grown at the Ames laboratory by the high-temperature flux technique as described elsewhere.[28] The grown crystals are platelets with the c-axis perpendicular to their flat surface. Since the size of the crystals is relatively small (approximately 5 x 5 x 0.5mm^3) for inelastic neutron scattering, most of the measurements on $LuNi_2B_2C$ were performed on a composite crystal, consisting of two crystals (mounted on a single holder) oriented to within 0.8 degrees. All measurements on YNi_2B_2C were performed on a single crystal of this compound.

The neutron scattering experiments were performed using the variable incident neutron energy triple-axis spectrometers H-7 and H-8 at Brookhaven National Laboratory's High Flux Beam Reactor and the constant incident neutron energy (13.7 meV) HB1A triple-axis spectrometer and variable incident neutron energy triple-axis spectrometers HB1, HB2, and HB3 at the Oak Ridge National Laboratory's High Flux Isotope Reactor. Pyrolitic graphite (PG), reflecting from the (002) planes, was used as monochromator and analyzer and a PG filter was used to eliminate higher order contamination. On the variable

incident spectrometers most of the data were collected using a fixed final neutron energy of 14.7 meV. Most of the data were collected with a collimation of 40-40-40-80 minutes of arc in the standard positions on the spectrometers.

Experimental Results and Discussion

The lowest lying branches of the $LuNi_2B_2C$ and YNi_2B_2C phonon dispersion curves have been measured at room temperature. Extensive studies have been made on the lowest 8 of 18 phonon branches extending up to around 40 meV along the $[\xi,0,0]$, $[0,0,\zeta]$, and $[\xi,\xi,0]$ directions for $LuNi_2B_2C$, while less work has been done on the Y compound. The measured phonon branches for $LuNi_2B_2C$ along these directions are given in Tables B.1, and B.2. Table B.1 deals only with the $[\xi,0,0]$ direction, while Table B.2 contains both the $[0,0,\zeta]$, and $[\xi,\xi,0]$ directions. Less extensive work has also been performed on the Y compound. The experimental data for the Y compound are given in Table B.3.

Since the two compounds have similar structure, we would reason that the dispersion curves of the two compounds should be very similar. The major difference in the two systems is the difference in mass. Lu is almost

twice as heavy as Y, thus we would expect some modification to the lowest lying phonon branches to reflect this difference in mass.

Three symmetry directions have been measured on the Lu compound, while only two directions have been measured on the Y compound. In the $[\xi,0,0]$ direction the 18 branches belong to four irreducible representations $6\text{-}\Delta_1$, $2\text{-}\Delta_2$, $4\text{-}D_3$, $6\text{-}\Delta_4$. As mentioned in the previous papers, the Δ_4 branches are purely transverse with atomic displacements along the c-axis at small wave vectors. For larger wave vectors, the RE and C displacements remain transverse, while the Ni and B atoms develop a longitudinal component. The Δ_1 representation is similar to the Δ_4 representation, except that the RE and C displacements are longitudinal, and the Ni and B atoms develop both longitudinal and transverse components. The last two representations are transverse in nature with polarization perpendicular to **c***. The Δ_2 representation has only the Ni and B atoms moving, while the Δ_3 representations have all 6 atoms moving in the **b*** direction. Along the $[0,0,\zeta]$, there are three representations, $5\text{-}\Lambda_1$, $1\text{-}\Lambda_2$, and $6\text{-}\Lambda_3$(degenerate). The degenerate Λ_3 representation is a transverse mode in this direction. Likewise, the Λ_1 representation is the longitudinal modes. The Λ_2 branch is longitudinal in nature, but only the two Ni atoms are allowed to move.

Lastly, along the [ξ,ξ,0], the irreducible representations are as follows; 5-Σ_1, 2-Σ_2, 6-Σ_3, and 5-Σ_4. Σ_1 is the longitudinal representation along this direction. The Σ_3 representations are transverse in nature with polarization perpendicular to **c***, while the Σ_4 branches are transverse with polarization parallel to **c***. The remaining two Σ_2 modes are mixed in nature with the RE and C atoms at rest.

In addition to the experimental data given in Tables B.1, B.2 and B.3, the four raman active modes (103 meV A_{1g}, 58.3 meV E_g, 35 meV E_g, 24.5 meV B_{1g})[29,30] were used to fit a Born-von Kármán model. The Born-von Kármán fit along with the experimental data to the lowest measured branches are plotted in Figure B.1 for $LuNi_2B_2C$ and Figure B.2 for YNi_2B_2C. Only the lowest lying branches are plotted along with the experimental data. To summarize the dispersion curves, the highest branch is around 150 meV, there is then a raman active mode at 105 meV, and the other 16 branches are scattered continuously below 65 meV. As mentioned in previous papers, the two lowest Δ_4 branches exhibit softening for $0.35 < \xi < 0.6$. Higher Δ_4 branches have not been studied for temperature dependence yet. It is also important to note that for the Y fit, the model predicts that the lowest Δ_1 branch is lower than in the Lu compound. This Δ_1 branch is within a meV of the Δ_4 branch in the region of softening. Since the Δ_1 branch also has

transverse components, it is possible to pick this mode up from the transverse scans which are used to pick up the softening Δ_4 branches. By looking at structure factor calculations, it appears that the structure factor from the (107) and (008) reciprocal lattice points are similar for both the Δ_4 and Δ_1 modes in the region of softening. Based on this, it is reasonable to assume that the 15 meV mode that does not soften around $\xi \cong 0.5$ is this Δ_1 branch.

From Figure B.1, and Figure B.2, the model appears to fit the system well given the lack of information about many of the higher energy branches. The force constants obtained by fitting the model are given in Table B.4 for $LuNi_2B_2C$ and YNi2B2C. Table B.4 also shows the distance between atoms and the atoms that correspond to each force constant.

The theoretical phonon density of states g(ν) from the Born-von Kármán model are shown in Figure B.3. This density of states is similar to the experimental density of states by Gompf et al.[23] The experimental density of states only goes up to 90 meV, but Gompf et al. did see the highest two modes at around 105 and 150 meV.

To evaluate the elastic constants[31,32,33] and lattice specific heat, the data was analyzed by a conventional Born-von Kármán model with force constants extending out one shell. From the model, we calculate a $\theta_D^{(0)}$calc = 545 K

from a room temperature fit to the model, which is well above the measured $\theta_D^{(0)}$exp = 360K[34]. Since we know that there is softening in the dispersion curves, we expect that there should also be temperature dependence in the density of states, which Gompf observed. This may explain the difference in Debye temperatures we see by using room temperature data to extract $\theta_D^{(0)}$calc. The elastic constants for this system are given in Table B.5.

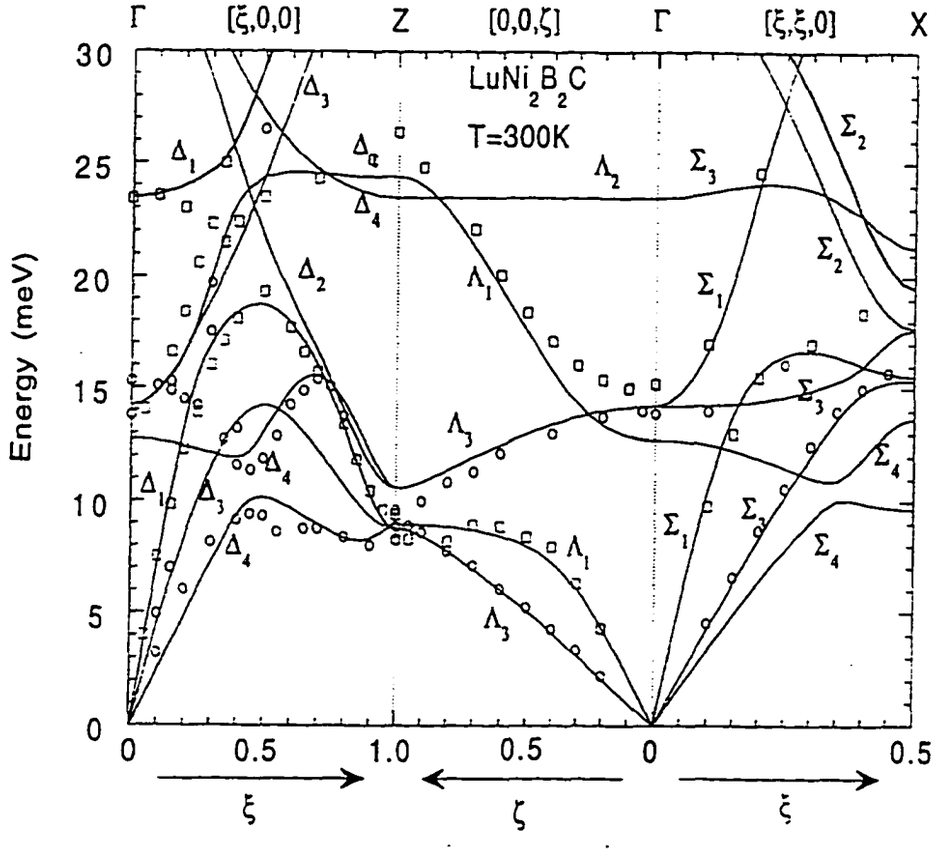

Figure B.1: Experimental dispersion curves of $LuNi_2B_2C$ at room temperature. The solid lines were obtained by fitting the data to a nearest-neighbot force-constant model.

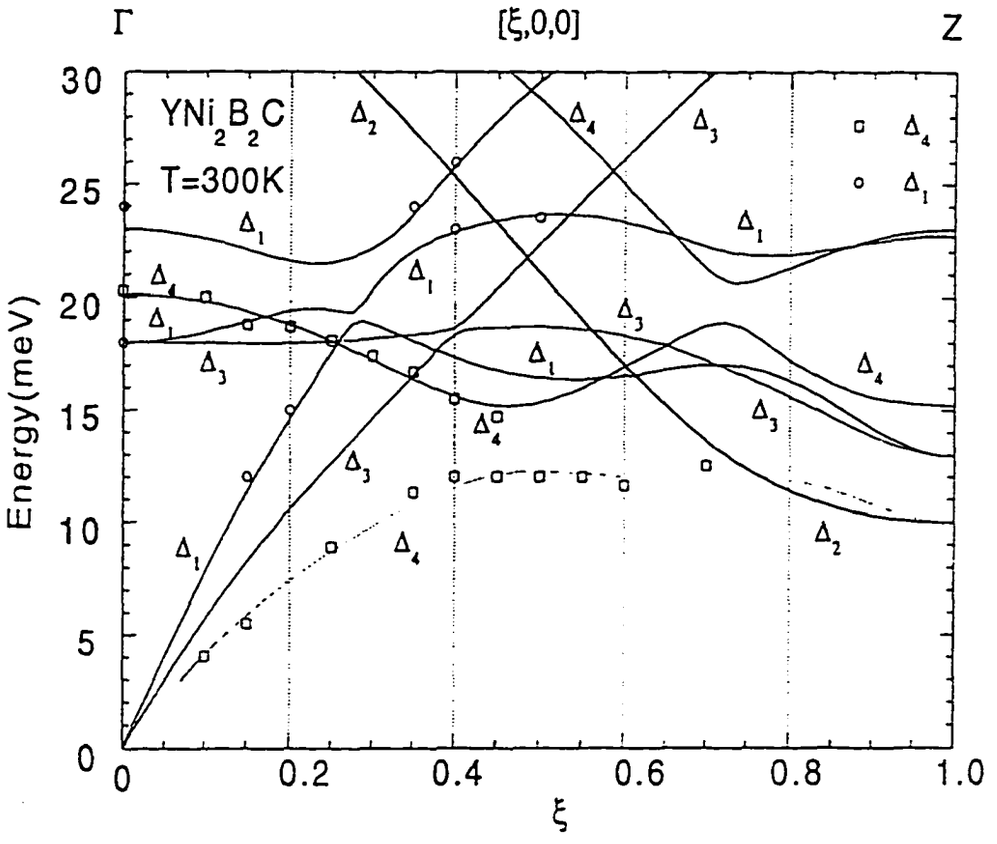

Figure B.2: Experimental dispersion curves of YNi_2B_2C at room temperature. The solid lines were obtained by fitting the data to a nearest-neighbor force-constant model.

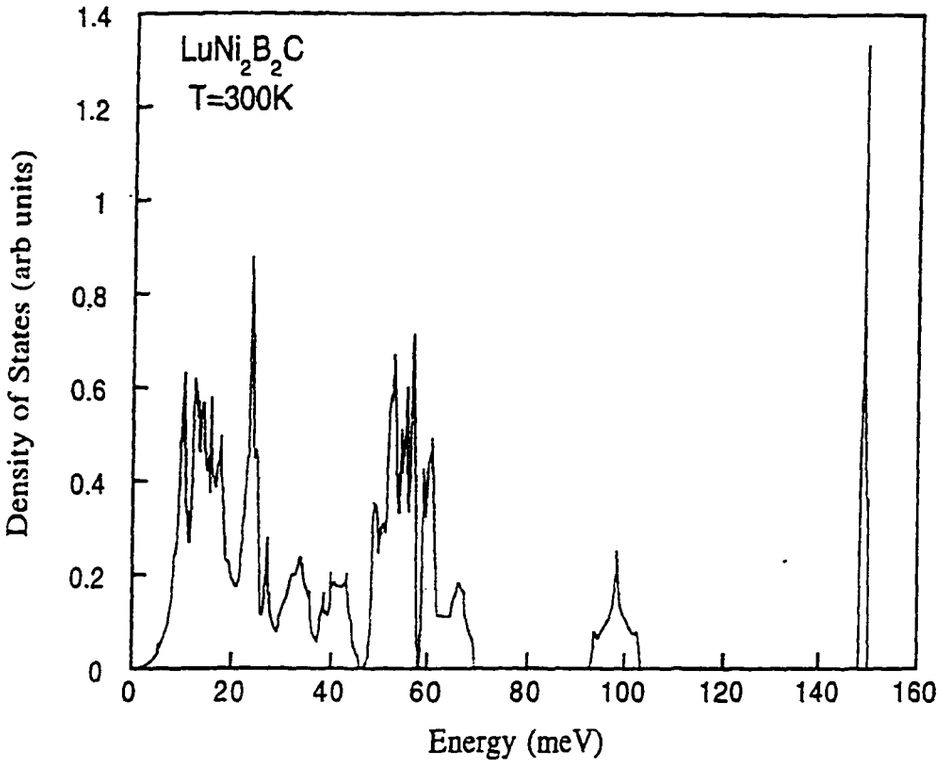

Figure B.3: Phonon density of states g(ν) of $LuNi_2B_2C$ at room temperature, evaluated using the force constants listed in Table B.4.

Table B.1: Measured phonon frequencies (meV) of $LuNi_2B_2C$ along the $[\xi,0,0]$.

ξ	Δ_4
0.1	3.2±.1
0.2	6.0±.1
0.3	8.2±.1
0.4	9.2±.2
0.5	9.4±.5
0.5	9.3±1.
0.7	8.8±.5
0.8	8.4±.4
0.9	8.0±.3
1.0	8.0±.3

ξ	Δ_4 #2
0.0	15.2±.2
0.1	15.1±.3
0.15	14.9±.2
0.2	14.5±.2
0.45	11.6±.4
0.5	11.4±.3
0.5	11.9±.3
0.6	14.2±.3
0.7	15.4±.3
0.8	13.7±.3

ξ	Δ_4 #3
0.6	26.1±.6
0.8	23.8±.7
1.0	23.8±.5

ξ	Δ_3
0.1	4.9±.2
0.2	7.1±.2
0.3	11.8±.4
0.4	12.2±.3

ξ	Δ_3 #2
0.0	13.8±.3
0.2	15.3±.3
0.3	19.6±.4
0.5	26.5±.4
0.8	32.8±.5
0.9	34.9±.7

ξ	Δ_2
0.1	7.5±.2
0.2	9.8±.2
0.2	12.3±.2
0.3	16.0±.4
0.4	18.1±.6
0.5	19.3±.5
0.6	17.7±.3
0.7	15.8±.2
0.8	13.4±.2
0.9	10.4±.2
1.0	10.4±.8

ξ	Δ_1 #2
0.0	13.8±.3
0.1	15.0±.3
0.2	16.5±.3
0.2	18.4±.3
0.4	22.5±.3
0.5	23.4±.5
0.6	23.7±.5
0.7	24.3±.8
0.8	25.6±.8
0.9	26.0±.4
1.0	26.4±.4

ξ	Δ_1 #3
0.0	23.4±.3
0.1	23.6±.3
0.2	23.0±.3
0.3	23.0±.4
0.4	27.0±.5
0.5	30.5±.5

Table B.2: Measured phonon frequencies (meV) of $LuNi_2B_2C$ along the $[0,0,\zeta]$ and $[\xi,\xi,0]$.

ζ	Λ_3	ζ	Λ_1 #2	ξ	Σ_1 #2
0.2	2.4±.2	0.1	15.4±.2	0.1	17.0±.3
0.3	3.3±.2	0.2	15.4±.2	0.2	24.6±.1
0.4	4.2±.1	0.3	16.0±.2	0.3	32.0±.3
0.5	5.2±.3	0.4	17.1±.2	0.5	35.8±1.
0.6	6.1±.2	0.5	18.4±.2		
0.7	7.1±.2	0.6	20.0±.3		
0.8	7.8±.2	0.7	22.0±.4		
0.9	8.6±.2	0.9	24.8±.3		
1.0	8.9±.2				

ζ	Λ_3 #2	ζ	Λ_2	ξ	Σ_3
0.1	14.2±.2	0.2	23.4±.3	0.1	4.6±.3
0.2	13.8±.2	0.4	23.7±.3	0.2	6.6±.2
0.4	13.0±.2	0.7	23.8±.4	0.2	8.7±.2
0.6	12.2±.2	0.8	24.1±.4	0.3	10.6±.3
0.7	11.4±.4			0.3	12.5±.3
0.8	10.8±.3			0.4	13.9±.3
0.9	10.0±.7			0.4	15.0±.4
				0.5	15.7±.3
ζ	Λ_1	ξ	Σ_1	0.5	16.9±.4
0.2	4.3±.4	0.1	6.2±.4		
0.3	6.3±.3	0.1	9.8±.4	ξ	Σ_3 #2
0.4	7.8±.2	0.2	13.0±.2	0.1	14.0±.5
0.5	8.4±.3	0.2	15.4±.6	0.2	15.0±.6
0.6	8.9±.3				
0.7	9.0±.3				
0.8	8.2±.2				
0.9	8.2±.3				
1.0	8.3±.3				

Table B.3: Measured phonon frequencies (meV) of YNi_2B_2C along the $[\xi,0,0]$ and $[0,0,\zeta]$ directions.

ξ	Δ_4
0.1	4.04
0.15	5.5
0.25	8.9
0.35	11.3
0.4	12
0.45	12
0.5	12
0.55	12
0.6	11.6
0.7	12.5

ξ	Δ_4 #2
0	20.3
0.1	20
0.15	18.8
0.2	18.7
0.25	18.1
0.3	17.4
0.35	16.7
0.4	15.5
0.45	14.7

ξ	Δ_1
0.15	12
0.2	15.4

ξ	Δ_1 #2
0	18
0.4	23
0.5	23.5

ξ	Δ_1 #3
0	24
0.35	24
0.4	26

ζ	Λ_3
0.2	2.6
0.6	7
0.95	9.5

Table B.4: The longitudinal (l) and transverse (t) short-range force constants for (D_0 + D_-) used in the Born-von Kármán model fit for the lowest lying branches of $LuNi_2B_2C$ and YNi_2B_2C.

		$LuNi_2B_2C$		
Pair	Shell	r Å	(l) 10^3 dyn/cm	(t) 10^3 dyn/cm
C-C	1st	3.46	23.03	2.67
C-Lu	1st	2.45	53.20	-21.76
C-B	1st	1.49	320.77	3.06
C-Ni	1st	3.17	9.60	4.77
Lu-Lu	1st	3.46	35.90	3.51
Lu-B	1st	2.87	18.86	6.68
Lu-Ni	1st	3.17	16.22	-7.15
B-B	1st	3.46	4.96	-10.93
B-B	1st	2.98	0.67	-10.14
B-Ni	1st	2.09	62.30	0.59
Ni-Ni	1st	3.46	-7.42	4.59
Ni-Ni	1st	2.45	72.36	-3.15

		YNi_2B_2C		
Pair	Shell	r Å	(l) 10^3 dyn/cm	(t) 10^3 dyn/cm
C-C	1st	3.55	45.97	35.07
C-Lu	1st	2.51	44.98	-20.80
C-B	1st	1.47	308.69	15.06
C-Ni	1st	3.16	11.03	4.06
Lu-Lu	1st	3.55	1.28	-15.26
Lu-B	1st	2.90	28.36	20.84
Lu-Ni	1st	3.16	8.07	-9.38
B-B	1st	3.55	-10.39	-3.78
B-B	1st	2.93	-24.26	-32.39
B-Ni	1st	2.11	34.91	17.14
Ni-Ni	1st	3.55	4.19	-12.91
Ni-Ni	1st	2.50	50.90	-2.05

Table B.5: Elastic constants (10^{12} dyn/cm^2) obtained by fittingthe room temperature data of LuNi2B2C to a model.

C_{11}	2.59
C_{12}	0.15
C_{33}	2.48
C_{44}	0.57
C_{66}	1.37

References

1. R. Nagarajan, C. Maxamundar, Z. Hossain, S.K. Dhar, K.V. Golparrishnan, L.C. Gupta, C. Godart, B.D. Padalia, and R. Vijazarahgavan, *Phys. Rev. Lett.* **72**, 274 (1994).

2. R.J. Cava, H. Takagi, H.W. Zandbergen, J.J. Krajewski, W.F. Peck, Jr., T. Siegrist, B. Batlogg, R.B. van Dover, R.J. Felder, K. Mizuhashi, J.O. Lee, H. Eisaki, And S. Uchida, *Nature* **367**, 252 (1994).

3. T. Siegrist, H.W. Zandbergen, R.J. Cava, J.J. Krajewski, and W.F. Peck, Jr., *Nature* **367**, 254 (1994).

4. R. Cava, H. Takagi, B. Batlogg, H.W. Zandbergen, J.J. Krajewski, W.F. Peck, Jr., R.B. van Dover, R.J. Felder, T. Siegrist, K. Mizuhashi, J.O. Lee, H. Eisaki, S.A. Cater, and S. Uchida, *Nature* **367**, 146 (1994).

5. H. Eisaki, H. Takagi, R.J. Cava, K. Mizuhashi, J.O. Lee, B. Batlogg, J.J. Krajewski, W.F. Peck, Jr., and S. Uchida, *Phys. Rev. B* **50**, 647 (1994).

6. B.K. Cho, P.C. Canfield, and D.C. Johnston, *Phys. Rev. B* **52**, 3844 (1997).

7. P. Dervenagas, J. Zarestky, C. Stassis, A.I. Goldman, P.C. Canfield, B.K. Cho, *Physica B* **212**, 1 (1995).

8. C. Stassis and A. Goldman, *J. Alloys and Comp.* **250**, 603 (1997).

9. J. Lynn, *J. Alloys and Comp.* **250**, 552 (1997).

10. J. Zarestky, C. Stassis, A.I. Goldman, P.C. Canfield, P. Dervenagas, B.K. Cho, and D.C. Johnston, *Phys. Rev. B* **51**, 678 (1995).

11. S.K. Sinha, J.W. Lynn, T.E. Grigereit, Z. Hossain, L.C. Gupta, R. Nagarajan, and C. Godart, *Phys. Rev. B* **51**, 681 (1995).

12. A.I. Goldman, C. Stassis, P.C. Canfield, J. Zarestky, P. Dervenagas, B.K. Cho, D.C. Johnston, *Phys. Rev. B* **50**, 9668 (1994).

13. T. Vogt, A. Goldman, B. Sternlieb, and C. Stassis, *Phys. Rev. Lett.* **75**, 2628 (1995).

14.P. Dervenagas, J. Zarestky, C. Stassis, A.I. Goldman, P.C. Canfield, B.K. Cho, *Phys. Rev. B* **53**, 8506 (1996).

15.C. Detlefs, A.I. Goldman, C. Stassis, P. Canfield, B.K. Cho, J.P. Hill, D. Gibbs, *Phys. Rev. B* **53**, 6355 (1996).

16.J.Y. Rhee, X. Wang, and B.N. Harmon, *Phys. Rev. B* **51**, 15585 (1995).

17.W.E. Pickett and D.J. Singh, *Phys. Rev. Lett.* **72**, 3702 (1994).

18.L.F. Mattheiss, *Phys. Rev. B* **49**, 13279 (1994).

19.R. Coehoorn, *Physica C* **228**, 5671 (1994).

20.L.F. Mattheiss, T. Siegrist, and R.J. Cava, *Sol. State Commun.* **91**, 587 (1994).

21.P. Dervenagas, J. Zarestky, C. Stassis, A.I. Goldman, P.C. Canfield, B.K. Cho, *Phys. Rev. B* **53**, 8506 (1996).

22.K. Kawano, H. Yoshizawa, H. Takeya, and K. Kadownki, *Phys. Rev. Lett.* **77**, 4628 (1996).

23.F. Gompf, W. Reichardt, H. Schober, B. Renker, and M. Bchgeister, *Phys. Rev. B* **55**, 9058 (1997).

24.I.K Yanson, V.V. Fisun, A.G.M. Jansen, P. Wyder, P.C. Canfield, B.K. Cho, C.V. Tomy, and D. McK. Paul, *Phys. Rev. Lett.* **28**, 935 (1997).

25.C. Stassis, M. Bullock, J. Zarestky, P. Canfield, A. Goldman, G. Shirane, S.M. Shapiro, *Phys. Rev. B* **55**, R8678 (1997).

26.M. Bullock, J. Zarestky, C. Stassis, A. Goldman, P. Canfield, Z Honda, G. Shirane, S.M. Shapiro, *Phys. Rev. B* (to be published).

27.M. Bullock, C. Stassis, J. Zarestky, A. Goldman, P. Canfield, G. Shirane, S. Shapiro, *Physica B*, (ICNS 97 conference preceedings to be published).

28.M. Xu, P.C. Canfield, J.E. Ostenson, D.K. Finnemore, B.K. Cho, Z.R. Wang, and D.C. Johnston, Physica C 227, 321 (1994).

29.V.G. Hadjiev, L.N. Bozukov, M.G. Baychev, *Phys. Rev. B* **50**, 16726 (1994).

30.H.J. Park, H.S. Shin, H.G. Lee, I.S. Yang, W.C. Lee, B.K. Cho, P.C. Canfield, D.C. Johnston, *Phys. Rev. B* **53**, 2237 (1996).

31.D. Royer, E. Dieulesaint, *J. Acoust. Soc. Am.* **76**, 1438 (1984).

32.R. Stoneley, *Proc. R. Soc. London, Ser. A* **232**, 447 (1955).

33.F.H. Featherston, J.R. Neughbours, *Phys. Rev.* **130**, 1324 (1963).

34.H. Michor, T. Holubar, C. Dasek, and G. Hilscher, *Phys. Rev B* **52**, 16165 (1995).

APPENDIX C: EXPERIMENTAL DATA FOR $LuNi_2B_2C$

The phonon dispersion curves for $LuNi_2B_2C$ were measured at the HFIR on the triple axis spectrometers HB1A, HB1, HB2, and HB3, and at the HFBR on the triple axis spectrometers H-7 and H-8. The dispersion curves were determined along the [100], [001], and [110] symmetry directions at varying temperatures from room temperature down to 1.8 K.

The typical experimental setup used for these scans are described in the introductory chapter of this thesis. To quickly summarize the experimental setup, most of the experimental data was obtained with phonon creation with a fixed final energy E_f equal to 14.7 meV. Some experiments were done at 30.5 meV also. Most of the experimental scan used constant Q, although some of the steeper dispersion curves were done in a constant energy configuration. Typically, we used collimation of 40'-monochromator-40'-sample-40'-analyzer-80'-detector, although tighter collimation was also used in some experiments. Most of the data collected at the HFIR was done with two crystal mounted together. For the low temperature experiments at HBRF, most of those experiments were done with only one single crystal.

The early work done on $LuNi_2B_2C$ was done at the HFIR reactor at Oak Ridge National Laboratory. This is where the

phonon softening of the two lowest Δ_4 branches was first observed, which resulted in our first paper which is chapter 2 of this thesis. After Kwano's paper on the YNi_2B_2C compound came out in *Physical Review Letters*, we then went back and studied the Lu compound in more detail. Those results are published in chapters 3-5 of this thesis. Most of this work was done in collaboration with Gen Shirane and Steve Shapiro of Brookhaven National Laboratory. These later experiments which looked exclusively at the phonon softening of the two lowest Δ_4 brances were done at BNL.

Table B.1 and B.2 contain a summary of most of the experimental phonon data collected on the $LuNi_2B_2C$ compound up to date. Table C.1 contains the temperature dependent data done at both the HFIR and HFRB for the two lowest Δ_4 branches. Table C.2 contains all other branches along the Δ direction as well as experimental data in the Λ and Σ directions. These tables differ from the experimental data in Appendix B in that this is a complete set of experimental data and the data in Appendix B is only the data used in the Born-von Kármán lattice dynamical calculations. The data in Appendix B are basically a summary of the room temperature data given in Tables C.1 and C.2.

Table C.1: Experimental data for the two Δ_4 branches that exhibit softening in $LuNi_2B_2C$.

Branch/q	Machine	Q	Date	T[K]	ω(meV)	Error
Δ_4						
0.10	HB3	(-0.1,0,8)	Apr-95	300	3.35	0.15
0.10	HB1A	(-0.1,0,8)	Mar-95	300	3.30	0.10
0.10	HB2	(0.1,0,8)	Feb-95	300	3.10	0.10
0.10	HB3	(-0.1,0,8)	Jun-95	300	3.32	0.10
0.20	HB3	(-0.2,0,8)	Apr-95	300	6.10	0.15
0.20	HB2	(0.2,0,8)	Feb-95	300	6.10	0.10
0.20	HB3	(-0.2,0,8)	Jun-95	300	6.00	0.10
0.20	HB3	(-0.2,0,8)	Apr-95	120	6.00	0.15
0.20	H8	(0.2,0,8)	Aug-96	15	5.50	0.20
0.20	H8	(0.2,0,8)	Aug-96	4	5.50	0.20
0.25	HB3	(-0.25,0,8)	Jun-95	2	6.90	0.10
0.30	HB3	(-0.3,0,8)	Apr-95	300	8.16	0.15
0.30	HB3	(0.3,0,8)	Feb-95	300	8.20	0.10
0.30	HB3	(-0.3,0,8)	Jun-95	300	8.10	0.15
0.30	HB3	(-0.3,0,8)	Apr-95	120	8.09	0.10
0.30	H8	(0.3,0,8)	Aug-96	15	7.50	0.20
0.30	HB3	(-0.3,0,8)	Apr-95	10	7.99	0.15
0.30	H8	(0.3,0,8)	Aug-96	4	7.50	0.20
0.30	HB3	(-0.3,0,8)	Jun-95	2	7.80	0.15
0.35	HB3	(-0.35,0,8)	Apr-95	120	8.60	0.20
0.35	H8	(-0.35,0,8)	Aug-96	30	8.00	0.40
0.35	H8	(-0.35,0,8)	Aug-96	15	8.00	0.30
0.35	H8	(-0.35,0,5)	Aug-96	4	7.70	0.20
0.36	H8	(-0.362,0,8)	Aug-96	15	8.00	0.40
0.36	H8	(-0.362,0,8)	Aug-96	4	8.00	0.30
0.38	H8	(-0.375,0,8)	Aug-96	75	8.00	0.40
0.38	H8	(-0.375,0,8)	Aug-96	30	8.00	0.40
0.38	H8	(-0.375,0,8)	Aug-96	15	5.00	0.40
0.38	H8	(-0.375,0,8)	Aug-96	4	5.50	0.30
0.38	H8	(-0.375,0,8)	Aug-96	4	7.50	0.50
0.40	HB2	(0.4,0,8)	Feb-95	300	9.60	0.20
0.40	HB3	(-0.4,0,8)	Jun-95	300	9.20	0.30
0.40	HB3	(-0.4,0,8)	Jun-95	300	9.15	0.20
0.40	HB3	(-0.4,0,8)	Jun-95	300	9.10	0.20
0.40	HB3	(-0.4,0,8)	Apr-95	120	8.49	0.25
0.40	HB3	(-0.4,0,8)	Jun-95	120	8.15	0.20
0.40	HB3	(-0.4,0,8)	Jun-95	60	7.60	0.20
0.40	HB3	(-0.4,0,8)	Aug-96	30	8.00	0.40
0.40	HB3	(-0.4,0,8)	Apr-95	25	7.70	0.25
0.40	HB3	(-0.4,0,8)	Jun-95	25	7.60	0.15
0.40	H8	(-0.4,0,8)	Aug-96	15	8.00	0.30

Table C.1 (continued)

0.40	HB3	(-0.4,0,8)	Apr-95	10	7.60	0.40
0.40	H8	(-0.4,0,8)	Aug-96	4	5.00	0.50
0.40	HB3	(-0.4,0,8)	Jun-95	2	7.50	0.20
0.41	HB3	(-0.41,0,8)	Apr-95	2	6.00	0.30
0.43	HB3	(-0.425,0,8)	Apr-95	120	8.43	0.20
0.43	HB3	(-0.425,0,8)	Apr-95	10	5.10	0.50
0.45	HB3	(-0.45,0,8)	Jun-95	300	8.90	0.50
0.45	HB3	(-0.45,0,8)	Jun-95	300	9.90	0.50
0.45	H8	(0.45,0,8)	Aug-95	75	8.00	0.50
0.45	HB3	(-0.45,0,8)	Jun-95	60	6.25	0.50
0.45	H8	(0.45,0,8)	Aug-95	30	6.00	0.50
0.45	HB3	(-0.45,0,8)	Jun-95	25	6.10	0.50
0.45	H8	(0.45,0,8)	Aug-95	15	6.00	0.30
0.45	HB3	(-0.45,0,8)	Jun-95	10	4.32	0.20
0.45	HB3	(-0.45,0,8)	Apr-95	10	4.20	0.40
0.45	H8	(0.45,0,8)	Aug-95	4	4.50	0.40
0.45	H8	(0.45,0,8)	Aug-96	4	5.00	0.50
0.45	HB3	(-0.45,0,8)	Jun-95	2	4.39	0.20
0.50	HB3	(0.5,0,8)	Jun-95	300	9.14	1.00
0.50	HB3	(-0.5,0,8)	Jun-95	300	9.50	1.00
0.50	HB3	(0.5,0,8)	Apr-95	120	8.74	0.30
0.50	HB3	(0.5,0,8)	Apr-95	120	8.70	0.50
0.50	H8	(0.5,0,8)	Aug-96	75	8.00	0.50
0.50	HB3	(0.5,0,8)	Apr-95	60	6.74	0.60
0.50	HB3	(-0.5,0,8)	Apr-95	60	7.74	0.40
0.50	H8	(0.5,0,8)	Aug-96	30	4.00	0.50
0.50	HB3	(0.5,0,8)	Apr-95	25	6.26	0.50
0.50	HB3	(-0.5,0,8)	Apr-95	25	6.52	0.60
0.50	HB3	(0.5,0,8)	Apr-95	10	3.80	0.50
0.50	HB3	(-0.5,0,8)	Apr-95	10	4.80	0.40
0.50	H8	(0.5,0,8)	Aug-96	4	4.00	0.40
0.50	HB3	(-0.5,0,8)	Jun-95	2	4.60	0.20
0.53	HB3	(-0.525,0,8)	Apr-95	10	6.00	0.30
0.55	HB3	(-0.55,0,8)	Jun-95	300	8.50	0.50
0.55	HB3	(-0.55,0,8)	Jun-95	300	8.60	0.50
0.55	HB3	(0.55,0,8)	Jun-95	300	8.70	0.50
0.55	HB3	(0.55,0,8)	Apr-95	10	5.76	0.40
0.55	H8	(0.55,0,8)	Aug-96	4	5.50	0.40
0.55	HB3	(-0.55,0,8)	Jun-95	2	6.00	0.20
0.60	HB3	(0.6,0,8)	Apr-95	120	8.59	0.15
0.60	HB3	(-0.6,0,8)	Apr-95	10	7.20	0.50
0.60	HB3	(-0.6,0,8)	Jun-95	2	7.00	0.50
0.70	HB3	(0.7,0,8)	Apr-95	300	8.75	0.30
0.70	HB2	(-0.7,0,8)	Feb-95	300	7.70	0.40

Table C.1 (Continued)

0.70	HB3	(0.7,0,8)	Apr-95	120	7.90	0.50
0.70	HB3	(0.7,0,8)	Apr-95	10	8.20	0.60
0.70	HB3	(0.7,0,8)	Jun-95	2	8.00	0.50
0.80	HB3	(0.8,0,8)	Apr-95	300	8.20	0.35
0.80	HB1A	(0.8,0,8)	Mar-95	300	8.00	0.60
0.80	HB2	(-0.8,0,8)	Feb-95	300	8.30	0.30
0.80	HB3	(0.8,0,8)	Apr-95	120	7.90	0.50
0.80	HB3	(0.8,0,8)	Apr-95	10	7.73	0.30
0.80	HB3	(0.8,0,8)	Jun-95	2	7.50	0.50
0.90	HB3	(0.9,0,8)	Apr-95	300	8.00	0.30
0.90	HB1A	(0.9,0,8)	Mar-95	300	8.00	0.70
0.90	HB2	(-0.9,0,8)	Feb-95	300	8.00	1.00
0.90	HB3	(0.9,0,8)	Apr-95	120	8.02	0.30
0.90	HB3	(0.9,0,8)	Apr-95	10	7.17	0.30
0.90	HB3	(0.9,0,8)	Jun-95	2	7.50	0.50
0.95	HB1A	(0.95,0,8)	Mar-95	300	7.45	0.15
0.95	HB3	(0.95,0,8)	Jun-95	2	7.00	0.30
1.00	HB3	(1,0,8)	Apr-95	300	8.34	0.30
1.00	HB1A	(1,0,8)	Mar-95	300	8.00	0.70
1.00	HB2	(-1,0,8)	Feb-95	300	8.30	0.30
1.00	HB2	(-1,0,10)	Feb-95	300	8.10	0.30
1.00	HB3	(1,0,8)	Apr-95	10	6.93	0.30
1.00	HB3	(1,0,8)	Jun-95	2	6.66	0.60
Δ_4 #2						
0.00	HB3	(0,0,8)	Apr-95	300	15.19	0.15
0.00	HB3	(1,0,7)	Apr-95	300	15.09	0.30
0.00	HB2	(1,0,7)	Feb-95	300	15.60	0.40
0.10	HB2	(0.9,0,7)	Feb-95	300	15.10	0.30
0.15	HB3	(0.15,0,8)	Apr-95	300	14.87	0.15
0.20	HB2	(0.8,0,7)	Feb-95	300	14.50	0.20
0.25	HB3	(0.25,0,8)	Apr-95	300	14.18	0.20
0.25	HB3	(0.25,0,8)	Jun-95	300	14.22	0.20
0.25	HB3	(0.25,0,8)	Apr-95	120	14.06	0.20
0.25	HB3	(0.25,0,8)	Apr-95	10	13.94	0.20
0.25	HB3	(0.25,0,8)	Jun-95	2	13.80	0.20
0.30	HB3	(0.3,0,8)	Jun-95	2	13.10	0.15
0.35	HB3	(0.35,0,8)	Apr-95	300	12.80	0.20
0.35	HB2	(0.65,0,7)	Feb-95	300	12.70	0.20
0.35	HB3	(0.35,0,8)	Jun-95	300	12.70	0.20
0.35	HB3	(0.35,0,8)	Apr-95	120	12.33	0.25
0.40	HB2	(-0.4,0,10)	Feb-95	300	11.40	0.40
0.40	HB3	(0.4,0,8)	Jun-95	300	11.85	0.20
0.40	HB3	(-0.4,0,8)	Jun-95	300	11.50	0.30
0.40	HB3	(0.4,0,8)	Apr-95	120	11.08	0.30

Table C.1 (Continued)

0.40	HB3	(0.4,0,8)	Jun-95	120	10.75	0.20
0.40	HB3	(0.4,0,8)	Jun-95	60	10.57	0.20
0.40	HB3	(0.4,0,8)	Apr-95	25	10.50	0.30
0.40	HB3	(0.4,0,8)	Jun-95	25	10.44	0.20
0.40	HB3	(0.4,0,8)	Apr-95	10	10.40	0.30
0.40	HB3	(0.4,0,8)	Jun-95	2	10.80	0.30
0.45	HB3	(0.45,0,8)	Jun-95	300	11.15	0.25
0.45	HB3	(0.45,0,8)	Jun-95	300	11.73	0.30
0.45	HB3	(0.45,0,8)	Jun-95	300	11.23	0.30
0.45	HB3	(0.45,0,8)	Jun-95	60	9.60	1.00
0.45	HB3	(0.45,0,8)	Jun-95	25	9.00	1.00
0.45	HB3	(0.45,0,8)	Jun-95	10	8.70	1.50
0.45	HB3	(0.45,0,8)	Jun-95	2	8.50	1.00
0.46	HB3	(0.46,0,8)	Apr-95	120	11.00	0.50
0.50	HB3	(0.5,0,8)	Apr-95	300	11.73	0.25
0.50	HB3	(0.5,0,8)	Apr-95	300	11.53	0.30
0.50	HB3	(-0.5,0,8)	Apr-95	300	12.20	0.15
0.50	HB3	(-0.5,0,8)	Apr-95	300	12.00	0.30
0.50	HB1A	(-0.5,0,8)	Mar-95	300	11.85	0.20
0.50	HB2	(0.5,0,8)	Feb-95	300	12.40	0.20
0.50	HB3	(0.5,0,8)	Jun-95	300	11.38	0.30
0.50	HB3	(-0.5,0,8)	Jun-95	300	11.80	0.30
0.50	HB3	(-0.5,0,8)	Jun-95	300	11.85	0.30
0.50	HB3	(0.5,0,8)	Apr-95	120	9.50	0.50
0.50	HB3	(-0.5,0,8)	Apr-95	120	9.50	0.40
0.50	HB3	(-0.5,0,8)	Apr-95	120	9.24	0.40
0.50	HB3	(-0.5,0,8)	Apr-95	10	9.30	0.40
0.50	HB3	(-0.5,0,8)	Jun-95	2	8.90	1.00
0.55	HB3	(-0.55,0,8)	Jun-95	300	12.93	0.30
0.55	HB3	(-0.55,0,8)	Jun-95	300	13.14	0.30
0.55	HB3	(-0.55,0,8)	Jun-95	300	12.88	0.30
0.55	HB3	(0.55,0,8)	Jun-95	300	12.48	0.30
0.55	HB3	(-0.55,0,8)	Apr-95	10	8.45	0.50
0.55	HB3	(-0.55,0,8)	Jun-95	2	8.50	1.00
0.60	HB3	(-0.6,0,8)	Apr-95	300	14.22	0.25
0.60	HB1A	(-0.6,0,8)	Mar-95	300	14.13	0.25
0.60	HB1A	(-0.6,0,8)	Mar-95	300	14.50	0.80
0.60	HB2	(0.6,0,8)	Feb-95	300	14.10	0.40
0.60	HB3	(0.6,0,8)	Jun-95	300	13.30	0.40
0.60	HB3	(-0.6,0,8)	Apr-95	120	12.91	0.20
0.60	HB3	(-0.6,0,8)	Apr-95	10	10.30	0.50
0.60	HB3	(0.6,0,8)	Jun-95	2	11.50	1.00
0.65	HB3	(-0.65,0,8)	Apr-95	300	15.06	0.30
0.65	HB3	(0.65,0,8)	Jun-95	300	14.72	0.30

Table C.1 (Continued)

0.65	HB3	(-0.65,0,8)	Apr-95	120	13.88	0.30
0.65	HB3	(-0.65,0,8)	Apr-95	60	13.36	0.25
0.65	HB3	(-0.65,0,8)	Apr-95	25	13.23	0.30
0.65	HB3	(-0.65,0,8)	Apr-95	10	13.00	0.60
0.70	HB3	(-0.7,0,8)	Apr-95	300	15.38	0.20
0.70	HB3	(0.7,0,8)	Apr-95	300	15.21	0.25
0.70	HB2	(-0.7,0,8)	Feb-95	300	15.60	0.20
0.70	HB1A	(-0.7,0,8)	Mar-95	300	16.30	0.70
0.70	HB3	(0.7,0,8)	Apr-95	120	14.80	0.40
0.70	HB3	(-0.7,0,8)	Apr-95	10	14.00	0.30
0.70	HB3	(0.7,0,8)	Jun-95	2	14.00	0.70
0.75	HB1A	(0.75,0,8)	Mar-95	300	15.06	0.30
0.80	HB3	(0.8,0,8)	Apr-95	300	13.75	0.30
0.80	HB1A	(0.8,0,8)	Mar-95	300	14.00	1.00
0.80	HB2	(-0.8,0,8)	Feb-95	300	13.50	1.00
0.80	HB3	(0.8,0,8)	Jun-95	300	13.76	0.40
0.80	HB3	(0.8,0,8)	Apr-95	120	13.70	0.50
0.80	HB3	(0.8,0,8)	Apr-95	10	13.42	0.30
0.80	HB3	(0.8,0,8)	Jun-95	2	13.30	0.50
0.85	HB3	(0.85,0,8)	Jun-95	300	12.20	0.50
0.90	HB3	(0.9,0,8)	Jun-95	300	11.00	1.00

Table C.2: Experimental data for the other branches in $LuNi_2B_2C$

Branch/q	Machine	Q	Date	ω(meV)	Error
Δ_1					
0.05	HB3	(2.05,0,0)	Jun-95	4.00	0.20
0.11	HB2	(2.11,0,0)	Mar-95	7.50	0.20
0.15	HB3	(2.15,0,0)	Apr-95	9.75	0.30
0.15	HB3	(2.15,0,0)	Aug-95	9.54	0.20
0.15	HB3	(2.15,0,0)	Aug-95	9.90	0.20
0.15	HB1A	(2.15,0,0)	Aug-95	9.90	0.20
0.20	HB2	(2.195,0,0)	Feb-95	12.00	0.30
0.20	HB2	(2.2,0,0)	Feb-95	12.30	0.20
0.25	HB3	(2.25,0,0)	Jun-95	13.90	0.35
0.29	HB2	(2.294,0,0)	Feb-95	16.00	0.40
0.35	HB3	(2.35,0,0)	Apr-95	17.00	0.30
0.35	HB1A	(2.35,0,0)	Feb-95	17.40	0.40
0.35	HB3	(2.35,0,0)	Jun-95	17.00	0.50
0.35	HB3	(2.35,0,0)	Aug-95	16.80	0.40
0.40	HB2	(2.4,0,0)	Feb-95	18.50	0.50
0.40	HB3	(0.6,0,9)	Jun-95	17.70	0.35
0.50	HB3	(2.5,0,1)	Apr-95	19.30	0.50
0.60	HB3	(2.4,0,1)	Apr-95	17.60	0.30
0.60	HB3	(2.4,0,1)	Jun-95	17.70	0.30
0.65	HB1A	(2.35,0,1)	Mar-95	16.60	0.60
0.70	HB3	(2.3,0,1)	Apr-95	15.60	0.20
0.80	HB1A	(2.2,0,1)	Apr-95	13.40	0.15
0.85	HB3	(2.15,0,1)	Jun-95	11.84	0.30
0.90	HB3	(2.1,0,1)	Apr-95	10.50	0.15
0.90	HB1A	(2.1,0,1)	Mar-95	10.40	0.15
0.95	HB1A	(2.05,0,1)	Mar-95	9.60	0.15
1.00	HB3	(2,0,1)	Apr-95	9.42	0.15
Δ_1 #2					
0.05	HB1A	(2.05,0,0)	Mar-95	14.05	0.30
0.15	HB1A	(2.15,0,0)	Mar-95	16.60	0.25
0.20	HB1A	(2.2,0,0)	Mar-95	18.40	0.25
0.25	HB1A	(2.25,0,0)	Mar-95	20.40	0.50
0.25	HB3	(2.25,0,0)	Jun-95	20.60	0.50
0.30	HB1A	(2.3,0,0)	Mar-95	23.00	0.40
0.30	HB3	(0.7,0,9)	Jun-95	22.30	0.60
0.40	HB1A	(0.6,0,9)	Mar-95	22.00	0.40
0.40	HB3	(0.6,0,9)	Jun-95	22.40	0.30
0.40	HB3	(0.6,0,9)	Jun-95	22.40	0.50
0.50	HB3	(0.5,0,9)	Apr-95	23.46	0.50
0.50	HB1A	(0.5,0,9)	Mar-95	23.42	0.60
0.60	HB1A	(0.4,0,9)	Mar-95	23.70	0.50

Table C.2 (Continued)

0.70	HB1A	(0.3,0,9)	Mar-95	24.50	0.80
0.80	HB1A	(1.8,0,9)	Mar-95	25.50	1.00
0.80	HB1A	(0.2,0,9)	Mar-95	25.80	0.70
0.90	HB3	(0.1,0,9)	Apr-95	25.15	0.40
0.90	HB1A	(0.1,0,9)	Mar-95	26.00	0.40
1.00	HB1A	(0,0,9)	Mar-95	26.40	0.40
Δ_1 #3					
0.00	HB1A	(1,0,9)	Mar-95	23.60	0.60
0.00	HB3	(1,0,9)	Jun-95	23.40	0.30
0.10	HB3	(0.9,0,9)	Apr-95	23.54	0.30
0.20	HB1A	(0.8,0,9)	Mar-95	25.50	0.40
0.20	HB3	(0.8,0,9)	Jun-95	23.00	0.25
0.40	HB1A	(2.4,0,0)	Mar-95	27.10	0.50
0.50	HB3	(2.5,0,0)	Jun-95	30.50	0.60
0.50	HB1A	(2.5,0,0)	Mar-95	30.70	0.50
Δ_3					
0.10	HB3	(2,0.1,0)	Aug-95	4.94	0.15
0.15	HB3	(2,0.15,0	Aug-95	7.00	0.20
0.15	HB3	(2,0.15,0)	Aug-95	7.10	0.15
0.30	HB3	(2,0.3,0)	Aug-95	11.75	0.50
0.40	HB3	(2,0.4,0)	Aug-95	13.20	0.30
Δ_3 #2					
0.15	HB3	(2,0.15,0)	Aug-95	15.25	0.30
0.30	HB3	(2,0.3,0)	Aug-95	19.70	0.40
0.50	HB3	(2,0.5,0)	Aug-95	26.50	0.40
0.75	HB3	(4,0.75,0)	Aug-95	32.80	0.50
0.90	HB3	(4,0.9,0)	Aug-95	34.90	0.70
1.00	HB3	(4,1,0)	Aug-95	36.00	2.00
Δ_4 #2					
0.60	HB3	(0.6,0,10)	Jun-95	26.05	0.60
0.70	HB3	(0.7,0,10)	Jun-95	24.30	0.60
0.80	HB3	(0.8,0,10)	Jun-95	23.80	0.70
1.00	HB3	(1,0,10)	Jun-95	23.90	0.50
Λ_3					
0.20	HB3	(2,0,0.2)	Jun-95	2.23	0.10
0.20	HB3	(2,0,0.2)	Apr-95	2.26	0.15
0.20	HB2	(2,0,-0.2)	Feb-95	2.20	0.15
0.30	HB3	(2,0,0.3)	Apr-95	3.34	0.15
0.30	HB1A	(2,0,0.3)	Mar-95	3.21	0.15
0.30	HB2	(2,0,-0.3)	Feb-95	3.50	0.10
0.30	HB3	(2,0,0.3)	Jun-95	3.32	0.15
0.40	HB3	(2,0,0.4)	Jun-95	4.26	0.10
0.50	HB3	(2,0,0.5)	Apr-95	5.22	0.15

Table C.2 (Continued)

0.50	HB2	(2,0,-0.5)	Feb-95	5.50	0.10
0.60	HB3	(2,0,0.6)	Jun-95	6.07	0.15
0.70	HB2	(2,0,-0.7)	Feb-95	7.10	0.10
0.80	HB3	(2,0,0.8)	Apr-95	7.78	0.15
0.80	HB1A	(2,0,0.8)	Mar-95	7.76	0.15
0.90	HB2	(2,0,-0.9)	Feb-95	8.60	0.10
0.90	HB3	(2,0,0.9)	Apr-95	8.57	0.15
0.95	HB3	(2,0,0.95)	Apr-95	8.89	0.15
0.95	HB3	(2,0,0.95)	Jun-95	8.80	0.10
1.00	HB3	(2,0,1)	Apr-95	9.42	0.10
1.00	HB2	(2,0,-1)	Feb-95	9.40	0.10
Λ_3 #2					
0.00	HB3	(2,0,0)	Apr-95	13.88	0.20
0.00	HB3	(2,0,0)	Jun-95	13.88	0.20
0.05	HB3	(2,0,-0.05)	Apr-95	14.01	0.15
0.20	HB3	(2,0,-0.2)	Apr-95	13.77	0.15
0.20	HB2	(4,0,0.2)	Feb-95	13.70	0.50
0.40	HB3	(2,0,-0.4)	Apr-95	13.01	0.20
0.40	HB1A	(2,0,-0.4)	Mar-95	12.95	0.30
0.40	HB2	(4,0,0.4)	Feb-95	13.30	0.30
0.60	HB3	(2,0,-0.6)	Apr-95	12.17	0.20
0.60	HB2	(4,0,0.6)	Feb-95	12.10	0.30
0.60	HB1A	(2,0,-0.6)	Mar-95	12.00	0.25
0.70	HB2	(2,0,0.7)	Feb-95	11.30	0.40
0.80	HB3	(2,0,-0.8)	Apr-95	10.85	0.25
0.80	HB1A	(2,0,-0.8)	Mar-95	10.50	0.25
0.90	HB3	(2,0,-0.9)	Apr-95	10.10	0.20
0.90	HB1A	(2,0,-0.9)	Mar-95	10.00	0.70
Λ_1					
0.20	HB3	(0,0,8.2)	Jun-95	4.30	0.40
0.30	HB2	(0,0,8.3)	Feb-95	6.30	0.30
0.40	HB3	(0,0,8.4)	Apr-95	8.08	0.20
0.40	HB1A	(0,0,8.4)	Mar-95	8.07	0.15
0.40	HB2	(0,0,8.4)	Feb-95	7.80	0.40
0.50	HB2	(0,0,8.5)	Feb-95	8.40	0.30
0.60	HB3	(0,0,8.6)	Apr-95	8.80	0.25
0.60	HB2	(0,0,8.6)	Feb-95	8.90	0.30
0.70	HB2	(0,0,8.7)	Feb-95	9.00	0.30
0.70	HB3	(0,0,8.7)	Jun-95	8.92	0.25
0.80	HB3	(0,0,8.8)	Jun-95	8.21	0.20
0.80	HB2	(0,0,10.8)	Feb-95	7.70	0.50
0.90	HB3	(0,0,8.9)	Apr-95	8.39	0.15
0.90	HB2	(0,0,10.9)	Feb-95	8.90	0.30
0.95	HB3	(1,0,7.95)	Jun-95	8.23	0.25

Table C.2 (Continued)

1.00	HB3	(1,0,8)	Jun-95	8.24	0.15
Λ_1 #2					
0.00	HB3	(0,0,8)	Apr-95	15.19	0.15
0.10	HB3	(0,0,8.1)	Jun-95	15.00	0.25
0.20	HB3	(0,0,8.2)	Apr-95	15.38	0.20
0.20	HB3	(0,0,8.2)	Jun-95	16.04	0.15
0.30	HB1A	(0,0,8.3)	Mar-95	16.04	0.15
0.40	HB1A	(0,0,8.4)	Mar-95	17.10	0.15
0.50	HB1A	(0,0,8.5)	Mar-95	18.40	0.20
0.60	HB1A	(0,0,8.6)	Mar-95	20.10	0.30
0.70	HB1A	(0,0,8.7)	Mar-95	22.10	0.10
0.90	HB3	(0,0,8.9)	Apr-95	24.96	0.20
0.90	HB1A	(0,0,8.9)	Mar-95	24.80	0.25
1.00	HB1A	(0,0,9)	Mar-95	26.40	0.40
Λ_2					
0.00	HB3	(1,0,9)	Jun-95	23.40	0.30
0.20	HB3	(1,0,9.2)	Jun-95	23.40	0.30
0.40	HB3	(1,0,9.4)	Jun-95	23.70	0.30
0.70	HB3	(1,0,9.7)	Jun-95	23.80	0.30
0.80	HB3	(1,0,9.8)	Jun-95	24.10	0.35
1.00	HB3	(1,0,10)	Jun-95	23.80	0.40
Σ_1					
0.06	HB3	(2.06,.06,0)	Aug-95	6.00	0.30
0.10	HB3	(2.1,2.1,0)	Aug-95	9.80	0.40
0.15	HB3	(2.15,2.15,0)	Aug-95	15.50	0.50
0.40	HB3	(1.6,2.4,0)	Aug-95	18.40	1.00
Σ_1 #2					
0.00	HB3	(2,2,0)	Aug-95	13.80	0.30
0.10	HB3	(2.1,2.1,0)	Aug-95	17.00	0.30
0.20	HB3	(2.2,2.2,0)	Aug-95	24.60	0.40
0.30	HB3	(2.3,2.3,0)	Aug-95	32.00	0.60
0.50	HB3	(2.5,2.5,0)	Aug-95	36.00	1.50
Σ_3					
0.10	HB3	(2.1,0.1,0)	Aug-95	4.54	0.25
0.13	HB3	(2.13,0.13,0)	Aug-95	6.60	0.20
0.20	HB3	(2.2,.2,0)	Aug-95	8.70	0.20
0.25	HB3	(2.25,0.25,0)	Aug-95	10.60	0.30
0.30	HB3	(2.3,0.3,0)	Aug-95	12.50	0.30
0.40	HB3	(1.6,2.4,0)	Aug-95	15.00	0.40
0.40	HB3	(3.6,0.4,0)	Aug-95	15.00	0.60
0.45	HB3	(2.45,0.45,0)	Aug-95	15.70	0.30
0.50	HB3	(1.5,2.5,0)	Aug-95	16.80	0.60
0.50	HB3	(1.5,2.5,0)	Aug-95	16.90	0.40

Table C.2 (Continued)

Σ_3 #2					
	0.10 HB3	(1.9,2.1,0)	Aug-95	14.00	0.50
	0.25 HB3	(1.75,2.25,0)	Aug-95	16.10	0.60

APPENDIX D. DYSON'S EQUATION

This appendix will follow the derivation given by Mattuck.[74]

Before we get to Dyson's equation, we will talk briefly about Green's function propagators. The Green's function propagator is usually in the form

$$G(k_2,k_1,t_2-t_1)=-i\langle\psi_0|T\{c_{k_2}(t_2)c_{k_1}^{\dagger}(t_1)\}|\psi_0\rangle,$$

where $c_k^{\dagger}(t)$ and $c_k(t)$ create and destroy a particle at time t, T is the Wick time-ordering operator, and ψ_0 is the exact normalized wave function of the ground state of the interacting N-particle system. These creation and destruction operators are in the 'Heisenberg picture' defined by

$$c_{k_1}^{\dagger}(t_1)=e^{iHt_1}c_{k_1}^{\dagger}e^{-iHt_1}$$

$$c_{k_2}^{\dagger}(t_2)=e^{iHt_2}c_{k_2}^{\dagger}e^{-iHt_2},$$

where H is the Hamiltonian of the interacting system. The Green's function propagator defined above destroys a particle at k_2, t_2, and creates a particle at k_1, t_1. Essentially, the Green's function propagator is a probability amplitude that the system will go from an initial state to a final state. The Green's function includes all intermediate states in the probability amplitude. Since there is an infinite number of possible intermediate states, the Green's function can end up representing an infinite series of possible states. Typically, instead of looking at this infinite number of

states, the series is transformed as a geometrical series into a single expression. This greatly simplifies the problem, but it still leaves the determination of the single expression.

To derive Dyson's equation, we will have to use methods that go beyond ordinary perturbation theory. This will require the infinite summation of possible states, many of these states are infinite. This geometric summation can be rewritten in such a way that is it possible to simplify the summation into a finite expression. This partial sum technique can be generalized to yield an extremely convenient exact expression for the propagator which is known as Dyson's equation. This sum is possible since we are only dealing with simple repeated parts of diagrams which are handing on the main directed $(\mathbf{k},\omega)$-line. These simple diagrams are bubbles, open oysters, rings, etc. which can be written without the main propagator line. Once we look at all possible cases that use these simple diagrams, the series is then summed into a finite form. If this sum is over all repetitions of all irreducible self-energy parts, we end up with Dyson's equation for a single particle. Translating Dyson's diagram into Green's function propagators, we end up with

$$G(\mathbf{k},\omega)=\frac{1}{\omega-\omega_k-\Sigma(\mathbf{k},\omega)+i\delta_k}.$$

In the above equation, $\Sigma(\mathbf{k},\omega)$ is related to the sum of all proper self-energy parts. Of course, for non-interacting systems, $\Sigma(\mathbf{k},\omega)=0$. Dyson's equation is the basic equation most propagator calculations start from. Of course, determining $\Sigma(\mathbf{k},\omega)$ is still very difficult, but the problem is simpler than trying to calculate the Green's function propagators for the entire infinite series of diagrams. Dyson's equation lets us simplify the problem immensely. Typically determining $\Sigma(\mathbf{k},\omega)$ is where the approximations come into play. Certain diagrams will dominate and only those are calculated, while the other less important diagrams are not calculated. It is important to note that Dyson's equation in this form is only valid when no external potentials exist, and the diagrams calculated are in $(\mathbf{k},\omega)$ space.

In the high-density electron gas, nearly the entire contribution to the self energy comes from the 'ring' diagrams('random phase approximation' or 'RPA'). This interaction can be interpreted as a 'screened' interaction between two particles. These rings are often called 'polarization diagrams' since they have one interaction line entering and one leaving the diagram. They show how the interaction causes the medium to become 'virtually polarized' in all possible ways. This approximation allows us to write the effective potential as

$$V_{eff(RPA)}(\mathbf{q},\omega) = \frac{V_q}{\varepsilon_{RPA}(\mathbf{q},\omega)},$$

where $\varepsilon_{RPA}(\mathbf{q},\omega)$ is the generalized dielectric constant. The dielectric properties of a medium arise because of the polarization of the medium by a field, and the sum of all ring diagrams represents the polarization of the electron gas by the field of one of the electrons in the gas itself.

The field theory related to this dissertation is discussed in Chapter 6. The theory starts out with Dyson's equation. From the optical theorem we know that the spectral function is related to the imaginary part of the green's function. In this case, the Green's function is for a collective excitation, and not a single particle excitation which was covered above. Similar to the single particle case, for the collective excitation, the Dyson's equation is given by

$$D(q,\omega) = \frac{1}{\omega^2 - \omega_0^2 - \Sigma(\mathbf{q},\omega)},$$

where D is the Dyson's Green's function, ω_0 is an undamped phonon frequency, and $\Sigma(\mathbf{q},\omega)$ is the exact self energy with no approximation. In this case, the important term to the self energy are the ring diagrams. Hence, we will approximate the self energy as

$$\Sigma(\mathbf{q},\omega) = |g(p)|^2 \Pi(\mathbf{q},\omega).$$

and all other contribution are considered to be non-important and ignored. In the above equations, $\Sigma(\mathbf{q},\omega)$ is the self energy which for this case has been approximated using only the simple ring diagrams, g(p) is the electron-phonon coupling constant, and $\Pi(\mathbf{q},\omega)$ is the irreducible polarizability. The problem arises in exactly how to determine $\Pi(\mathbf{q},\omega)$ which contains a very difficult integral. To perform this integral some assumptions must be made. Schuster extended the limits on integration out to infinity, while Varma made assumptions about the fermi surface to perform the integral. The results of these calculations are talked about in Chapter 6.

REFERENCES

1. For a review, see S. Roth, *Applied Physics*, **15**, 1 (1978).

2. For a review of magnetic superconductors as of 1990, see O. Fisher, *Ferromagnetic materials*, Vol. 5, ed. K.H.J. Bushow and E.P. Wohlfarth (North Holland, Amsterdam, 1990) P. 465.

3. G.K. Shenoy, B.D. Dunlap, F.Y. Fradin (eds.), Proc. Int. Conf. on Ternary Superconductors (North-Holland, Amsterdam, 1981).

4. M.B. Maple and O. Fischer (eds.), *Superconductivity in Ternary Compounds, Vols. I and II, Topics in Current Physics* (Springer, Berlin, Heidelberg and New York, 1982).

5. S.K. Sinha, H.A. Mook, O.A. Pringle, D.G. Hinks, in: Superconductivity in Magnetic and Exotic Materials: Proc. 6th Taniguchi Internat. Symp. Kashikojima, Japan, November 14-18, 1983, eds. T. Matsubara and A. Kotani, (Springer-Verlag, New York, 1984) pp. 14-28.

6. W.A. Fertig, D.C. Johnston, L.E. DeLong, R.W. McCallum, M.B. Maple, and B.T. Mattheis, *Phys. Rev. Lett.* **38**, 987 (1977).

7. D.E. Moncton, *J. Appl. Phys.* **50**(3), 1880 (1979).

8. D.E. Monctom, G. Shirane, and W. Thominson, *J. of Magnetism and Magnetic Materials* **14**, 172 (1979).

9. D.E. Monctom, D.B. MeWhan, P.H. Schmidt, G. Shirane, W. Thomlinson, M.B. Maple, H.B. MacKay, L.D. Woolf, Z. Fisk, and D.C. Johnston, *Phys. Rev. Lett.* **45**, 2060 (1980).

10. J.W. Lynn, G. Shirane, W. Thomlinson, and R.N. Shelton, *Phys. Rev. Lett.* **46**, 368 (1981).

11. S.K. Sinha, G.W. Crabtree, D.G. Hinks, and H. Mook, *Phys. Rev. Lett.* **48**, 950 (1982).

12. J.W. Lynn, J.A. Gotaas, R.W. Erwin, R.A. Ferrel, J.K. Bhattacharjee, R.N. Shelton, and P. Klavins, *Phys. Rev. Lett.* **52**, 133 (1984).

13. J.A. Gotaas, J.W. Lynn, R.N. Shelton, P. Klavins, and H.G. Braun, *Phys. Rev. B* **36**, 7277 (1987).

14. *Proceedings of the International Conference on Ternary Superconductors*, edited by G.K. Shernoy, B.D. Dunlap, and F.Y. Fradin (North-Holland, Amstardam, 1981).

15. *Superconductivity in Ternary Compounds, Vols, I and II of Topics in Current Physics*, edited by M.B. Maple, and O. Fisher (Springer, Berlin, 1982).

16. R. Nagarajan, C. Maxumundar, Z. Hosain, S.K. Dhar, K.V. Golparrishnan, L.C. Gupta,C. Godart, B.D. Pedalia, and R. Vijayaraghavan, *Phys. Rev. Lett.* **72**, 274, (1994).

17. R.J. Cava, H. Takagi, H.W. Zandbergen, H.H. Krajewski, W.F. Peck, Jr., T. Siegrist, B. Batloff, R.B. van Dover, R.J. Felder, K. Mizuhashi, J.O. Lee, H. Eisaki, and S. Uchida, *Nature* (London) **367**, 252 (1994).

18. T. Siegrist, H.W. Zandbergen, R.J. Cava, J.J. Krajewski, and W.F. Peck, Jr., *Nature* (London) **367**, 254 (1994).

19. R. Cava, H. Takagi, B. Batloff, H.W. Zndbergen, J.J. Krajewski, W.F. Peck, Jr., R.B. van Dover, R.J. Felder, T. Siegrist, K. Mizuhashi, J.O. Lee, H. Eisasi, S.A. Cater, and S. Uchida, *Nature* (London) **367**, 146 (1994).

20. Ming Xu, B.K. Cho, P.C. Canfield, D.K. finnemore, and D.C. Johnston, *Physica C* **235-240**, 2533 (1994).

21. Ming Xu, P.C. Canfield, J.E. Ostenson, D.K. Finnemore, B.K. Cho, Z.R. Wang, D.C. Johnston, *Physica C* **227**, 321 (1994).

22. B.K. Cho, Ming Xu, P.C. Canfield, L.L. Miller, and D.C. Johnston, *Phys. Rev. B* **52**, 3676 (1995).

23. B.K. Cho, P.C. Canfield, L.L. Miller, and D.C. Johnston, *Phys. Rev. B* **52**, 3684 (1995).

24. K.D.D. Rathnayaka, D.G. Naugle, B.K. Cho, P.C. Canfield, *Phys. Rev. B* **53**, 5688 (1996).

25. B.K. Cho, P.C. Canfield, and D.C. Johnston, *Phys. Rev. B* **52**, R3844, (1995).

26. P. Dervenagas, J. Zarestky, C. Stassis, A.I. Goldman, P.C. Canfield, B.K. Cho, *Physica B* **212**, 1 (1995).

27. P.C. Canfield, B.K. Cho, K.W. Dennis, *Physica B* **215**, 337 (1995).

28.B.K. Cho, P.C. Canfield, D.C. Johnston, *Phys. Rev. B* **53**, 8499 (1996).

29.C. Stassis and A. Goldman, *J. Alloys and Comp.* **250**, 603 (1997).

30.A.I. Goldman, C. Stassis, P.C. Canfield, J. Zarestky, P. Dervenagas, B.K. Cho, D. C. Johnston, And B. Sternlieb, *Phys. Rev B* **50**, 9668 (1995)

31.T.E. Grigereit, J.W. Lynn, Q. Huang, A. Santoro, *Phys. Rev. Lett.* **73**, 2756 (1994).

32.T. Vogt, A. Goldman, B. Sternlieb, and C. Stassis, *Phys. Rev. Lett.* **75**, 2628 (1995).

33.J. Zarestky, C. Stassis, A.I. Goldman, P.C. Canfield, P. Dervenagas, B.K. Cho, and D. C. Johnston, *Phys. Rev. B* **51**, 678 (1995).

34.S.K. Sinha, J.W. Lynn, T.E. Griegereit, Z. Hossain, L.C. Gupta, R. Nagarajan, and C. Godart, *Phys. Rev. B* **51**, 681 (1995).

35.C. Detlefs, A.I. Goldman, J.P. Hill, D. Gibbs, C. Stassis, P.C. Canfield, and B.K. Cho, *Phys. Rev. B* **53**, 6355 (1996).

36.P. Dervenagas, J. Zarestky, C. Stassis, A.I. Goldman, P.C. Canfield, and B.K. Cho, *Phys. Rev. B* **53**, 8506 (1995).

37.M.A. Ruderman, C. Kittel, *Phys. Rev.* **96**, 99 (1954).

38.T. Kasuya, *Progr. Theoret. Phys.*(Japan), **16**, 45 (1956).

39.K. Yosida, *Phys. Rev.* **106**, 893 (1957).

40.J.H. Van Vleck, *Rev. Mod. Phys.* **34**, 681 (1962).

41.J.M. Ziman, Principles of the Theory of Solids (Cambridge, 1972).

42.W. Kohn, *Phys. Rev. Lett.* **2**, 393 (1959).

43.B.N. Brockhose, T. Arase, G. Cagliota, K.R. Rao, and A.D.B. Woods, *Phys. Rev.* **128**, 1099 (1962).

44.J.Y. Rhee, X. Wang, and B.N. Harmon, *Phys. Rev. B* **51**, 15585 (1995).

45.J. Rath and A.J. Freeman, *Phys. Rev. B* **11**, 2109 (1975).

46.F. Gompf, W. Reichardt, H. Schober, B. Renker, M. Buchgeister, *Phys. Rev. B* **55**, 9058 (1997).

47.I.K. Yanson, V.V. Fisun, A.G.M. Jansen, P. Wyder, P.C. Canfield, B.K. Cho, C.V. Tomy, D. McK. Paul, *Phys. Rev. Lett.* **78**, 935 (1997).

48.H. Kwano, H. Yoshizawa, H. Takeya, K. Kadowaki, *Phys. Rev. Lett.* **77**, 4628 (1996).

49.M. Xu, P.C. Canfield, J.E. Ostenson, D.K. Finnemore, B.K. Cho, Z.R. Wang, and D.C. Johnston, *Physica C* **227**, 321 (1994).

50.B. Cho, *Anisotropic superconducting and normal state magnetic properties of single crystals of RNi2B2C compounds (R = Y,Gd,Dy,Ho,Er, and Tm)* (ISU Dissertation, 1995).

51.R. Celotta and J. Levine, Methods of Experimental Physics Vol 23-part A, (Academic Press, 1986).

52.G.E. Bacon, Neutron Diffraction (Clarendon Press, 1975).

53.H. Dachs, Neutron Diffraction (Springer Press, 1978).

54.P. Brüesch, Phonons: Theory and Experiments II (Springer Press, 1982).

55.P. Brüesch, Phonons: Theory and Experiments II (Springer Press, 1986).

56.P. Brüesch, Phonons: Theory and Experiments III (Springer Press, 1987).

57.J. Harada, J.D. Axe, G. Shirane, *Phys. Rev. B* **4**, 155, (1971).

58.J.D. Axe, J. Harada, G. Shirane, *Phys. Rev. B* **1**, 1227 (1970).

59.J.D. Axe and G. Shirane, *Phys. Rev. Lett.* **30**, 214 (1973).

60.S.M. Shapiro, G. Shirane, J.D. Axe, *Phys. Rev. B* **12**, 4899 (1975).

61.T. Ekino, H. Fujii, M. Kosugi, Y. Zenitani, J. Akimitsu, *Phys. Rev B* **53**, 9 (1996).

62.G.T. Jeong, J.I. Kye, S.H. Chun, Z.G. Khim, W.C. Lee, P.C. Canfield, B.K. Cho, D.C. Johnston, *Physica C*, **253**, 48 (1995).

63.N. Pyka, W. Reichardt, L. Pintschovius, G. Engel, J. Rossat-Mignod, J.Y. Henry, *Phys. Rev. Lett.* **70**, 1457 (1993).

64.H.A. Mook, B.C. Chakoumakos, M. Mostoller, *Phys. Rev. Lett.* **69**, 2272 (1992).

65.B. Friedl, C. Thomsen, M. Cardona, *Phys. Rev. Lett.* **65**, 915 (1990).

66.F. Marsiglio, *Phys. Rev. B* **47**, 5419 (1993).

67.M.V. Klein, S.B. Dierker, *Phys. Rev. B* **29**, 4976 (1984).

68.R. Zeyher and G. Zwicknagl, *Z Phys. B* **78**, 175 (1990).

69.P.B. Allen, V.N. Kostur, N. Takesue, and G. Shirane, *Phys. Rev. Lett.* -to be published.

70.H.Y. Kee and C.M. Varma(preprint)

71.H.G. Schuster *Solid State Comm.* **13**, 1559 (1973).

72.R. Zeyher, *Phys. Rev. B* **44**, 9596 (1991).

73.J.M. Ziman, Principles of the theory of Solids (Cambridge University Press, 972).

74.R.D. Mattuck, A Guide to Feynman diagrams in the many-body problem (McGraw-Hill Internationsl Book Company, 1976).